TABLE OF CONTENTS

CHAPTER 1 INTRODUCTION

The series of operations in a mineral processing plant to produce a valuable metal product from mined ore is illustrated in Fig. 1.1. The first process in the mineral processing plant, comminution, consists of a sequence of crushing, grinding, and classification. Crushing reduces the particle size of run-of-mine ore through compression against rigid surfaces for the ore to be within a manageable size for subsequent grinding. Grinding is achieved by mills where the metals are liberated from gangue through impact, abrasion, and attrition breakage. The classification process returns ore requiring further breakage to the grinding process. The combination of the grinding and classification process is generally referred to as a grinding mill circuit, or milling circuit. The aim of comminution is to convert run-of-mine ore into fine particles in order to liberate valuable metals within the ore (Wills 2006, Sbarbaro and del Villar 2010).

The subsequent separation process shown in Fig. 1.1 receives the comminution product and separates the valuables metals from waste (gangue). Two streams exit the separation process: a concentrate of

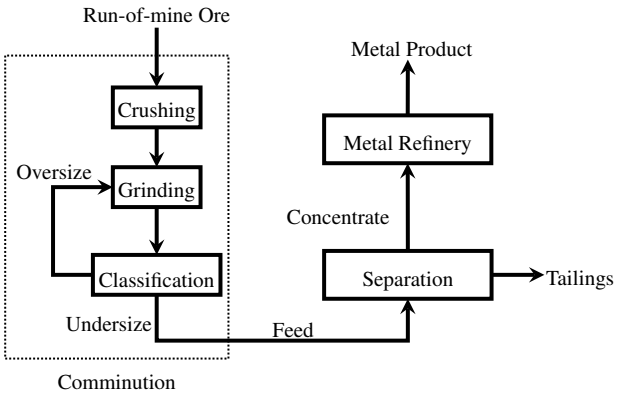

Figure 1.1. The chain of processes in a mineral processing plant. (The metal refinery is excluded from the mineral processing plant.)

valuables and a stream of gangue to be discarded (tailings). A mineral processing plant in this study excludes the extractive metallurgy at a metal refinery and comprises only of the comminution and separation processes. The mineral processing plant sells the concentrate to a metal refinery where the metal is extracted from the concentrate through pyro-, hydro, or electro-metallurgy to produce the final marketable metal product. A common refinery method is the pyrometallurgy process of smelting. If the run-of-mine ore is processed directly by the smelter, the cost of smelting will outweigh the product value in the ore. Therefore, the objective of the mineral processing plant is to maximise the economic value of the separator concentrate sold to the smelter by reducing the bulk of ore and increasing the contained value of the ore (Hodouin, Jämsä-Jounela, Carvalho and Bergh 2001, Wills 2006).

Given the crucial part a grinding mill circuit plays in the energy and cost-intensive comminution process of extracting valuable metals and minerals from mined ore, the ability of downstream processes to extract the greatest benefit from milled ore is dependent on the metal liberation in the product that leaves the mill. In order to achieve the desired product specification in terms of quality and production rate, adequate control of the milling circuit is required. The general control objectives for a milling circuit are to improve the quality of the product, to maximise the throughput, to decrease the power consumption, to reduce the usage of grinding media and to improve process stability. However, these objectives are interrelated and necessitate certain trade-offs to be made (Craig and MacLeod 1995, Edwards, Vien and Perry 2002).

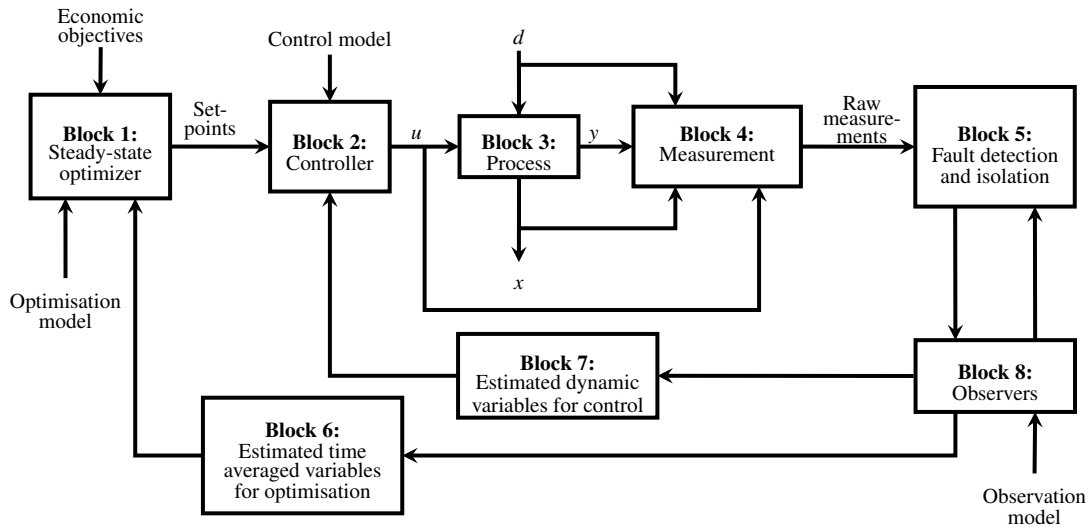

Figure 1.2. Generalised control loop for mineral processing. (Adapted from Hodouin (2011) with permission.)

The generalized control loop shown in Fig. 1.2 indicates the flow of data between the process, the controller, and various peripheral control tools (Hodouin 2011). It provides a structural separation between the various aspects to be considered to achieve a specific control objective. However, within the structure of Fig. 1.2, three issues needs to be resolved (Qin and Badgwell 2003, Dochain, Marquardt, Won, Malik, Kinnaert and Lunze 2008, Craig, Aldrich, Braatz, Cuzzola, Domlan, Engell, Hahn, Havlena, Horch, Huang, Khanbaghi, Konstantellos, Marquardt, McAvoy, Parisini, Pistikopoulos, Samad, Skogestad, Thornhill and Yu 2011):

- The realistic approach to system analysis and synthesis for complex systems.
- The development of advanced control strategies which can be implemented with relative ease.
- The design of accurate process models to be used for model-based control and observer design.

Developing economic objectives and incorporating them within a steady-state optimiser (Block 1) can be associated with the first issue of system analysis and synthesis. This also requires correct differentiation between variables required for optimisation (Block 6) compared to variables required for control (Block 7). Once desired set-points have been identified, the second issue of advanced controller design (Block 2) can be addressed. For model-based advanced process control, the third issue of developing accurate control-relevant process models needs to be addressed. Tied to this is observer design for state and parameter feedback (Block 8) using the relevant process models and plant measurements (Block 4).

This thesis aims to address these issues for a single-stage grinding mill circuit in the order they are listed above. A realistic approach to plant-wide control synthesis is developed, which defines the requirements for an advanced process control strategy. An advanced model-based control strategy with reduced computational cost is subsequently developed. For state-feedback, an observer model is developed with states which can be realistically estimated from measurements commonly available on industrial plants.

1.1 PROBLEM STATEMENT

1.1.1 Context

1.1.1.1 Plant-wide control synthesis

In general, the objective of comminution is to produce a product with a consistent fineness while maximising throughput, whereas the objective of separation is to maintain a constant concentrate grade while trying to maximise metal recovery. The value of the concentrate sold to the smelter depends on the relationship between the recovery and grade of the concentrate. The recovery is the fraction of total valuable metals in the concentrate recovered from the separator feed. (A recovery of 0.85 means that 85% of the minerals in the feed is recovered in the concentrate and 15% is lost in tailings.) The concentrate grade is the fraction marketable product content in the concentrate. (A concentrate grade of 0.01 means there is 10 kg of valuable content in 1 tonne of concentrate.)

Optimisation of the comminution and separation objectives individually may lead to a sub-optimal solution. Because the concentrate produced by the separation process is the main revenue generator of the plant, economic optimisation of the comminution circuit only makes sense if done with reference to the separation circuit. In the case of McIvor and Finch (1991), a size-by-size analysis of the recovery of metals in a separation circuit is used to estimate the recoverable value of metals distributed throughout the comminution circuit product size distribution. This is then used to define the steady-state target grind size for the comminution circuit to improve economic performance of the metal processing plant. In a similar study, Sosa-Blanco, Hodouin, Bazin, Lara-Valenzuele and Salazar (2000) provide a step-wise procedure to optimally tune a comminution circuit to maximise the economic efficiency of a separation circuit. An empirical relationship is used to describe the comminution circuit product ore size distribution to the separation metal recovery. To address the effect of the dynamics of the comminution circuit on the separation circuit, Munoz and Cipriano (1999) propose a predictive controller which optimises an economic objective function based on metallurgical performance indices. The economic objective function describes the income generated by the plant as a function of the comminution feed ore grade, the separator tailings grade, and the metal refinery recovery per tonne of ore processed. Wei and Craig (2009a) make use of an economic performance function based on the relation between the comminution product quality to separation concentrate recovery to compare the

economic performance of non-linear Model Predictive Control (NMPC) to single-loop Proportional-Integral-Derivative (PID) control for a comminution circuit. In all the cases mentioned above, a relationship between the comminution product particle size and the concentrate recovery and grade is used to define the revenue generated from selling the concentrate to a metal refinery (see also Matthews and Craig (2013)).

Optimisation of the economic objective function for the grinding mill circuit depends on the operating range of the grinding mill circuit. The comminution product particle size which will optimise the economic objective function for different market conditions may not necessarily be achievable by the grinding mill circuit. The model used to describe the grinding mill circuit needs to be capable of capturing the range of feasible operating conditions of the grinding mill. The non-linear population balance models used in the optimisation studies above remain limited to a relatively small region of operation. The model parameters need to updated for different feasible operating regions of the grinding mill circuit.

The grindcurves of Van der Westhuizen and Powell (2006) are quazi-static descriptions of the operable regions of the grinding mill. It relates the mill's performance indicators - power draw, grind size, and discharge flow-rate - to the mill's filling and its rotational speed. The grindcurves therefore provide the feasible operating conditions for the grinding mill to achieve a specific product size specification. The grindcurves can be regarded as a mechanism for optimisation of the mill as a unit (Powell, van der Westhuizen and Mainza 2009). Consequently, it enables optimisation of the economic objective function over a larger range of mill operating conditions without the need to update the mill's model parameters.

However, once the operating condition which will optimise the economic objective function is defined, the regulatory and supervisory control layer needs to be able to maintain the circuit at the desired operating condition. This raises additional questions, such as which variables should be controlled apart from the product particle size, which should be manipulated, which should be measured, what links should be made between them, and which set-points are appropriate for the controlled variables? The plant-wide control analysis of Skogestad (2004) answers these questions by providing a structured approach to construct a control architecture capable of achieving the demands specified by the optimisation of the economic objective function. This assists achieving the final goal of this industry: plant-wide economic optimisation (Hodouin *et al.* 2001).

1.1.1.2 Computational cost of model-based control

Regulatory and supervisory control of a grinding process face the following challenges: strong coupling between variables, large time delays, uncontrollable and unmeasured disturbances, variation of parameters over time, non-linearities in the process, and instrumentation inadequacies (Chen, Li and Fei 2008, Coetzee, Craig and Kerrigan 2010). Although process industries, in general, have benefited considerably from advanced process control to resolve similar challenges, the mineral processing industry, in particular, has yet to take full advantage of model-based advanced process control (Craig *et al.* 2011).

Traditionally milling circuits are controlled by decentralized PID controllers (Wei and Craig 2009b) despite the multivariable nature of the circuits (Pomerleau, Hodouin, Desbiens and Gagnon 2000). Significant improvement in product quality, throughput and power consumption is possible through multivariable control techniques. This is illustrated by the industrial implementation of a multivariable controller on a run-of-mine ore grinding circuit documented in Hulbert, Craig, Coetzee and Tudor (1990) and Craig, Hulbert, Metzner and Moult (1992), the robust controller applied to an industrial semi-autogenous (SAG) mill in Craig and MacLeod (1995) and Craig and MacLeod (1996), and the linear model predictive control for an industrial ball mill circuit in Chen, Zhai, Li and Li (2007). The industrial controller applications mentioned above are based on linear process models. Because of the slow time-varying nature of the process and the large process disturbances, the controllers are limited to a narrow range of process operation. Although non-linear model-based control is preferable, an impediment to applying non-linear control to grinding mill circuits is the computational burden to minimise a non-linear controller objective function (Coetzee *et al.* 2010, Wolf and Marquardt 2016).

The computational burden of detailed fundamental non-linear models with large parameter sets and large state vectors increases the difficulty of developing feasible non-linear model based controllers. Linearized models are generally used when applying optimal control in the form of Model Predictive Control (MPC) to grinding mill circuits (Ramasamy, Narayanan and Rao 2005, Chen *et al.* 2008, Apelt and Thornhill 2009), but the use of NMPC with fundamental non-linear models is more desirable because of the highly non-linear nature of the grinding process. Even though the modelling of comminution processes improved over the past years (Powell and Morrison 2007), many of the available fundamental non-linear models are not necessarily suitable for process control. These non-

linear models are mainly used for steady-state plant design and for a better understanding of load behaviour, breakage mechanisms and energy dissipation (Hodouin *et al.* 2001).

The non-linear model in (Le Roux, Craig, Hulbert and Hinde 2013b) of a single-stage closed grinding mill circuit was developed to produce reasonably accurate model responses using as few parameters and states as possible. This makes the model well suited for control purposes. Coetzee *et al.* (2010) made use of this model to apply robust NMPC in simulation to a grinding mill circuit. Although excellent regulatory results were achieved in the presence of large disturbances and parameter uncertainties, the robust NMPC controller was not regarded suitable for on-line application unless computational time was significantly reduced.

As noted in the review by Wolf and Marquardt (2016), a vast array of NMPC schemes based on fast updated methods are available. The fast update approximates the solution to the parametric non-linear program obtained when the optimal control problem is discretized. In the case of regulatory NMPC, recursive feasibility alone suffices to guarantee stability for these methods (Scokaert, Mayne and Rawlings 1999). The basis for these fast NMPC methods were NMPC schemes where the model is linearised and only a few quadratic-program iterations are conducted. These schemes are generally developed for quadratic objective functions with box path constraints and no endpoint constraints. Li and Biegler (1989) and De Oliveira and Biegler (1995) provide examples of regulatory NMPC schemes based on linearisation of the system. A first-order correction of the outputs is iteratively computed beginning with the reference solution until the change in the objective function is below a certain threshold. The first iteration uses the control applied previously to the process as the reference for the entire time horizon.

Alternatively, explicit MPC evaluates the state of a linear system at every sampling instance and looks up the corresponding optimal control input from a pre-computed map of critical regions. The computational effort of solving the optimisation problem is thereby moved off-line (Bemporad, Borrelli and Morari 2002a, Summers, Jones, Lygeros and Morari 2011, Rivotti and Pistikopoulos 2015). However, there is a rapid increase in the computational burden to solve the off-line optimisation problem as the prediction horizon increases. Also, explicit MPC is generally only suited to small-scale problems (Bemporad, Morari, Dua and Pistikopoulos 2002b). As a possible solution to these problems, Pannocchia, Rawlings and Wright (2007), and Wang and Boyd (2010) combine explicit MPC with online optimisation methods.

A suboptimal control design technique called Model Predictive Static Programming (MPSP) was developed by Padhi and Kothari (2009) for finite-horizon non-linear problems with terminal constraints. This technique combines the philosophies of MPC and approximate dynamic programming to reduce a dynamic optimisation problem to a low dimensional static optimisation problem. This strategy borrows from explicit MPC, where the optimisation problem is reduced to an explicit function (Bemporad *et al.* 2002a), and borrows also from NMPC methods where the system is linearised so that only a few quadratic-program iterations are required (De Oliveira and Biegler 1995). Additionally, numerical values of the sensitivity matrices are calculated recursively, similar to the robust explicit multi-parametric MPC of Kouramas, Panos, Faisca and Pistikopoulos (2013). Finally, even though the sensitivity matrices used in the optimisation problem can be calculated off-line in symbolic form, MPSP is executed on-line (Wang and Boyd 2010).

Therefore, MPSP is one technique among many which attempts to reduce computational complexity for real-time application of NMPC (Chawla, Sarmah and Padhi 2010). The particular attractiveness of MPSP is that it only makes use of matrix algebra calculations, and is therefore relatively simple to understand and implement. The computational effectiveness of MPSP is well attested in the aerospace industry, e.g. Padhi and Kothari (2009), Oza and Padhi (2012), Joshi and Padhi (2013), Maity, Oza and Padhi (2013), Bhitre and Padhi (2014), and Halbe, Raja and Padhi (2014).

However, MPSP is yet to be extended to regulatory control for output tracking. Applying the MPSP technique with a receding horizon mechanism for output tracking problems may provide a viable control solution for industrial comminution circuits where computational complexity limits the implementation of advanced process control (Coetzee *et al.* 2010). As far as the author is aware, fast MPC techniques has yet to be applied to comminution circuits.

1.1.1.3 State and parameter estimation

Apart from the concern of computational complexity, another impediment to implementing model-based control in grinding mill circuits, is the lack of sufficient real-time measurements to estimate the necessary model states and parameters for state-feedback (Hodouin *et al.* 2001, Edwards *et al.* 2002). The number of available real-time measurements on industrial circuits are generally far less than the size of the state vector to be measured (Wei and Craig 2009b). Therefore, the peripheral tools

of the control loop such as observers and soft sensors become as important as the controller itself (Hodouin 2011, Olivier, Huang and Craig 2012).

In general terms, the grinding performance of a mill depends on the hold-up of steel balls, ore and water. Consequently, estimation of these three hold-ups is desirable. Although the total mill hold-up is generally measured in industrial circuits (Wei and Craig 2009b), the steel ball, ore, and water hold-ups cannot be measured directly with the currently available instrumentation. Measurement of these three mill inventories, which influence the product throughput and product quality of the mill, can significantly improve plant performance if used to inform a control loop. Steel balls form very effective grinding media because of their higher density and hardness compared to ore. The balls enhance impact breakage to quickly break the coarser rocks which would otherwise have been broken through the slower abrasion and attrition processes. A very low level of balls in the mill reduces the rate at which coarse ore is broken through impact breakage, and a too high level of balls reduces the amount of coarse ore necessary to produce a fine ore product through abrasion and attrition. If the ball level is increased to very high levels, the impact on the fineness of the product is reduced, but considerably more power is required to turn the mill because of the high mass of balls. It is also necessary to maintain the correct ratio between ball and ore hold-up. If the ore hold-up is significantly less than the ball hold-up, the mill-liners become too exposed to the steel balls and the mill-liner life-time is consequently reduced. Furthermore, with regards to the ore hold-up, a harder ore causes an increase in ore hold-up as more time is required to break the harder ore, and vice-versa for a softer ore. In the case of SAG mills, the harder ore generally produces a finer grind at a lower throughput, whereas a softer ore produces a coarser grind at a higher throughput. Finally, the water in the mill is responsible for transporting the broken media through the mill. If the water hold-up is too high, a slurry-pool forms at the bottom of the mill absorbing the breaking power of the falling balls and rocks. On the other hand, a too low water hold-up causes the build-up of a thick non-flowing mud which also reduces the efficiency of ore breakage (Napier-Munn, Morrell, Morrison and Kojovic 2005).

The model structure used to describe a comminution process has a significant impact on the success of state and parameter estimation. Models aimed at plant design are generally not suited for model-based control, and vice-versa. Steady-state phenomenological models, a combination between theoretical and empirical models, are well established and are valuable for comminution plant design and steady-state optimisation (King 2001, Napier-Munn *et al.* 2005, Gupta and Yan 2006). The model parameters are generally divided into the ore to be processed and the comminution unit processing the ore. Laboratory

drop-weight and pendulum-breakage tests provide the ore specific parameters, and sampling campaigns provide the processing unit's parameters (Napier-Munn *et al.* 2005). Since the characteristics of run-of-mine ore fed to industrial mills change over time, results from laboratory tests used to estimate ore specific parameters do not necessarily reflect the range of ore breakage conditions in the industrial mill (Powell and Morrison 2007). Also, sampling campaigns used to estimate the processing unit's parameters assume steady-state operation at a specific operating point, but steady-state is difficult to guarantee over a long period given the variation of run-of-mine ore characteristics. It is usually assumed the functions describing the milling environment can be expressed as simple equations with parameters that can be estimated from sampling campaign data through back-calculation. Because of the heavy reliance on back-calculation, small measurement errors can lead to large variances in parameters (Hinde and Kalala 2009). With the advancements in computing power, computational fluid dynamics (CFD) and discrete element method (DEM) models have provided valuable insight into the charge motion of grinding processes. A difficulty associated with these fundamental models is the correct estimation of the force contact model's parameters as ore characteristics vary over time (Morrison, Shi and Whyte 2007). Additionally, fundamental models remain too computationally intensive to be used in advanced process control strategies (Mishra 2003a, Mishra 2003b).

The mathematical models of comminution circuits proving most useful for industrial automatic control so far are developed on-line (Wills 2006). These empirically derived linear-time-invariant transfer function models have been successfully applied in model-based controller strategies to industrial circuits, e.g. by Hulbert *et al.* (1990), Craig and MacLeod (1996), Chen *et al.* (2007), and Chen *et al.* (2008). However, these linear models are restricted to the domain around the nominal operating point of the plant and require constant management to accommodate variations in grinding conditions (Hodouin *et al.* 2001, Desbiens, Najim, Pomerleau and Hodouin 1997). System identification is particularly difficult given the inherent uncontrollable disturbances, measurement noise and high tonnage operation (Hodouin 2011). Ideally, real-time measurements should be used to estimate model states and parameters.

Considerable work has been done to estimate grinding mill process variables using different modelling approaches (Herbst, Pate and Oblad 1992). A very simple model along with power and bearing pressure measurements is used by Herbst, Pate and Oblad (1989) to estimate mill filling and rock hardness. This work is extended in Herbst and Pate (1996) to estimate ore, water, and ball inventories. A commercialised soft-sensor is described by Herbst and Pate (1999) to estimate mill inventories

and breakage rates. The soft-sensor assumes the parameters used to describe the measurements are known and remain constant. In all cases above, a Kalman filter is used to estimate the unknown state vector. Although the filters capture the qualitative trend of the unknown states, the studies above do not explicitly include observability analyses to indicate if the filters can produce reliable solutions.

A linear observability test is included in the inferential measurement work of Apelt, Asprey and Thornhill (2002a). The SAG mill model of Napier-Munn *et al.* (2005) was used to describe the grinding process, along with a novel ball charge model and a mill-liner model. Using measurements of the mill charge weight and size-by-size solids discharge, Apelt *et al.* (2002a) used 29 measurements to estimate 37 states and 7 parameters with an Extended Kalman Filter (EKF). However, the rank of the observability matrix of the linearised system was only 20, which meant a unique solution for the parameters and states was not available.

As shown by Le Roux and Craig (2016), it is theoretically possible to uniquely fit the simplified non-linear grinding mill circuit model of Le Roux *et al.* (2013b) to real-time plant measurements. However, the algebraic fitting procedure is too sensitive to uncertainties in measurements as the procedure involves the calculation of first and second order time-derivatives from noisy data. Although a relatively simple model is used, there are so many parameters to be defined that the value of this procedure is limited.

The model of Le Roux *et al.* (2013b) is used by Olivier *et al.* (2012) to estimate the mill inventories and grinding environment parameters in simulation. Assuming measurements of the mill discharge are available, a dual particle filter is used to estimate the hold-up of balls, rocks, solids, fines, and water as states, and the fraction of rock entering the circuit and the power needed per tonne of fines produced as parameters. The technique achieves good quantitative estimation if constant rock abrasion rates, ball abrasion rates, and step disturbances are assumed, but these assumptions may not necessarily hold true for industrial operation.

To ensure efficient model-plant mismatch rejection and integral action for MPC, correct state and parameter feedback is required (Meadows and Rawlings 1997, Qin and Badgwell 2003, Olivier and Craig 2013). The aim is therefore to construct an observer model for a SAG mill with states and parameters which can be realistically estimated from commonly available real-time measurements on industrial circuits (Wei and Craig 2009b).

1.1.2 Research questions

Therefore, the research questions listed below are addressed in this thesis:

- How should the output of the comminution circuit be related to the economic objective of the mineral processing plant?
- Given the plant-wide economic objective, how should the control framework of the comminution circuit be structured to enable the plant to achieve its optimum economic performance?
- Once the optimal operating conditions for the comminution circuit is defined, can MPSP be used to provide a non-linear model-based controller with sufficient computational simplicity for industrial application?
- For state-feedback for model-based control, which states and parameters can be observed and estimated from commonly available real-time measurements on industrial circuits, or at least from measurements which can be realistically made on industrial circuits?

1.2 CONTRIBUTION AND PUBLICATIONS

The contribution envisioned by this research is listed below:

- An economic objective of the comminution circuit in relation to the economic objective of the larger mineral processing plant is defined (Chapter 2).
- A plant-wide control framework (Skogestad 2004) capable of maintaining the comminution circuit at its optimal operating condition is developed (Chapter 3).
- Grindcurves (Van der Westhuizen and Powell 2006, Powell *et al.* 2009) are used within the larger plant-wide control framework to define the range of feasible operating conditions of the grinding mill (Chapter 3).

- MPSP (Padhi and Kothari 2009) is applied to a grinding mill circuit in simulation to assess the viability of industrial application (Chapter 4).

- The MPSP controller's performance is compared to an NMPC controller's performance for the same operating conditions (Chapter 4).

- An observer model with states and parameters which are linearly observable from measurements of the mill's inflow, discharge flow-rate, discharge density, and total volumetric filling is developed (Chapter 5).

- The observer model is applied in simulation through an EKF to estimate the states and parameters of a SAG mill (Chapter 5).

In terms of publications, the plant-wide control framework is to be submitted as:

- Le Roux, J.D., Skogestad, S. and Craig, I.K. (2016). Plant-wide control of a single-stage closed grinding mill circuit, To be submitted to *Control Engineering Practice*

The application of the MPSP controller was published in:

- Le Roux, J.D., Padhi, R. and Craig, I.K. (2014). Optimal control of grinding mill circuit using model predictive static programming: A new non-linear MPC paradigm, *J. Process Control* **24**: 29-40

The observer model and its simulation application is to be submitted as:

- Le Roux, J.D., Steinboeck, A., Kugi, A. and Craig, I.K. (2016). An EKF observer to estimate semi-autogenous grinding mill hold-ups, To be submitted to *J. Process Control*

The non-linear model of the grinding mill circuit used in this study was previously published in:

- Le Roux, J.D. Craig, I.K. Hulbert, D.G. and Hinde, A.L. (2013). Analysis and validation of a run-of-mine ore grinding mill circuit model for process control, *Minerals Eng.* **43-44**: 121-134

The model is also used in the following control study where an NMPC structure uses a non-linear state estimator for state feedback:

- Le Roux, J.D., Olivier, L.E., Naidoo, M.A., Padhi, R. and Craig, I.K. (2016). Throughput and product quality control for a grinding mill circuit using non-linear MPC, *J. Process Control* **42**: 35-50

The conference articles listed below are a result of this study:

- Le Roux, J.D., Craig, I.K. and Padhi, R. (2013). State and parameter estimation for a grinding mill circuit from operational input-output data, *Proc. 10th IFAC Symposium Dynamics Control Process Systems*, Mumbai, India, pp. 178-183, doi: 10.3182/20131218-3-IN-2045.00046

- Le Roux, J.D., Craig, I.K. and Padhi, R. (2014). Output Tracking for a Milling Circuit using Model Predictive Static Programming, *Proc. 19th Int. IFAC World Congress*, Cape Town, South Africa, pp. 9792-9797, doi: 10.3182/20140824-6-ZA-1003.01902

- Le Roux, J.D., Steinböck, A., Kugi, A. and Craig, I.K. (2016). Non-linear observability of grinding mill conditions, *Proc. 17th IFAC Symposium Mining Mineral Metal Processing*, Vienna, Austria, (Accepted)

- Le Roux, J.D., and Craig, I.K. (2016). State and parameter identifiability of a non-linear grinding mill circuit model, *Proc. 17th IFAC Symposium Mining Mineral Metal Processing*, Vienna, Austria, (Accepted)

- Le Roux, J.D., Skogestad, S., and Craig, I.K. (2016). Plant-wide control of grinding mill circuits: Top-down analysis, *Proc. 17th IFAC Symposium Mining Mineral Metal Processing*, Vienna, Austria, (Accepted)

1.3 ORGANISATION

The organisation of this thesis addresses the research questions in the order in which the questions are listed above:

1. Chapter 2 describes the economic objectives of the mineral processing plant in terms of the product of the comminution circuit.

2. Chapter 3 constructs a control strategy to achieve the operational goals determined by the economic objective of the larger mineral processing plant.

3. Chapter 4 investigates the application of MPSP to the grinding mill circuit to achieve the regulatory and supervisory control aims specified by the plant-wide control framework at reduced computational cost.

4. Chapter 5 develops an observer model a SAG mill with states and parameters that are linearly observable from mill inflow, discharge flow-rate, discharge density, and total volumetric filling measurements, and applies the observer model to a SAG mill in simulation using an EKF.

5. Chapter 6 concludes the thesis.

CHAPTER 2 COMMINUTION: PROCESS DESCRIPTION AND ECONOMIC OBJECTIVES

The aim of this section is to describe the comminution process, specifically a single-stage closed grinding mill circuit, and develop the economic objectives of the comminution circuit with reference to the mineral processing plant. This provides a mechanism to develop a control strategy for the comminution circuit to achieve the plant-wide economic objectives. The work below is organised as shown below:

1. Section 2.1 describes the operation and the control challenges of the comminution process considered.

2. Section 2.2 addresses the effect of comminution on the separator concentrate sold to the refinery.

3. Section 2.3 describes the revenue of a mineral processing plant in terms of the grade and recovery of the separator concentrate.

4. Section 2.4 concludes the chapter.

2.1 COMMINUTION PROCESS: SINGLE-STAGE GRINDING MILL CIRCUIT

The survey by Wei and Craig (2009b) shows the prevalence of equipment type and configurations of milling circuits in mineral processing plants:

- Mill type: ball mills (54%), followed by SAG and autogenous (AG) mills (38%). (For ball mills only balls contribute to the grinding media; for SAG mills both balls and ore contribute to the grinding media; for AG mills only ore is used as grinding media.)

- Mill discharge type: grates (40%), followed by over-flow (22%).

- Circuit configuration: single-stage closed circuit (37%), followed by two-stage with the first open and then a closed mill circuit (30%).

- Classification type: cluster cyclone (37%), followed by single cyclones (27%) and screens (22%).

A single-stage grinding mill circuit closed by a cyclone, as shown in Fig. 2.1, is used throughout this study. The three main elements in the circuit are a SAG mill, a sump, and a cyclone. The motivations for using a SAG mill in a mineral processing plant are: low operating costs compared to conventional grinding, the increased demand to process large amounts of low-grade ore, reduced grinding media consumption, and the capability to handle larger sized ore which reduces preceding crushing requirements (Salazar, Magne, Acuña and Cubillos 2009).

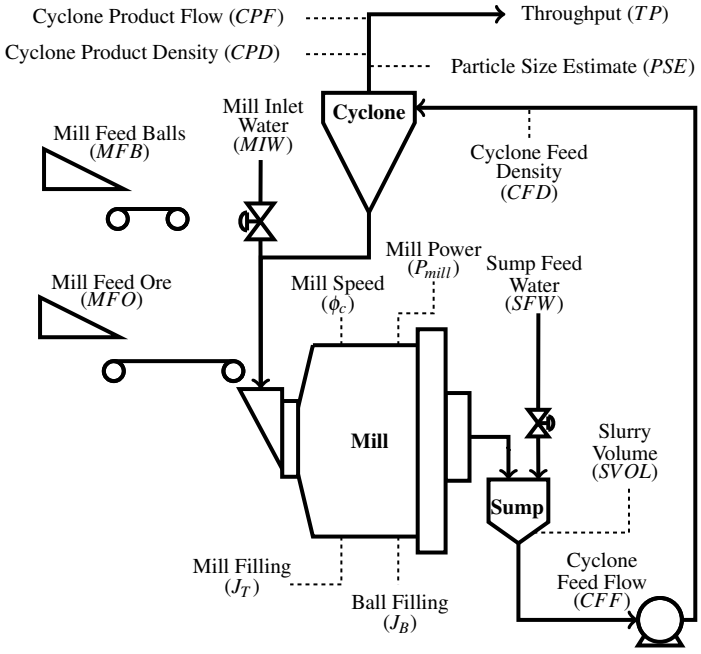

Figure 2.1. A single-stage closed grinding mill circuit.

2.1.1 Process description

The variables of the circuit in Fig. 2.1 are listed in Table 2.1. The mill receives four streams: mined ore (MFO) (t/h), water (MIW) (m^3/h), additional steel balls (MFB) (t/h) to assist with the breakage of ore, and underflow from the cyclone. The mill charge constitutes a mixture of grinding media and slurry. Grinding media refers to the steel balls and large rocks used for breaking the ore, and slurry refers to the mixture of fine ore material and water such that the mixture exhibits the same flow characteristics as water. The fraction of the mill filled with charge is denoted by J_T, and the fraction of the mill filled with balls by J_B.

The mill is rotated along its longitudinal axis by a motor. As shown in Fig. 2.2, the charge in the mill is lifted by the inner liners on the walls of the mill to a certain height from where it cascades down, only to be lifted again by the liners through the rotating action of the mill. If the rotational speed is sufficiently fast the material in the charge will become airborne after reaching the top of its travel on the mill shell. The uppermost point where material leaves the mill shell is called the shoulder of the charge. The airborne particles follow a parabolic path reaching a maximum, called the charge head, and making contact again with the mill charge at the bottom of the mill, called the charge toe. The cascading motion of the charge causes the ore to break through impact breakage, abrasion, and attrition. The mill grind (ψ) is the fraction of material in the discharge of the mill below the specification size and indicates the efficiency of the mill to break the ore. The power draw (P_{mill}) (kW) of the motor turning the mill is an indication of the kinetic and potential energy imparted to the charge. The rotational speed of the mill is generally expressed as a fraction of the critical mill speed

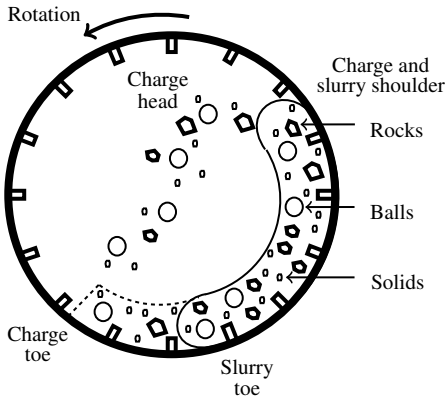

Figure 2.2. Cross-section of a SAG mill.

(ϕ_c), where the critical mill speed is the rotational speed where the centrifugal acceleration of a particle at the mill shell is equal to its gravitational acceleration.

The ground ore in the mill mixes with the water to create a slurry. The slurry in a mill begins to form at the shoulder of the charge. The toe of the slurry starts to grow downwards towards the toe of the charge as the slurry flow-rate through the mill increases. While the toe of the slurry is less than or equal to the

Table 2.1. Description of comminution circuit variables.

Variable	Unit	Description
		Manipulated Variables
MFB	[t/h]	Feed-rate of steel balls to the mill
MFO	[t/h]	Feed-rate of ore to the mill
MIW	[m^3/h]	Flow-rate of water to the mill
SFW	[m^3/h]	Flow-rate of water to the sump
CFF	[m^3/h]	Flow-rate of slurry to the classifier
ϕ_c	[-]	Fraction of critical mill speed
		Controlled Variables
J_T	[-]	Fraction of mill volume filled by total charge
PSE	[-]	Particle size estimate, i.e. fraction of particles < 75 μm in cyclone overflow
$SVOL$	[m^3]	Volume of slurry in sump
		Additional Circuit Variables
CFD	[t/m^3]	Cyclone feed density
CPD	[t/m^3]	Cyclone product density
CPF	[m^3/h]	Cyclone product flow-rate
J_B	[-]	Fraction of mill volume filled with balls
P_{mill}	[kW]	Mill power draw
Q	[m^3/h]	Mill discharge flow-rate
Q_S	[t/h]	Mill solids discharge flow-rate
Q_W	[m^3/h]	Mill water discharge flow-rate
ρ_Q	[t/m^3]	Mill slurry density
TP	[t/h]	Solids throughput, i.e. mass flow-rate of solids at cyclone overflow
ψ	[-]	Mill grind, i.e. fraction of particles in mill discharge < 75 μm

toe of the charge, discharge occurs via the grinding media. When the toe of the slurry exceeds the toe of the charge, a slurry pool forms at the bottom of the mill. Slurry discharge is then a combination of flow via the grinding media and the slurry pool (Latchireddi and Morrell 2003). Slurry pool conditions should be avoided as they decrease the mill power draw and the breakage rate by cushioning material falling from the charge shoulder to the charge toe.

The slurry is discharged through an end-discharge grate where the aperture size of the end-discharge grate limits the particle size of the discharged slurry. Ore larger than the discharge-grate aperture are referred to as 'rocks', and ore smaller than the aperture size as 'solids'. The flow-rate of slurry at the mill discharge is given by Q (m^3/h), where Q_S (t/h) denotes the solids component of Q, and Q_W (m^3/h) denotes the water component of Q. It is assumed the in-mill slurry density is equal to the discharge slurry density (ρ_Q) (t/m^3).

The discharged slurry is collected in a sump. The total volume of slurry in the sump is represented by $SVOL$ (m^3). The slurry in the sump is diluted with water (SFW) (m^3/h) before it is pumped to the cyclone via a variable-speed pump. The flow-rate of slurry from the sump to cyclone is given by CFF (m^3/h) and the density of the cyclone feed by CFD (t/m^3).

The cyclone is responsible for the classification of material discharged from the sump. The lighter and smaller particles in the slurry pass to the overflow of the cyclone, while the heavier and larger particles pass to the underflow. The 'cut-size' of the cyclone is defined as the size which divides equally to overflow and underflow, and the efficiency of the cyclone refers to the sharpness of the cut. The underflow is passed to the mill for further grinding. The overflow is the cyclone product passed to the downstream separation process. The fraction of particles in the product flow smaller than a specification size, i.e. the product particle size estimate (PSE), defines the quality of the product. Ore smaller than the specification size are referred to as 'fines', and ore larger than the specification size but smaller than the discharge-grate aperture size as 'coarse' ore. Solids are the combination of coarse ore and fines. The mass flow-rate of solids in the overflow is the throughput (TP) (t/h) of the circuit and is equal to MFO at steady-state operation of the circuit. The cyclone product density and flow-rate is given by CPD (t/m^3) and CPF (m^3/h) respectively (Stanley 1987, Napier-Munn *et al.* 2005).

2.1.2 Controlled and manipulated variables

2.1.2.1 Fraction of the mill filled with charge (J_T)

The combined mass of the mill and mass of the charge inside the mill is generally measured using either load cells or bearing pressure. Because this is not a direct measurement of J_T, the relation between J_T and a mass measurement needs to be determined whenever a mill survey is performed (Powell and Mainza 2006). For different mill charges, accurate mill filling measurements after mill stops can be used to calibrate the relationship between the mass measurement and J_T. The calibration exercise should be repeated at reasonable intervals as the loss of liner mass through wear and tear will cause a drift in the accuracy of the relationship. Once the drift in the data is quantified, an empirical liner wear model can be constructed to predict the service life of liners and adjust the relationship between the mass measurement and J_T over time. With careful planning, the mass to J_T relationship can easily be checked within half an hour from mill stop to start (Powell *et al.* 2009).

When plants choose the set-point for J_T, the efficiency of power consumption is the primary factor, followed by the stability of the system (Wei and Craig 2009b). If J_T is too high the mill needs to be stopped and the load manually reduced. The stoppage interrupts production and the additional human resources required increases operational cost. If J_T is too low in relation to J_B, the power applied to turn the mill is wasted on the energy transfer between ball-ball contact and ball-liner contact. This causes unnecessary liner damage, increases ball abrasion, and reduces Q_S. As no solids are added to the system at the sump, Q_S is split by the cyclone. The solids overflow at the cyclone (i.e. TP) is therefore a function of Q_S. If J_T is too low, it reduces Q_S which in turn reduces TP.

A primary prerogative of any controller is to stabilize the slow integrating action of the mill on its contents. To achieve this industrial plants primarily manipulate J_T by adjusting MFO, otherwise by ϕ_c if a variable speed drive is fitted, or as a last option by manipulating MIW. Control of J_T by MFO is relatively straightforward as an increase or decrease in MFO results in a direct increase or decrease in J_T. In case MFO is not available as a manipulated variable, a decrease in ϕ_c will reduce the rate at which ore is broken and more ore is allowed to accumulate within the mill. On the other hand, by increasing ϕ_c the ore is broken quicker as more energy is imparted to the charge. Once the ore is broken small enough it discharges from the mill which causes a decrease in J_T. Finally, because water

is the main transporting medium of ore through the mill, an increase in MIW will wash material out of the mill and reduce J_T. Conversely, a reduction in MIW increases the density of the slurry in the mill which reduces the fluidity of the slurry. This causes a build up of slurry in the mill which results in an increase in J_T.

2.1.2.2 Sump slurry volume ($SVOL$)

Because of the fast integrating action of the sump and the relatively small volume of the sump, care should be taken not too overflow or run the sump dry. In the case of slurry overflow, there is not only a loss of potential valuable product, but also a waste in the energy spent to produce the fine material in the lost slurry. Often sumps are not well mixed and a build-up of solids occur at the bottom. In the case of an almost dry sump, the pump may not only start to cavitate, but some of the build-up may be sucked in by the pump causing spikes in CFD. This not only damages the pump and piping, but causes the cyclone to pass a very coarse product to the downstream process. The variations in the underflow as a result of cavitation reduces the stability of the circuit.

An undesired increase in $SVOL$ can be countered by reducing SFW to maintain a constant $SVOL$. However, if the increase in $SVOL$ was as a result of increased solids discharge from the mill, the reduction in SFW will cause CFD to increase, PSE to decrease, and CPD to increase. The undesired increase in $SVOL$ can also be countered by increasing CFF, but this will cause PSE to increase. A controller must manage the loop interactions between $SVOL$ at the sump and PSE at the cyclone. In industrial plants SFW is used more frequently than CFF to control $SVOL$ (Wei and Craig 2009b).

Because the sump acts as a buffer between the mill and the cyclone, the available volume between overfill and underfill can be used to manipulate the desired CFD and CFF such that PSE is not affected. This requires a multi-variable controller capable of decoupling the dependencies between the variables (Hulbert *et al.* 1990, Coetzee *et al.* 2010, Le Roux, Olivier, Naidoo, Padhi and Craig 2016a).

2.1.2.3 Cyclone feed density (CFD)

The downstream separation process requires CPD to be within a specific range for correct operation. The CFD can be used to correct for CPD as they are directly proportional. However, CFD influences

both CPD and PSE. A low CFD increases PSE as less coarse ore report to the overflow. A high CFD has the opposite effect. At a critically high CFD, the underflow at the cyclone apex will change from a wide 'umbrella' spray shape to a high density rope. The high density rope impedes flow to the underflow, i.e. the cyclone underflow chokes. The cyclone then functions as a T-pipe where CFF splits between the under- and overflow with the majority of CFF reporting to the cyclone overflow. This causes PSE to drop and CPD to rise beyond acceptable limits. If CFD is too high, the cyclone underflow will choke and the entire CFF will report to the cyclone overflow. Therefore, the operating range of CFD is chosen based on system stability, avoiding roping conditions, and the PSE and CPD set-points.

As mentioned above, CFD can easily be manipulated by SFW. A more indirect change can be made by changing MFO as this changes the solids content in the circuit. Similarly, MIW can also be used to alter CFD. The order in which the manipulated variables were listed - SFW, MFO and MIW - is the order of preference for plants to control CFD (Wei and Craig 2009b).

2.1.2.4 Cyclone product particle size estimate (PSE) and cyclone product throughput (TP)

There are two general philosophies when controlling a grinding mill circuit:

- Maintain a specified PSE and maximize TP.
- Maintain a specified TP and minimize deviation of PSE from its desired set-point.

In the second control philosophy above where TP is fixed, it is tempting to mirror the first philosophy and write the secondary control objective aim as maximising PSE. However, grinding the ore too fine may result in unnecessary losses of valuable material in the tailings as many separation circuits cannot separate too fine material from gangue. It is also necessary to consider the energy cost of grinding material too fine. Although a desired PSE may be specified, the circuit may not necessarily be able to achieve it for the TP required. Naturally, there is a limit to the degree of coarseness in the slurry for the separation circuit to operate efficiently. In these cases it may be necessary to sacrifice TP simply to maintain a minimum allowable PSE.

At steady-state TP is equal to the MFO. The availability of ore from the mine provides a practical upper limit for TP and MFO. Also, the physical structure of the mill limits the volume of ore the mill can grind efficiently and provides an additional constraint on TP. The cyclone may also be a limiting factor of TP. Given the size of the spigot and vortex finder, the cyclone limits the maximum CPF. This also translates to an upper limit on CFF. Since the manufacturing, maintenance and operation costs associated with a cyclone are very low compared to a mill, a well-designed circuit should not allow the cyclone to dictate the circuit's throughput capacity.

At the cyclone PSE is a function of both CFD and CFF. The effect of a higher CFF is to reduce the cyclone cut size and consequently increase PSE. The capacity of the cyclone limits the maximum CFF that may be applied, and the lower bound of CFF is determined by the minimum cyclone inlet pressure allowed to keep the cyclone within its operable region. It is important that the pump at the sump discharge is correctly sized to achieve the desired CFF.

Although CFF and CFD can alter the cut-size of the cyclone, the cyclone does not break material. The achievable PSE depends on ψ. A significant increase in PSE is achieved through a significantly improved ψ. Manipulation of MFO can alter ψ, but the effect on J_T and TP should not be neglected. An increase in MFO increases J_T and the overall TP of the circuit, but it decreases ψ and therefore the achievable PSE. A lower J_T produced by a lower MFO is more conducive to producing a higher ψ and a better PSE, but it sacrifices TP and consequently reduces the mass of tradable final concentrate product.

2.1.3 Additional circuit variables

A control strategy should be informed by process measurements generally and readily available at industrial circuits. The survey of Wei and Craig (2009b) indicates that P_{mill}, JT, and CFD are commonly measured variables, whereas CPD and the ore feed size distribution are less commonly measured. The variables CPF, TP, ψ, Q, ρ_Q, and J_B are not explicitly included as real-time measured variables for any of the plants surveyed.

Assuming steady-state operation, CPF should be equal to the sum of $\frac{MFO}{\rho_O}$, MIW, and SFW, where ρ_O (t/m^3) is the density of the ore. Also, at steady-state TP should equal MFO by definition. Because

steady-state is rarely achieved by a circuit, real-time measurements of CPF and CPD are desirable to control the dynamics of the process. TP does not necessarily need to be measured in real-time as it can be inferred from measurements of CPF and CPD. Real-time measurements are difficult because of the amount of air in the cyclone overflow pipe. A possible solution would be to pass the cyclone overflow through a U-shaped pipe to create an airless volume of flowing slurry of which the flow-rate can be measured more easily.

Because of space restrictions at the discharge trommel of the mill, inclusion of flow, density and particle size instrumentation at the mill discharge is not yet a viable reality (Napier-Munn *et al.* 2005). Through careful planning and design of greenfield comminution circuits it should be possible to install existing flow, density and particle size measurement instrumentation technology at a mill discharge trommel. In the case where the mill discharges into a sump, both ρ_Q and Q can be back-calculated from a flow-balance around the sump if accurate measurements of $SVOL$, SFW, CFF, and CFD are available. In a similar manner, ψ can be back-calculated if a particle size measurement is made at either the outflow of the sump or at the overflow of the cyclone. However, the accuracy of the back-calculations are sensitive to errors in the measurements and in the modelling of the process units.

In general MIW is kept at a constant ratio of MFO to maintain ρ_Q within reasonable bounds. A very high density slurry will result in a non-flowing thick mud which reduces Q. On the other hand, a very high water content in the mill may cause a low-density slurry pool to form at the toe of the charge. The slurry pool absorbs the impact energy of falling material. This not only reduces P_{mill}, but also the rate at which fines are produced. If the discharge-grate conditions are such that no slurry pooling occurs, an increase in MIW will reduce the residence time of solids in the mill and increase Q. These conditions are typically a high fractional open area of the discharge grate, high relative radial position of the open area, and high relative radial position of the outermost grate aperture (Apelt *et al.* 2002a).

SAG mills are usually designed with a constant J_B in mind. Because accurate real-time measurement of J_B is generally not available, J_B is difficult to include in control schemes to manipulate ψ and Q. J_B can be approximated inferentially using models and measurements of P_{mill} or J_T (Apelt, Asprey and Thornhill 2001), assuming the model parameters are correctly fitted to process data. In practice, a linear proportionality between the rock volume and the energy required per tonne of steel balls consumed (κ_B) (kWh/t) is assumed, although this is not necessarily always the case. This assumption allows for the calculation of MFB to maintain an approximately constant J_B in terms of the ton of ore

milled. At steady-state this relates to MFB being a constant fraction of MFO.

A consistent ψ can be achieved through a high J_B (as in the case of a ball mill), but the heavy balls increase the power required to turn the mill and consequently increase the energy cost. κ_B depends on the ore characteristics, the mill liner type, the ball material, the ore grinding media hold-up, and J_B. A high J_B increases κ_B as there is more ball-ball and ball-liner contact rather than ball-ore contact. Although a low J_B reduces κ_B, it also reduces the grinding ability of the mill. For a very high mill rotational rate the balls may collide with exposed liners causing unnecessary liner wear and a higher κ_B.

The survey by Wei and Craig (2009b) indicates most plants desire better measurement instruments rather than more actuators. However, the one actuator most plants do desire is a variable speed drive to manipulate ϕ_c. Because this variable has a large impact on the operating region of a mill (Powell *et al.* 2009), care should be taken when changing ϕ_c. Viklund, Albertsson, Burstedt, Isaksson and Soderlund (2006) show how ϕ_c is used to change the grinding efficiency of a mill processing different types of ore. Since ϕ_c and P_{mill} are approximately linearly related, the maximum available power provides the upper limit for ϕ_c (Van der Westhuizen and Powell 2006).

2.1.4 Disturbances

The equilibrium of the mill is perturbed when MFO, the ore feed size distribution, or the ore feed hardness varies. The effect of the variations in these variables on the behaviour of the grinding mill requires time to decay. Although it is desirable to control all three of these disturbances, only MFO can be controlled. Any grinding mill circuit contends with the feed size distribution or the feed hardness as disturbances. These two disturbances vary both in the short and long term. If the disturbances are not rejected effectively by a control system, there is a lower recovery of valuable product in the downstream processes.

Variations in the feed size distribution will result in changes in the grinding media size distribution affecting the breakage characteristics in the mill. An increase in the size distribution of the feed ore means more rocks are available to assist with breakage, but the critical sized material in the mill responsible for fines production is reduced. Conversely, a reduction in the size distribution of the feed

ore reduce the availability of rocks for impact breakage (Valery and Morrell 1995). A manner of feed size distribution control is possible if run-of-mine ore is not used (Steyn 2011).

Variation of the hardness of the ore will cause P_{mill} to vary. An increase in the hardness of the ore means more energy is required to break ore in the mill, which means fines are produced at a slower rate. If the throughput is not altered through changes in MFO, an increase in the hardness of the ore can result in an increase in J_T. The increase in J_T requires more power to rotate the charge at the desired speed. If the hardness decreases, more fines can be produced at a quicker rate and J_T can potentially decrease. This decrease causes a reduction in P_{mill}. It should be noted that changes in MFO and feed hardness do not directly change P_{mill}. Rather, the feed hardness and MFO change J_T which consequently alters P_{mill} (Napier-Munn *et al.* 2005).

2.2 RELATIONSHIP BETWEEN COMMINUTION AND SEPARATION

Efficient comminution is essential for efficient separation of valuable elements and gangue. The degree of liberation by comminution refers to the percentage of minerals occurring as free particles in the ore in relation to the total mineral content. The desired degree of liberation depends on the ore properties and the separation method. If there is a pronounced difference in density or magnetic susceptibility between the particles and the gangue, separation is possible through gravimetric and magnetic separation even when valuable minerals are completely locked inside gangue. In the case of chemical leaching some part of the surface of a valuable component locked in gangue needs to be exposed to achieve separation. For effective separation through froth flotation the valuable particle's surface needs to be as large as possible, but if the particle is too small it is lost in the tailings. Although the low degree of liberation sufficient for magnetic or gravimetric separation is less energy intensive, more gangue may possibly report to the concentrate. Less gangue may report to the concentrate in the case of froth flotation and leaching, but the higher degree of liberation required is more energy intensive (Wills 2006). Throughout the rest of this study it is assumed separation is achieved through froth flotation as this is the most common separation technique employed.

The comminution circuit has only limited influence on the variables that determine the performance of a separation circuit. Laurila, Karesvuori and Tiili (2002) suggest a number of key variables to control the flotation process:

- Slurry feed-rate and density
- Particle size distribution, shape, and degree of mineral liberation
- Mineral concentrations in the feed, concentrate, and tailings
- Mineralogical composition of ore
- Electrochemical parameters
- Chemical reagents and their addition rate
- Cell pulp levels and air inlet flow-rates
- Froth properties and wash water rate

Variations in the content of valuable metals or minerals in the ore, *CPF*, *CPD*, and *PSE* are considered the main disturbances to the flotation circuit, of which only the latter three disturbances can be influenced by the comminution circuit. Should the comminution circuit be controlled efficiently, there should be minimal variations in *CPF*, *CPD*, and *PSE* (Shean and Cilliers 2011). Although this study assumes flotation as the method used for separation, the same disturbances apply to a gold leaching plant (Hodouin 2011).

An overview of stabilizing flotation control is given in Laurila *et al.* (2002). The review of Shean and Cilliers (2011) considers current and future trends in the instrumentation, base level control, advanced control and optimisation control of flotation circuits. The simulation studies of Desbiens, Hodouin, Najim and Flament (1994), Bergh and Yianatos (2011) and Putz and Cipriano (2015) use different types of process models to develop predictive controllers for flotation circuits. An example of an industrial application of a simple single-input/single-output generalized predictive controller is shown in Suichies, Leroux, Dechert and Trusiak (2000). As shown by Craig and Koch (2003), monetary benefits can be achieved by reducing the variation of the flotation level around a particular set-point. An economic performance comparison between a multi-variable controller and a single-loop proportional-integral (PI) controller at an industrial flotation circuit is given by Craig and Henning (2000). It is reported

that improved level control improved metal recovery by 1%, which translated to an increase in yearly revenue of approximately $ 830k. However, since the recovery is affected by a number of variables which are not under the control of the experimenter, a valid statistically significant comparison between controllers can only made after correct experimental design (Craig and Koch 2003).

2.2.1 Separator concentrate grade and recovery

The concentrate grade (γ_C) and recovery (Υ), depicted in Fig. 2.3, are accepted measures of the metallurgical performance of a mineral processing plant, but are not measures of the economic performance by themselves. Rather, the optimal economic operation of the separation process is determined by establishing the most profitable region on the grade-recovery curve. As shown in Fig. 2.4, if a very high γ_C is desired from the separation process, a large quantity of valuable metals will report to the tailings which reduces Υ. If a high Υ is required, more gangue may report to the final

Table 2.2. Nomenclature for mineral processing plant.

Parm	Unit	Description
C_{sep}	[t/h]	Separator concentrate mass flow-rate
T_{sep}	[t/h]	Separator tailings mass flow-rate
γ_{ROM}	[-]	Run-of-mine ore grade
γ_C	[-]	Separator concentrate grade
γ_T	[-]	Separator tailings grade
γ_{TP}	[-]	Comminution circuit throughput grade
Υ	[-]	Recovery
NSR	[$/h]	Net smelter return
$P_{\$p}$	[$/t]	Processing cost
$P_{\$t}$	[$/t]	Transportation cost
$P_{\$s}$	[$/t]	Cost of steel
$P_{\$v}$	[$/t]	Metal Price
$P_{\$W}$	[$/kWh]	Energy cost
κ_B	[kWh/t]	Energy required per tonne of steel balls consumed
κ_{1-6}	[-]	Constants

concentrate which reduces γ_C. The challenge is to improve both γ_C and Υ through process control (Wills 2006).

If only one metal is extracted from the separator concentrate, the material balance for the separation process at steady-state operation can be expressed as

$$F_{sep} = C_{sep} + T_{sep} \tag{2.1}$$

where F_{sep}, C_{sep}, and T_{sep} (t/h) are the separator feed, concentrate, and tailings respectively. The valuable concentrate balance is

$$\gamma_F F_{sep} = \gamma_C C_{sep} + \gamma_T T_{sep} \tag{2.2}$$

where γ_F and γ_T are the separator feed and tailing grades respectively. It is assumed the product of the comminution circuit is fed directly to the separation circuit, i.e. $TP = F_{sep}$ and $\gamma_{TP} = \gamma_F$ where γ_{TP} is the grade of the comminution circuit product. Using (2.1) and (2.2) it is possible to express Υ as

$$\Upsilon = \frac{\gamma_C C_{sep}}{\gamma_{TP} TP} = \frac{\gamma_C (\gamma_{TP} - \gamma_T)}{\gamma_{TP} (\gamma_C - \gamma_T)}. \tag{2.3}$$

The nomenclature is shown in Table 2.2.

2.2.2 Effect of cyclone product flow-rate (*CPF*) and density (*CPD*) on recovery-grade curve

The throughput capacity of the flotation plant should be designed to match the throughput capacity of the milling circuit. Assuming the cyclone product of the milling circuit is fed directly to the flotation circuit, variations in *CPF* cause disturbances in the slurry levels of the flotation cells. The flotation circuit cell capacity therefore constrains *CPF*. Given adequate flotation control and no violation of the *CPF* constraint, it is assumed *CPF* has negligible effect on the recovery-grade relationship of the flotation circuit.

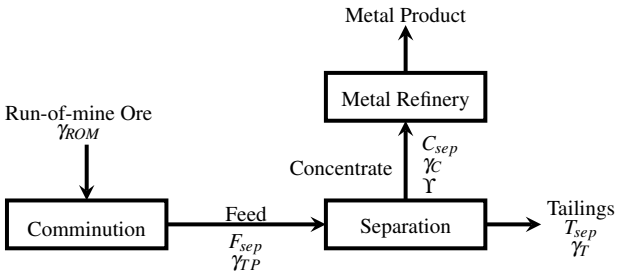

Figure 2.3. The flow-rates and grades of the various streams in the mineral processing plant.

CPD describes the split between water and solids content in *CPF*. Increased dilution in the flotation feed lowers the mean residence time of particles in the flotation circuits. This disturbance can be handled if the capacity of the flotation circuit is large enough, but if the disturbance is too large it may require the use of a dewatering process prior to flotation (Sosa-Blanco *et al.* 2000). If maintained within constraints, it is assumed that under good flotation circuit control *CPD* has negligible effect on the recovery-grade relationship of the flotation circuit.

2.2.3 Effect of cyclone product particle size estimate (*PSE*) on recovery-grade curve

The Υ as a function of particle size for a flotation circuit is shown in Fig. 2.5. The particle size should not be confused with *PSE*, where the former is measured in millimeter and the latter represents the percentage of ore passing a given size. The particles in the flotation feed are roughly divided into three sizes: very small, intermediate and large. Because the very small particles have low momentum and a low rate of collision with bubbles, the probability of adhesion and subsequent flotation is reduced. With an increase in particle size, the degree of hydrophobicity necessary for a high level of flotation increases. For large particles, the rapid consumption of reagents by smaller particles leads to less complete surface coverage of the large particles and results in less floatable particles. The relationship between Υ and the ore particle size is relatively independent of moderate changes in *PSE*, *CPD*, and the mineral content (Trahar 1981).

From Fig. 2.5 it is clear that the aim of a comminution circuit is to maintain a narrow distribution of intermediately sized particles to maximise the separation capability through flotation. Grinding material

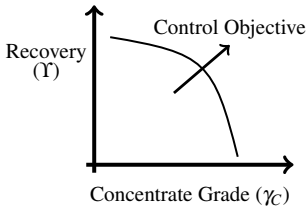

Figure 2.4. Typical concentrate grade (γ_C) and concentrate recovery (Υ) curve.

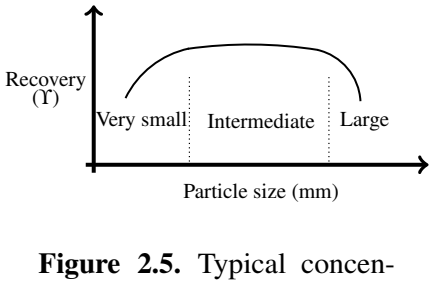

Figure 2.5. Typical concentrate recovery (Υ) of a separation circuit as a function of the flotation feed particle size distribution.

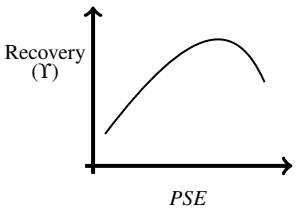

Figure 2.6. Concentrate recovery (Υ) as a function of the particle size estimate (*PSE*).

too fine not only reduces flotation capability, it also translates to unnecessary energy expenditure to achieve the high grind. Grinding material too coarse drastically reduces separation capabilities. In the case where *PSE* deviates to above/below set-point (overgrind/undergrind), the impact is to decrease/increase γ_C and increase/decrease Υ of the separation circuit. If the separation plant operates at the optimum recovery-grade ratio in terms of the refinery return, any deviation in *PSE* reduces the return from selling the concentrate to the smelter (McIvor and Finch 1991).

As shown in Fig. 2.6, the relationship between Υ and *PSE* is a simple second order polynomial (Wei and Craig 2009a). Although flotation is considered here, a similar relationship between Υ and *PSE* as shown in Fig. 2.6 is seen for leaching plants (Craig *et al.* 1992). The corresponding γ_C can be determined from the grade-recovery relationship depicted in Fig. 2.4. Therefore, both Υ and γ_C are empirically defined in terms of *PSE* as

$$\Upsilon(PSE) = \kappa_1 \cdot (PSE)^2 + \kappa_2 \cdot PSE + \kappa_3 \tag{2.4}$$

$$\gamma_C(PSE) = \frac{\kappa_4}{\Upsilon(PSE) - \kappa_5} + \kappa_6 \quad ; \quad \Upsilon(PSE) < \kappa_5 \tag{2.5}$$

where the constant parameters $\kappa_{1,2,\ldots 6}$ can be fitted to process data.

2.3 MINERAL PROCESSING PLANT REVENUE

A mineral processing plant generates revenue by selling the separator concentrate to a smelter. The revenue should cover the mineral processing cost of comminution and separation for the plant to be economically viable. The revenue is approximated as

$$\text{Mineral Processing Revenue} = \text{Net Smelter Return} - (\text{Comminution Cost} + \text{Separation Cost}) \tag{2.6}$$

2.3.1 Net smelter return

The price a smelter would be willing to pay for a concentrate depends on the metal recovery, metal prices, operating costs, capacity constraints, deleterious elements, transport issues, metal premiums and discounts, types of flotation concentrates, processing capital costs, metal grades etc. A thorough comprehension and appreciation of market conditions, the characteristics of the concentrate, and the abilities of potential buyers to process the concentrate is required to negotiate the best possible contract

between the smelter and the mineral processing plant (Cramer 2008). Although simplified, a basic contract may stipulate the items listed below:

- Valuation $P_{\$v}$ (\$/t): pay the lowest market price per ton of metal recoverable from the concentrate
- Transport $P_{\$t}$ (\$/t): cost for transport per ton of concentrate between mineral processing plant and refinery
- Process $P_{\$p}$ (\$/t): cost per ton of concentrate processed by the smelter

The net smelter return (NSR) (\$/h) can therefore be expressed as

$$\begin{aligned} \text{NSR} &= \text{Concentrate Metal Value} && - && (\text{Transport cost} + \text{Process cost}) \\ &= P_{\$v} \cdot (\text{Concentrate Metal Mass}) && - && \left(P_{\$t} + P_{\$p}\right) \cdot (\text{Concentrate Total Mass}) \\ &= P_{\$v} \cdot C_{sep} \cdot \gamma_C && - && \left(P_{\$t} + P_{\$p}\right) \cdot C_{sep}. \end{aligned} \tag{2.7}$$

It is assumed the metal content of the ore fed to the separation process is equal to the metal content of the unprocessed run-of-mine ore fed to the comminution circuit. In other words, the grade of the run-of-mine ore fed to the comminution circuit (γ_{ROM}), also known as the mill-head grade, is equal to the grade of the separator feed (γ_{TP}). Using (2.3) to (2.5), NSR in (2.7) can be expressed in terms of Υ, γ_{ROM}, γ_C and PSE as

$$\text{NSR} = P_{\$v} \cdot \Upsilon(PSE) \cdot \gamma_{ROM} \cdot TP - \left(P_{\$t} + P_{\$p}\right) \cdot \Upsilon(PSE) \frac{\gamma_{ROM}}{\gamma_C(PSE)} \cdot TP. \tag{2.8}$$

Given possible improvements in the separation of gangue from valuable minerals, a company may decide to reprocess tailings. Because the ore has already been broken, there is no energy cost if the particle size distribution is already within specification (Wills 2006). The economic value in the tailings is given by

$$\text{Tailing Value} = P_{\$v} \cdot (1 - \Upsilon(PSE)) \cdot \gamma_{ROM} \cdot TP. \tag{2.9}$$

The NSR depends on the trade-off between Υ and γ_C as illustrated by Fig. 2.4. A high γ_C is less costly to smelt, but the lower Υ yields a lower return on the final product. A low γ_C with high Υ is costly to smelt but returns more final product. If the metal price is high, a low γ_C can be targeted by the separation circuit to improve Υ and increase return. For the low γ_C and high Υ, the comminution circuit may need to run at a constant and high TP at the cost of a consistently correct ψ. If the metal price decreases, the separation circuit may target a higher γ_C at the cost of Υ. In this case the comminution

circuit may need to focus on achieving a correct and constant ψ while sacrificing a consistently high TP. In the case of a high grade ore, the comminution circuit may aim to maintain a consistently correct ψ while maximising TP to extract the maximum value. If a low grade ore is processed, the aim may be to operate at a constantly high TP while attempting to maintain ψ as close as possible to its desired value.

2.3.2 Comminution and separation cost

The cost of comminution accounts for approximately 50% of the operational cost of the mineral processing plant, followed by the cost of separation at less than 20% of the operational cost (Joe 1979, Wills 2006). The main operating cost for the separation circuit is the cost of reagents added to separate gangue and minerals. A constant separation process cost is assumed as the economics of the separation circuit falls outside the scope of this study. These costs can be included if a sufficient model of the flotation process is available (Seppälä, Sorsa, Paavola, Ruuska, Remes, Kumar, Lamberg and Leiviskä 2016). The high comminution cost is due to the high power required to turn the grinding mill (Matthews and Craig 2013). The consumption of steel balls as grinding media is the second largest operational cost of comminution, but is only a small fraction of the milling power cost. The pumping energy cost in the comminution circuit itself is negligible compared to the power used by the mill (Halbe and Smolik 2002). If $P_{\$W}$ (\$/kWh) is the cost of energy, and $P_{\$s}$ (\$/t) is the cost of steel balls, the comminution circuit operating cost (\$/h) can be approximated as (Munoz and Cipriano 1999)

$$\text{Comminution cost} = P_{mill} \cdot (P_{\$W} + P_{\$s}/\kappa_B)\,. \tag{2.10}$$

2.4 CONCLUSION

This chapter aims to formulate the economic impact of a comminution circuit's product on the mineral processing plant revenue. This provides a mechanism to define the operational goals of the comminution circuit in terms of the economic objectives of the mineral processing plant. The revenue of the mineral processing plant is defined in terms of the output variables of the grinding mill circuit by relating the grade and recovery of the separator concentrate to the product quality and quantity of the comminution circuit. It is assumed the control of the separation circuit is such that a constant functional description can be used to relate the comminution circuit's output to the separation circuit's output. Once the operational goals of the comminution circuit are defined, a sufficient control structure

needs to be constructed for the comminution circuit to achieve these goals. Such a control structure is proposed in the next chapter.

CHAPTER 3 PLANT-WIDE CONTROL

Reflecting on chemical process control of the 1970's, the seminal review article by Foss (1973) deplored the gap which existed between the theory of process control and its application. The significant theoretical advances made during that time in optimal control and state estimation were successfully translated for application in the aerospace industry, but these advances were not yet translatable to the chemical process industry. Kestenbaum, Shinnar and Thau (1976) demonstrated how a classical PID controller applied to a chemical process performed better than prevalent optimisation-based design methodologies in the presence of model uncertainties, unmeasured process disturbances, and changing process parameters. The main thesis of Foss (1973) and Kestenbaum *et al.* (1976) was that the theoretician and not the practitioner was responsible for closing the gap between control theory and the more stringent and rigorous demands of industrial process control. Furthermore, apart from addressing issues such as inclusion of process dynamics and uncertainty in the controller design, the main and most critical issue for theoreticians and practitioners to address for industrial processes was the configuration of the control system. For successful control of any plant, they stated that a systematic framework was required to guide qualitative and quantitative decisions regarding the variables to measure, manipulate, and control (control objective), as well as the relationship between these variables to achieve a specific control objective (control structure) (Stephanopoulos 2014).

The unit-based approach of Umeda, Kuriyama and Ichidawa (1978) decomposes the plant into individual units of operation, generates a control structure for each unit, combines the structures, and then eliminates possible conflicts in the combined control structure. However, as the size of the plant grows, this procedure becomes impractical given the number of conflicts which arise. Also, it does not provide a framework to capture the broad range of objectives for the plant as a whole.

As a response to the need for systematic control structure configurations which considers the plant-wide

objectives, Morari, Arkun and Stephanopoulos (1980) cast the problem in a multi-layer multi-echelon decomposition framework. In the vertical, multi-layer decomposition, the control tasks are decomposed into a series of control tasks with different frequencies. This is similar to the common hierarchical separation of control tasks starting with base layer control, supervisory control, optimisation, and process planning (Seborg, Edgar and Mellichamp 2004). The use of hierarchy representations reduces the complexity of the problem by allowing the designer to address process goals within different ranges of a time-horizon. In Morari *et al.* (1980), the scope of each layer is determined by a series of quantitative criteria reflecting the sensitivities of the operating objectives to various variables. In the horizontal, multi-echelon decomposition, the control tasks are organized according to different segments of the process. This is based on the sensitivity conveyed by Lagrangian multipliers associated with the interconnections among process sub-systems. The structure of these hierarchical control tasks provide the boundaries of regulatory control tasks (Ng and Stephanopoulos 1996, Stephanopoulos and Ng 2000).

Rather than following a mathematically orientated approach as in Morari *et al.* (1980), a process orientated approach to control structure configuration is proposed by Luyben, Tyreus and Luyben (1997). Their plant-wide procedure, specifically for chemical process plants, is listed below:

1. Establish control objectives, i.e. determine the controlled variables.

2. Determine the control degrees of freedom by counting the number of independent valves.

3. Establish energy inventory control to remove the exothermic heats of reactions and to prevent propagation of thermal disturbances.

4. Set the production rate using a variable which can increase the reaction rate in the reactor.

5. Ensure product quality and handle safety, operational and environmental constraints.

6. Do inventory control and fix the flow in liquid recycle loops.

7. Check component balances, and return to Step 4 if required.

8. Control individual unit operations.

9. Use the remaining control degrees of freedom to optimise economics or improve dynamic controllability.

The rationale for the order of these steps is as follows: Steps 1 and 2 determine the objectives and the available degrees of freedom. Since the methods of heat removal are intrinsic to heat reactor design, and reactors are considered the heart of any process, Step 3 ensures heat generated by an exothermic reaction is efficiently dissipated. Step 4 determines where the production rate is set. Step 5, where product quality is set, follows Step 4 as the control of product quality is of higher priority than inventory control in Step 6. Variability in inventories is not as critical as ensuring the variability in product quality is as small as possible. After the total process mass balance is satisfied, the individual component balances can be checked in Step 7. If in Step 7 it is evident the choice of throughput manipulator is invalid given other plant-wide control considerations, it is necessary to return to Step 4. The plant-wide control issues are accomplished when Step 7 is completed, such that Step 8 can be used to improve performance of unit operations, and Step 9 can be used to address higher level concerns.

From a review of the mathematically and process orientated approaches to plant-wide control, Larsson and Skogestad (2000) proposed a plant-wide control design framework using elements of both these approaches. The framework, which was expanded by Skogestad (2004), distinguishes between economic control and regulatory control by dividing structural decisions into two parts: a top-down and a bottom-up analysis. The aim of the top-down analysis is to define an economic supervisory control structure that achieves close-to-optimal steady-state economic operation (Le Roux, Skogestad and Craig 2016b). The aim of the bottom-up analysis is to define a stable and robust regulatory control structure capable of operating under the conditions imposed by the economic supervisory layer. In comparison to Luyben *et al.* (1997), Skogestad (2004) combines Steps 1 and 9 since the selection of controlled variables should depend on the plant economics. The procedure is given below:

1. Top-down analysis (to address steady-state operation)

   (a) Define the operational economic objective, and determine the steady-state degrees of freedom.

(b) Determine the optimal steady-state operation.

(c) Select the primary controlled variables influencing the economic cost function.

(d) Select the variable responsible for manipulating the process throughput.

2. Bottom-up analysis (to address dynamic operation)

(a) Select the regulatory control structure.

(b) Select the supervisory control structure.

(c) Select the the real-time optimisation structure.

(Additional guidelines on decisions specific to each step are provided by Minasidis, Skogestad and Kaistha (2015).)

The plant-wide control design framework of Skogestad (2004) is applied by Downs and Skogestad (2011) to industrial processes operated by the Eastman Chemical Company. It is noted that since the dawn of the holistic approach to process control design, the variety of frameworks to address the design problem illustrates the difficulty in finding a unified approach. At least from the industrial perspective of J. Downs, one of the original proposers of the "Tennessee Eastman challenge problem" (Downs and Vogel 1993), the procedure outlined by Skogestad (2004) is adequate to design a controller capable of optimising the process economics of a plant (Downs and Skogestad 2011).

The aim of this chapter is to construct a control strategy for a comminution circuit to achieve operational goals determined by the economic objectives of the larger mineral processing plant. The control strategy is developed according to the plant-wide control design procedure outlined by Skogestad (2004). The chapter is organised according to the top-down and bottom-up analysis steps listed above.

3.1 TOP DOWN ANALYSIS

3.1.1 Operational economic objective

The questions to answer in this step are: what is the scalar cost function which defines the economic objective of operation, and what are the available dynamic and steady-state degrees of freedom to achieve this economic objective? Given the mineral processing plant economic objective defined in (2.6), the comminution process economic scalar cost function is defined in terms of (2.8) and (2.10) as

$$J_{comm} = \Upsilon(PSE) \cdot \gamma_{ROM} \cdot TP \cdot \left(P_{\$v} - \frac{P_{\$t} + P_{\$p}}{\gamma_C(PSE)} \right) - P_{mill} \cdot \left(P_{\$W} + \frac{P_{\$s}}{\kappa_B} \right). \tag{3.1}$$

The cost function in (3.1) is constrained by downstream operation requirements and by operating limits.

The economics of the plant are primarily determined by its steady-state behaviour. In general the steady-state degrees of freedom are the same as the economic degrees of freedom. Identifying the dynamic degrees of freedom is generally easier than identifying the economic (steady-state) degrees of freedom. However, it is the number of economic degrees of freedom (N_{SS}) and not the variables themselves which is important to determine. N_{SS} gives the number of controlled variables to be selected in the third step of the top-down analysis (Skogestad 2012).

N_{SS} is determined by subtracting the number of manipulated and controlled variables with no economic steady-state effect (N_0) from the number of dynamic degrees of freedom (N_D). Since there are six manipulated variables, it means $N_D = 6$:

- Mill ore feed-rate (MFO)
- Mill inlet water flow-rate (MIW)
- Mill ball feed-rate (MFB)
- Sump feed water flow-rate (SFW)

- Cyclone feed flow-rate (CFF)

- Mill rotational speed (ϕ_c)

The liquid levels in tanks generally form part of the variables with no economic steady-state effect. There are four levels throughout the circuit to consider:

- Total charge filling in the mill (J_T)

- Ball filling in the mill (J_B)

- Mill slurry volume

- Sump slurry volume ($SVOL$)

As discussed in Section 2.1, J_T, J_B and the mill slurry volume can all affect TP, PSE and P_{mill}. Therefore, these three levels in the mill remain crucial steady-state degrees of freedom to define. At the sump, $SVOL$ has no economic steady-state effect and can be controlled through either SFW or CFF. This means $N_0 = 1$. Consequently, there are five steady-state degrees of freedom

$$N_{SS} = N_D - N_0 = 6 - 1 = 5.$$

3.1.2 Optimal steady-state operation: Grindcurves

Once the cost function is identified, the question is what are the operational conditions for optimal steady-state operation? In other words, how should the set-points be chosen for optimal circuit operation? The optimal steady-state of operation for the single-stage grinding mill circuit is primarily determined by the operating performance of the mill. The main mill performance indicators are P_{mill}, Q_S and ψ. The quazi-static curves of P_{mill}, Q_S and ψ as functions of J_T and ϕ_c are called grindcurves and can be used to determine the optimal steady-state operating region of a mill (Van der Westhuizen and Powell 2006, Powell *et al.* 2009).

Van der Westhuizen and Powell (2006) developed grindcurves of an industrial open-circuit SAG mill with a ball filling of 7.9%. These grindcurves were developed assuming J_B and ρ_Q remained constant for all equilibrium conditions produced by different combinations of J_T and ϕ_c. It is possible to maintain J_B relatively constant by setting MFB at a constant ratio of MFO. Similarly, MIW is generally set at a constant ratio of MFO to maintain a constant ρ_Q. Grindcurves should not necessarily be defined only in terms of two degrees of freedom: J_T and ϕ_c. Adequate manipulation of J_B and ρ_Q within system constraints can allow the grindcurves to be defined in terms of four degrees of freedom.

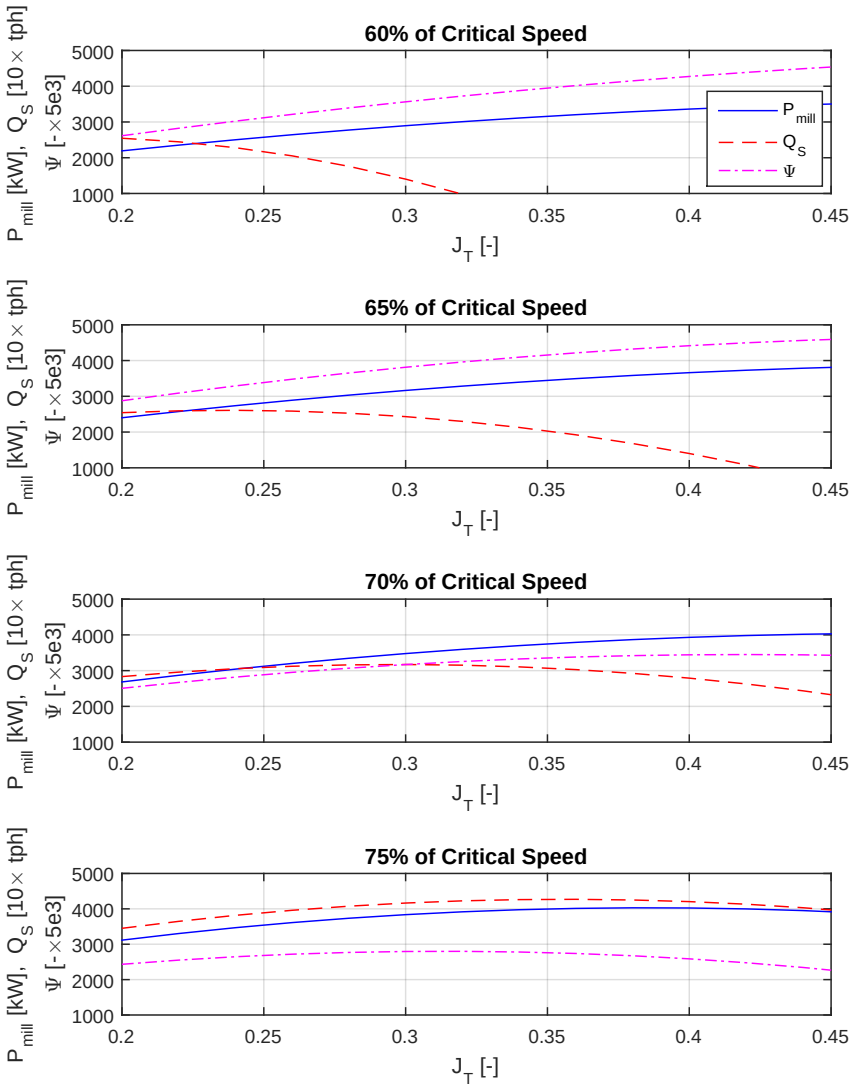

Figure 3.1. Mill grindcurves for an open circuit SAG mill. (Re-created from data in Van der Westhuizen and Powell (2006).)

Fig. 3.1 illustrates the general parabolic shape of the grindcurves in Van der Westhuizen and Powell (2006) for J_T in the range of 0.18 to 0.45 and ϕ_c in the range of 0.60 to 0.75. Certain conclusions can be drawn from the grindcurves:

- The peaks of Q_S and P_{mill} do not coincide.
- Q_S increases with ϕ_c.
- The curve shapes are dramatically changed by ϕ_c.
- The peak values change according to changes in ϕ_c.
- Q_S becomes coarser as ϕ_c increases, implying ψ reduces as ϕ_c increases.

The grindcurves provided by Van der Westhuizen and Powell (2006) are for an open-circuit grinding mill. If the circuit is closed, the grindcurve peaks move slightly relative to the open-circuit case, but the curve shapes do not change (Powell *et al.* 2009). Although not labelled as such, Craig *et al.* (1992) developed grindcurves for a closed-circuit single-stage grinding mill at a single fixed speed. The circuit was controlled by the multi-variable Inverse Nyquist Array controller of Hulbert *et al.* (1990). The steady-state data showed a clear parabolic relationship between TP and J_T. The peak of TP occurred at a lower J_T as the peak of P_{mill}. Therefore, the results of the open-circuit grindcurves can be extrapolated to the closed-circuit case. Also, it can be assumed that for the closed-circuit case the cyclone maintains a consistent cut-size and water recovery to underflow, and that the variations in CFF to maintain a consistent cut-size and water recovery has a negligible effect on the grindcurves. If the cyclone maintains a consistent cut-size and recovery, the following relations apply

$$\begin{aligned} TP &= \kappa_{TP} Q_S \\ PSE &= \kappa_{PSE} \psi \end{aligned} \tag{3.2}$$

where κ_{TP} and κ_{PSE} are constants. Therefore, the grindcurves in terms of J_T and ϕ_c can be used to define the circuit's performance in terms of PSE and TP.

3.1.2.1 Description of grindcurves in terms of J_T and ϕ_c

The data in Table 3.1 as provided by Van der Westhuizen and Powell (2006) can be used to construct functions of the mill performance indicators, P_{mill}, Q_S and ψ, where J_T and ϕ_c are independent variables. As noted by (Powell *et al.* 2009), second order polynomials are best suited to fit the data where ϕ_c is fixed and J_T is an independent variable. Therefore, the grindcurves as functions of J_T for a fixed ϕ_c are defined as

$$Y = \kappa_a J_T^2 + \kappa_b J_T + \kappa_c \tag{3.3}$$

where $Y = [P_{mill}, Q_S, \psi]^T$, κ_a and κ_b are vector constants, and $\kappa_c = [P_{NL}, 0, 0]$. It is assumed that at zero mill filling both Q_S and ψ is equal to zero and P_{mill} is equal to the no-load power draw (P_{NL}). Table 3.1 provides the location of the grindcurve peaks for different ϕ_c. Therefore, for a specific ϕ_c the constants can be written as

$$\kappa_a = \frac{Y_{peak}}{J_{T_{peak}}^2} \tag{3.4a}$$

$$\kappa_b = -2\kappa_a J_{T_{peak}} \tag{3.4b}$$

where Y_{peak} is the peak value of the performance indicator, and $J_{T_{peak}}$ is the value of J_T at Y_{peak}. Since the peaks are given in Table 3.1 in terms of ϕ_c, the peaks can be fitted to low order polynomials with ϕ_c as independent variable.

$$Y_{peak} = f(\phi_c) \tag{3.5a}$$

$$J_{T_{peak}} = g(\phi_c) \tag{3.5b}$$

Table 3.1. Data of grindcurve peaks from Van der Westhuizen and Powell (2006). (* - indicates peaks that are extrapolated to above 50% mill filling.)

Mill Speed	Power Peak		Discharge Peak		Grind Peak	
ϕ_c	J_T	P_{mill}	J_T	Q_S	J_T	ψ
0.60	0.54*	3603*	0.18	261	0.63*	1.00*
0.65	0.55*	3931*	0.23	252	0.58*	0.94*
0.70	0.47	4028	0.31	326	0.37	0.69
0.75	0.39	4037	0.35	424	0.33	0.56

In summary, ϕ_c is used in (3.5) to define the peaks of the performance indicators, the peak locations in turn define the vector constants in (3.4), and the vector constants define the grindcurves in (3.3). Using the data in Table 3.1, the mill performance indicators as functions of J_T and ϕ_c are shown in Figs. 3.2 to 3.4. A brief discussion of the surface shapes is provided below.

3.1.2.2 Power (P_{mill}) for different mill fillings (J_T) and speeds (ϕ_c)

Since P_{mill} is an indication of the rate of kinetic and potential energy imparted to the charge, P_{mill} is determined by J_T. An increase in J_T means an increase in mass in the mill which allows more charge to absorb the energy available from the rotating mill. This increase in J_T results in a higher P_{mill}. At very high J_T the movement of the centre of mass of the charge towards the centre of the mill dominates the increase in mass, which reduces the torque of the mill. At the same time, the increase in J_T lifts the toe of the charge which reduces the potential energy imparted to the charge. Therefore, P_{mill} peaks somewhere between low and high J_T.

As ϕ_c increases, more kinetic and potential energy is imparted to the charge and results in a higher P_{mill}. A second order polynomial passing through the origin can be used to describe the relationship between P_{mill} and J_T. For higher ϕ_c, the curve between P_{mill} and J_T is steeper and the peaks are more pronounced. The peaks move from higher to lower J_T as ϕ_c is increased (Van der Westhuizen and

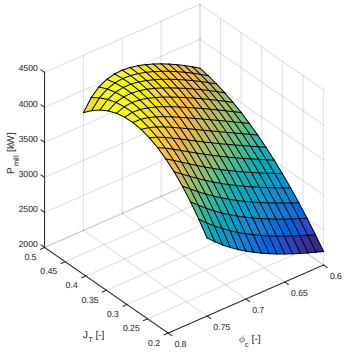

Figure 3.2. Mill power (P_{mill}) as a function of mill filling (J_T) and mill speed (ϕ_c).

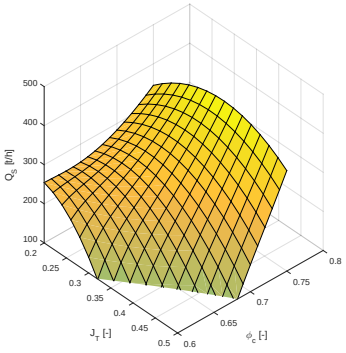

Figure 3.3. Mill solids discharge (Q_S) as a function of mill filling (J_T) and mill speed (ϕ_c).

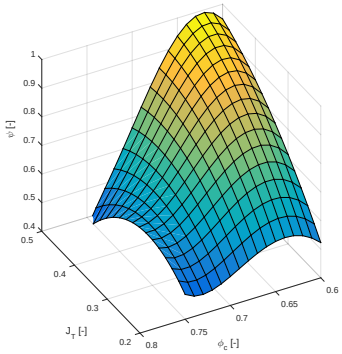

Figure 3.4. Mill grind (ψ) as a function of mill filling (J_T) and mill speed (ϕ_c).

Powell 2006).

The generally held belief by the mineral processing industry is that ψ is maximised when P_{mill} is at its maximum (Stanley 1987). The rationale is that since P_{mill} is an indication of the rate of energy imparted to the charge, the maximum breakage of ore occurs at maximum P_{mill}. Plants may therefore decide to operate at the point where maximum P_{mill} occurs. However, as seen from the grindcurves, maximum ψ and Q_S does not necessarily coincide with maximum P_{mill}. In most cases the maximum of P_{mill} is reached only after the peak of Q_S and ψ is passed (Borell, Backstrom and Soderberg 1996). If the difference between the peaks of Q_S and P_{mill} in terms of J_T is very small, a power-peak-seeking controller can be used as a relatively simple solution to increase circuit throughput (Craig *et al.* 1992). Otherwise, if the difference is significant, operating at maximum P_{mill} may not be the best operating strategy.

3.1.2.3 Solids discharge rate (Q_S) for different mill fillings (J_T) and speeds (ϕ_c)

If there are no discharge limitations or slurry pooling, Q_S is determined by the rate of breakage of coarse sizes to below the discharge grate size. The breakage rate of coarse material ($>$ 10 mm) decreases as the mill filling J_T increases. Because the coarser material is broken by impact breakage, the increase in J_T lifts the toe of the charge and reduces the drop height from shoulder to toe. However, the mass breakage rate, which is the total mass of coarse ore multiplied by the coarse ore breakage rate parameter, determines the value of Q_S. As J_T is increased from a low level, the coarse ore breakage rate parameter will decrease slower than the mass of coarse ore will increase. The cumulative effect is therefore a higher Q_S. At high J_T the coarse ore breakage rate constant will decrease faster than the mass of coarse ore will increase and the consequent effect is a reduced Q_S. A peak for Q_S occurs between these two effects.

For J_T in the range 20%-40%, moving from $\phi_c = 65\%$ to $\phi_c = 75\%$ results in a dramatically higher Q_S. Changes in ϕ_c below 65% or above 75% does not have the same large influence. The Q_S peak shifts to higher J_T as ϕ_c increases. This is opposite to the P_{mill} peaks which move to lower J_T as ϕ_c increases. Similar to power curves, the Q_S curves become steeper as ϕ_c increases. Mill control at higher ϕ_c becomes more difficult as a small change in J_T can have a large impact on Q_S.

3.1.2.4 Grind (ψ) for different mill fillings (J_T) and speeds (ϕ_c)

The production of fines is influenced by the breakage rate constant of fines and the slurry content of the mill. Theoretically, for an increased J_T the breakage rate of fines and the solids content in the slurry both increase. Therefore, the total mass breakage rate, which is the product of the slurry solids content and the fines breakage rate, increases as J_T increases.

Although a higher ϕ_c results in an increased Q_S and P_{mill}, a higher ϕ_c also results in a coarser product. Reducing ϕ_c will improve ψ, but this will sacrifice Q_S. Whereas the P_{mill} and Q_S curves are steeper for a higher ϕ_c, the ψ becomes less influenced by J_T as ϕ_c increases. The ψ is expected to increase as P_{mill} increases and Q_S reduces. As seen in Fig. 3.1, the larger the difference between the P_{mill} and Q_S curves at a high J_T, the finer the product will be.

The findings above may suggest that for a finer product the mill must be run at a lower ϕ_c. However, because of the consequent reduction in Q_S, a lower ϕ_c may not increase the discharge rate of fines. The discharge rate of fines is highest at a high ϕ_c even though ψ is lower. (In other words, at high ϕ_c the percentage of material passing 75 μm may be lower, but the tonnes per hour of material passing 75 μm is higher.) The ϕ_c should thus be chosen depending on whether Q_S or ψ is a priority.

3.1.3 Primary (economic) controlled variables

Once optimal operation is defined, the question is which five economic (steady-state) degrees of freedom should be controlled to maintain optimal operation? These five variables are listed below, if the grindcurves are used to define the optimal circuit operation:

- Total charge filling in the mill (J_T)
- Ball filling in the mill (J_B)
- Mill slurry density (ρ_Q)
- Particle size estimate (PSE)

- Throughput (TP)

In accordance with the assumptions made in the development of the grindcurves, J_B, ρ_Q, and the cyclone's cut are to be kept constant. Consequently, it is suggested to control J_T as this determines Q_S and ψ which in turn determine TP and PSE. However, Q_S and ψ are also dependent on ϕ_c. The cost function in (3.1) should therefore be maximised with respect to J_T and ϕ_c with the grindcurves as equality constraints.

The prominent economic controlled variable is therefore J_T. This is confirmed by the study of Borell *et al.* (1996) were a heuristic on/off supervisory controller to maximize the throughput of an industrial open-circuit AG mill was applied. In their case, J_T was adjusted using MFO to optimise the mill power usage for improved Q_S.

The maximum of the cost function in (3.1) gives the desired PSE as functions of J_T and ϕ_c. If the mill is disturbed through ore hardness or feed size distribution variations, it will affect PSE. These disturbances can be rejected to some extent by adjusting CFF as long as the sump does not run dry or overflow. This is in accordance with the demand to keep the cut-size of the cyclone constant for the grindcurves to be applicable.

Because TP passes through a maximum as given by the grindcurves, it cannot be selected as a controlled variable. Setting TP at a too high value may lead to an infeasible operating condition. Rather, a manipulator of TP should be selected and its value chosen based on the operating condition that produces the maximum of the cost function in (3.1).

3.1.4 Location of throughput manipulator

The location of the manipulator of TP is a dynamic issue, but it has significant economic implications. There are three options to manipulate throughput: MFO, CFF, or ϕ_c. Since TP has a maximum as given by the grindcurves, using MFO as manipulator for TP may produce unfeasible operation. Skogestad (2004) suggests locating the throughput manipulator close to the bottleneck of the process, and in the case of a recycle stream, the throughput manipulator should be located within the recycle loop. Within the loop, either the mill capacity or the cyclone capacity can constrain TP. Ideally the

constraint should be determined by the mill as the capacity of cyclones are relatively inexpensive and easy to adapt. Therefore, the mill is the bottle-neck of the process. For this reason, ϕ_c and not CFF is chosen as the variable responsible for manipulating the throughput. Also, the influence of ϕ_c on the production of solids in the mill is much greater than that of CFF.

The cost function in (3.1) suggests the overall profit can be increased if TP is increased. However, the inverse relationship between TP and PSE as illustrated by Fig. 3.5 may negate any potential benefits from the increase in TP (Bauer and Craig 2008). The use of ϕ_c as manipulated variable provides a degree of leverage to increase TP without sacrificing PSE (Le Roux *et al.* 2016a, Viklund *et al.* 2006). As seen from the grindcurves, as ϕ_c increases the peak of Q_S (or equivalently the peak of TP) increases, and the peak of ψ (or equivalently the peak of PSE) reduces. Thus, optimisation of (3.1) with respect to ϕ_c with the grindcurves as constraint equations already considers the inverse relationship between PSE and TP.

3.1.5 Summary

In summary, the cost function in (3.1) indicates the economic objective of the grinding circuit with reference to the final product produced by the mineral processing plant. The cost function is defined in terms of the product quality (i.e. PSE) and quantity (i.e. TP) of the circuit. Both PSE and TP, performance measures of the circuit, can be related to the mill's performance measures, Q_S and ψ, if the cyclone is regarded as a classification device with a constant cut. Since grindcurves describe Q_S and ψ as functions of J_T and ϕ_c, the revenue of the plant can be expressed as a function of J_T and ϕ_c. The primary economic controlled variable is therefore J_T, with ϕ_c the manipulator of TP.

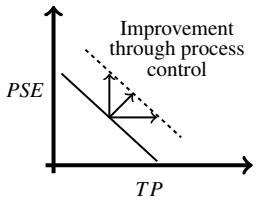

Figure 3.5. Relationship between throughput (TP) and particle size estimate (PSE).

3.2 BOTTOM-UP ANALYSIS

3.2.1 Regulatory control

The aim of the regulatory layer is to stabilize the plant generally through simple single-loop PID controllers. The regulatory layer should ensure that the plant does not drift too far away from its nominal operating point and that the supervisory layer can handle disturbances on the primary plant outputs (Skogestad 2004). In light of the top-down analysis in the previous section, the control scheme listed below is proposed to pair the six available manipulated variables with the control variables to stabilise the circuit:

- ϕ_c is set by the operator to achieve the desired TP.
- MFO is used to control J_T.
- MIW is used to maintain a constant ρ_Q.
- MFB is used to maintain a constant J_B.
- SFW is used to reject disturbances in PSE.
- CFF is used to control $SVOL$.

The slow integrating effect of the mill on J_T is managed through MFO. However, MFO can only adjust the ore content. The water and ball content also needs to be stabilised. As mentioned in Section 2.1.3, if a linear proportionality between the rock volume and ball breakage rate is assumed, a relatively constant J_B can be maintained by setting MFB as a constant fraction of MFO. If ρ_Q is measured, MIW can be used to control ρ_Q. Since ρ_Q is generally not measured, MIW is set at a constant ratio of MFO to maintain a relatively constant ρ_Q.

The fast integrating action of the sump on its contents necessitates regulatory control of $SVOL$ through either SFW or CFF. As shown in 2.1, since SFW is closer to $SVOL$ and CFF is closer to PSE,

the natural pairing appears to be $SFW \leftrightarrow SVOL$ and $CFF \leftrightarrow PSE$, which is in accordance with the guidelines in Minasidis *et al.* (2015) for regulatory control. However, the transfer function model developed in Craig and MacLeod (1995) from step-tests at an industrial circuit indicates there is a quicker and larger response between changes in SFW and PSE, than for changes in CFF and PSE. The mechanism by which SFW affects PSE is by changing CFD (see Section 2.1.2.4). Therefore, as in the list above, the following pairing is made: $SFW \leftrightarrow PSE$ and $CFF \leftrightarrow SVOL$.

The survey of Wei and Craig (2009b) confirms that plants prefer the pairing of $SFW \leftrightarrow PSE$ rather than $CFF \leftrightarrow PSE$. However, the survey also indicates that plants prefer reducing SFW, rather than increasing CFF, to reduce $SVOL$. Because of the coupling between these variables, a multi-variable controller capable of managing the available volume in the sump is recommended to keep $SVOL$ between extreme limits and reduce the variability in PSE (Hulbert *et al.* 1990, Coetzee *et al.* 2010, Le Roux *et al.* 2016a).

The regulatory control scheme is illustrated in Fig. 3.6. The level controller (LC) for J_T manipulates MFO. The flow controllers (FC) manipulate MIW and MFB which are set as constant ratios of MFO. The level controller (LC) for slurry volume manipulates SFW. The analyser controller (AC) for PSE manipulates CFF. These controllers can be implemented using PID controllers. No distinct connection is shown in the figure between TP and ϕ_c, as this should be set by the operator.

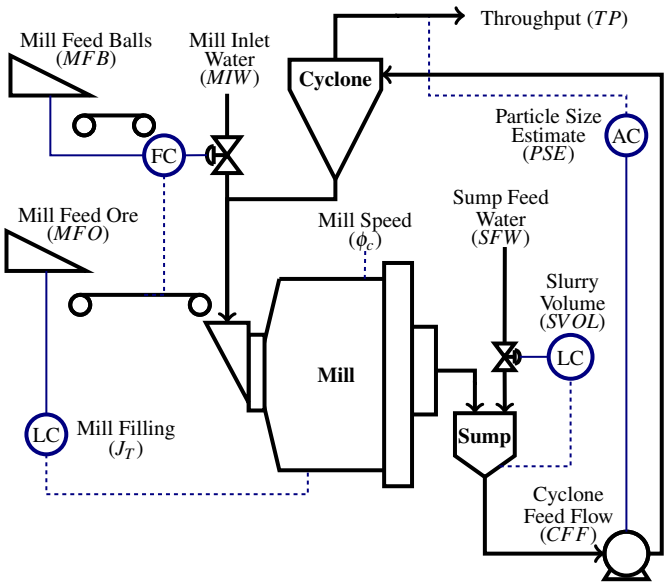

Figure 3.6. Plant-wide regulatory control scheme.

3.2.2 Supervisory control

The supervisory control layer aims to control the primary economic controlled variables using the set-points to the regulatory layer as manipulated variables. The supervisory layer should preferably avoid saturation of manipulated variables used for regulatory control. For grinding mill circuits, the regulatory and supervisory layer are often combined into one layer. The two general alternatives are advanced single loop control or multi-variable control.

The majority of industrial mineral processing plants make use of SISO PID controllers to achieve their control objectives even though the success of advanced process controllers in other process industries are well attested (Wei and Craig 2009b, Craig *et al.* 2011). Model-based controllers, such as MPC, provide significant advantages over PID when applied to grinding mill circuits (Niemi, Tian and Ylinen 1997, Pomerleau *et al.* 2000, Ramasamy *et al.* 2005, Remes, Aaltonen and Koivo 2010). The economic performance of PID control compared to non-linear MPC when applied to a grinding mill circuit was evaluated by Wei and Craig (2009a) and results showed that NMPC can improve performance with respect to recovered mineral value in downstream flotation circuits. Further improvements to overall MPC performance can be achieved by incorporating peripheral control tools such as inferential measurements, disturbance observers or model-plant mismatch detection (Hodouin 2011, Apelt and Thornhill 2009, Yang, Li, Chen and Li 2010, Olivier and Craig 2013). The ability of MPC to negotiate strong coupling between variables, long time delays, variable constraints, and plant non-linearities, qualifies it as a good candidate for a regulatory and supervisory controller (Darby and Nikolaou 2012).

As seen in Section 3.1.3, the primary economic controlled variables are J_T and ϕ_c. The set-points of J_T and ϕ_c are specified by the optimisation layer. As summarized in Section 3.1.5, these set-points define the desired PSE and TP. The manipulator to achieve the desired TP is ϕ_c. For a specific J_T and ϕ_c, disturbances to PSE can be managed through changes to CFF and SFW.

Assuming MPC is used for regulatory and supervisory control, the MPC controller must perform the tasks delineated for the regulatory controller and the supervisory controller. If MFB and MIW are constant ratios of MFO, the controller can make use MFO, SFW, and CFF as manipulated variables to control the primary economic controlled variable J_T, as well as the variables $SVOL$ and PSE. Control of $SVOL$ is required to ensure the sump does not run dry or overflows, and control of PSE is required

to maintain a constant cut-size at the cyclone amid plant disturbances. Since each of the manipulated variables impact each of the controlled variables, an adequate plant model is required for the controller to decouple the variable interaction. Because the sump acts as a buffer between the mill and the cyclone, it can assist to reduce the effect of feed ore hardness and size distribution disturbances on PSE. The degree of disturbance rejection depends on the size of the sump and the ability of the MPC controller to allow $SVOL$ to drift between its minimum and maximum value.

3.2.3 Optimisation

The task of the optimiser is to update the primary controlled variables and to detect changes in the active constraint regions that require switching of controlled variables. A good example of this is seen in the demand side management simulation study of Matthews and Craig (2013), where an optimiser varies the mill power draw depending on the cost of electricity in certain time periods. Over a one week period, the controller is able to maintain the total required TP for the week and maintain the specified PSE while reducing the cost of grinding for the week. The increase profit is not a result of increased TP, but rather the reduction in power consumption. An example of real-time optimisation using linear programming to maximise TP of a grinding mill circuit is found in Lestage, Pomerleau and Hodouin (2002).

For this study, the optimisation layer maximises the economic cost function in (3.1) in terms of the equality constraints defined by the grindcurves in Section 3.1.2. This provides a set-point for the primary economic controller variables J_T and ϕ_c. The variables J_T and ϕ_c need to be updated whenever there are significant changes in the cost of electricity, the grade of the ore from the mine, the market price for concentrator product, or the processing and transportation cost of the concentrator product.

3.3 CONCLUSION

This chapter aims to formulate a control structure capable of achieving the operational economic goals of the comminution circuit developed in Chapter 2. The operational economic objective is defined by the cost function in (3.1). The cost function is defined in terms of the performance indicators of the milling circuit as a whole: PSE and TP. The circuit performance indicators can be related to the mill

performance indicators - Q_S and ψ - through (3.2), if it is assumed the cyclone maintains a constant cut and the variations in CFF to maintain a consistent cut has a negligible effect on the grindcurves. The grindcurves define the mill performance indicators in terms of J_T and ϕ_c, if it is assumed J_B and ρ_Q remains constant for all ranges of J_T and ϕ_c. The optimisation layer maximises (3.1) in terms of J_T and ϕ_c, the primary economic controlled variables, to optimise the revenue the mineral processing plant can generate. The grindcurves act as equality constraints for the maximisation of (3.1).

The regulatory and supervisory layer aims to control the plant at the operating condition specified by the optimisation layer. Because the process contains non-linearities, long time delays and strong interaction between variables, a multi-variable controller such as MPC is well-suited to control the grinding mill circuit (Chen *et al.* 2007, Yang *et al.* 2010, Salazar, Valdez-Gonzalres, Vyhmesiter and Cubillos 2014). For a target J_T at a specific ϕ_c, the MPC controller can make use of MFO, SFW, and CFF to regulate J_T, reject disturbances in PSE, and maintain $SVOL$ within operation bounds. The other two manipulated variables, MFB and MIW, are set as constant fractions of MFO to maintain a constant J_B and ρ_Q in the mill. The capacity of the circuit, i.e. the final TP, is manipulated by ϕ_c as defined by the optimisation layer.

Advanced process control, which is a mature technology in the broader process industry, is not yet widely adopted in the mineral processing industry (Craig *et al.* 2011). Although industrial plants recognize the plant non-linearities and the coupling between process variables, most appear to remain satisfied with the performance achievable through single-input-single-output (SISO) PID controllers (Wei and Craig 2009b). There are a number of examples of industrial applications of multi-variable control to grinding mill circuits (Hulbert *et al.* 1990, Craig *et al.* 1992, Craig and MacLeod 1996, Bouche, Brandt, Broussaud and Drunick 2005, Chen *et al.* 2007), but these are mostly linear controllers based on linear process models. Because of the slow time-varying nature of the process and the large process disturbances, these linear controllers are limited to a narrow range of process operation. Non-linear control is the desired option, but one of the main impediments to applying non-linear process control to grinding mill circuits is the computational burden to minimise a non-linear controller objective function (Coetzee *et al.* 2010).

To enable the application of non-linear control on industrial milling circuits, the next chapter develops a non-linear model-based controller with significantly reduced computational cost. The aim is to provide a suitable option for non-linear model-based optimal control for output tracking in large

industrial processes, especially if computational time and complexity is a limiting factor for the real-time application of a model-based optimal controller.

CHAPTER 4 MODEL PREDICTIVE STATIC PROGRAMMING

The aim of this chapter is to develop a non-linear model-based optimal controller capable of achieving the regulatory and supervisory control goals described in the previous chapter at a reduced computational cost and complexity.

This chapter describes the mathematical formulation of MPSP for output tracking where the output is a non-linear function of both the states and the input. The proposed MPSP technique is applied in simulation to a grinding mill circuit, and is evaluated against conventional NMPC in terms of the ability to reject noise and disturbances while tracking a desired set-point. The aim is to illustrate the ability of MPSP to track a desired set-point, where similar control performance to NMPC is achieved, but without the computational burden associated with NMPC (Le Roux, Padhi and Craig 2014).

The chapter is organized as shown below:

1. Section 4.1 discusses the non-linear model used to describe the grinding mill circuit.

2. Section 4.2 gives an overview of MPSP for non-linear problems.

3. Section 4.3 gives a brief description of the NMPC used in this study.

4. Section 4.4 describes the simulation of both controllers.

5. Section 4.5 discusses the results.

4.1 MILLING CIRCUIT MODEL DESCRIPTION

Similar to the MPC studies for grinding mill circuits by Coetzee *et al.* (2010) and Salazar *et al.* (2014), the same non-linear grinding circuit model is used to simulate the plant and develop the controller. In this study, the continuous time dynamic phenomenological non-linear population balance model validated by Le Roux *et al.* (2013b) is used to describe the single-stage closed grinding mill circuit in Fig. 2.1. The model was developed with the aim to produce reasonably accurate model responses using as few parameters and states as possible. The input and output variables of the circuit are described in Table 2.1. Each process unit in the circuit is modelled separately.

The model divides the ore into the three size classes mentioned in Section 2.1.1: rocks, coarse ore and fine ore. Although only three size classes are used to describe the ore in the circuit, they are sufficient for the model to produce qualitatively accurate responses (Le Roux and Craig 2013).

The model defines fives states to describe the mill charge volumetric hold-ups: water (x_{mw}), solids (x_{ms}), fines (x_{mf}), rocks (x_{mr}), and steel balls (x_{mb}). Because of the end-discharge grate, only three states are necessary to describe the sump slurry volumetric hold-ups: water (x_{sw}), solids (x_{ss}), and fines (x_{sf}).

For the population balance model equations, V denotes a flow-rate in m^3/h and x denotes the states of the model as volumes in m^3. Table 4.1 provides a description of the subscripts for V and x. The first subscript indicates the module considered (mill, sump or cyclone), the second subscript specifies which state is considered (rocks, solids, coarse, fines, balls, or water), and in the case of flow-rates the final subscript indicates an inflow, outflow or underflow. Only a brief overview of the model is presented here. A detailed description of the model is provided in Le Roux *et al.* (2013b). The model nomenclature is shown in Table 4.2.

4.1.1 Mill model

The population volume balance of mill hold-ups - water (x_{mw}), solids (x_{ms}), fines (x_{mf}), rocks (x_{mr}), and steel balls (x_{mb}) - are defined in terms of the inflow, outflow and generation/consumption of each

state

$$\dot{x}_{mw} = V_{mwi} + V_{cwu} - V_{mwo} \tag{4.1a}$$

$$\dot{x}_{ms} = V_{msi} + V_{csu} - V_{mso} + RC \tag{4.1b}$$

$$\dot{x}_{mf} = V_{mfi} + V_{cfu} - V_{mfo} + FP \tag{4.1c}$$

$$\dot{x}_{mr} = V_{mri} - RC \tag{4.1d}$$

$$\dot{x}_{mb} = V_{mbi} - BC \tag{4.1e}$$

where V_{mwi}, V_{msi}, V_{mfi}, V_{mri} and V_{mbi} (m^3/h) are the flow-rates of water, solids, fines, rocks and balls into the mill respectively; V_{mwo}, V_{mso} and V_{mfo} (m^3/h) are the discharge flow-rates of water, solids and fines respectively; RC, BC and FP (m^3/h) are the rock consumption, ball consumption and fines production respectively; V_{cwu}, V_{csu} and V_{cfu} (m^3/h) represent the cyclone water, solids and fines underflow flow-rates respectively.

4.1.1.1 Mill feed

The flow of material into the mill is defined as

$$V_{mwi} = MIW \tag{4.2a}$$

$$V_{msi} = (1 - \alpha_r) MFO / \rho_O \tag{4.2b}$$

$$V_{mfi} = \alpha_f MFO / \rho_O \tag{4.2c}$$

$$V_{mri} = \alpha_r MFO / \rho_O \tag{4.2d}$$

$$V_{mbi} = MFB / \rho_B \tag{4.2e}$$

where ρ_O (t/m^3) is the ore density, ρ_B (t/m^3) is the ball density, and parameters α_f and α_r represent the fraction of fines and rocks in MFO respectively. Variations in feed size distribution which perturb the

Table 4.1. Description of subscripts

Subscript	Description
$x_{\square -}$	m-mill; s-sump; c-cyclone
$x_{- \square}$	w-water; s-solids; c-coarse; f-fines; r-rocks; b-balls
$V_{- - \square}$	i-inflow; o-outflow; u-underflow

Table 4.2. Circuit parameter values and uncertainty

Parm	Value	Unit	Δ	Description
α_f	0.055	[-]	50%	Fraction fines in the mill feed ore
α_r	0.465	[-]	50%	Fraction rock in the mill feed ore
α_P	1.0	[-]		Fractional power reduction per fractional reduction in mill speed
α_{κ_f}	0.01	[-]		Fractional change in kW/fines produced per change in fractional mill filling
α_{su}	0.916	[-]	5%	Parameter related to fraction solids in underflow
C_1	0.6	[-]		Constant
C_2	0.7	[-]		Constant
C_3	4.0	[-]		Constant
C_4	4.0	[-]		Constant
C_5	0.6	[-]		Constant
δ_{P_s}	17.5	[-]		Power-change parameter for fraction solids in the mill
δ_{P_v}	17.5	[-]		Power-change parameter for volume of mill filled with charge
δ_{P_c}	0.0	[-]		Cross-term for maximum power draw
ρ_B	7.85	[t/m^3]		Density of steel balls
ρ_O	3.20	[t/m^3]		Density of feed ore
ρ_W	1.00	[t/m^3]		Density of water
ε_{sv}	0.6	[-]		Maximum fraction solids by volume of slurry at zero slurry flow
ε_c	126.9	[m^3/h]	5%	Parameter related to coarse split
ϕ_c	0.72	[-]		Fraction of critical mill speed
κ_B	90.0	[kWh/t]	5%	Energy required per tonne of steel balls consumed
κ_F	29.5	[kWh/t]	50%	Energy required per tonne of fines produced
κ_R	6.72	[kWh/t]	20%	Energy required per tonne of rock consumed
$\varphi_{P_{max}}$	0.57	[-]		Rheology factor for maximum mill power draw
P_{max}	1670	[kW]		Maximum mill motor power draw
v_{mill}	59.1	[m^3]		Mill volume
$v_{P_{max}}$	0.34	[-]		Fraction of mill volume filled for maximum power draw
d_H	88.0	[1/h]		Volumetric flow per “flowing volume” driving force

equilibrium of the mill is represented by changes to α_r and α_f. The implicit assumption when dividing by ρ_O in (4.2b) to (4.2d) is that the ore is non-porous.

4.1.1.2 Mill discharge

The mill discharge flow-rates are defined as

$$V_{mwo} = \varphi d_H x_{mw} \left(\frac{x_{mw}}{x_{ms} + x_{mw}} \right) \tag{4.3a}$$

$$V_{mso} = \varphi d_H x_{mw} \left(\frac{x_{ms}}{x_{ms} + x_{mw}} \right) \tag{4.3b}$$

$$V_{mfo} = \varphi d_H x_{mw} \left(\frac{x_{mf}}{x_{ms} + x_{mw}} \right) \tag{4.3c}$$

where d_H (1/h) is the discharge rate, and φ is an empirical function called the rheology factor. The rheology factor attempts to incorporate the effect of the fluidity and density of the slurry on the milling circuit's performance and is defined as

$$\varphi = \left[\max \left(0, 1 - \left(\frac{1}{\varepsilon_{sv}} - 1 \right) \frac{x_{ms}}{x_{mw}} \right) \right]^{0.5} \tag{4.4}$$

where ε_{sv} is the maximum fraction of solids by volume of slurry at zero slurry flow. A rheology factor of unity corresponds to $\frac{x_{ms}}{x_{mw}} = 0$, indicating the slurry consists only of water. A rheology factor of zero corresponds to $\frac{x_{ms}}{x_{mw}} = \frac{\varepsilon_{sv}}{1-\varepsilon_{sv}}$, indicating the slurry is a non-flowing mud.

4.1.1.3 Material consumption and production

The general formulation of the breakage equations finds its parallel in the cumulative breakage rates expressions in Hinde and Kalala (2009) and Amestica, Gonzalez, Menacho and Barria (1996). The rock consumption (RC), ball consumption (BC) and fines production (FP) are defined as

$$RC = \frac{x_{mr} \varphi P_{mill}}{\rho_O \kappa_R \left(x_{mr} + x_{ms} \right)} \tag{4.5a}$$

$$BC = \frac{x_{mb} \varphi P_{mill}}{\kappa_B \left[\rho_O \left(x_{mr} + x_{ms} \right) + \rho_B x_{mb} \right]} \tag{4.5b}$$

$$FP = \frac{P_{mill}}{\rho_O \kappa_F \left[1 + \alpha_{\kappa_f} \left(J_T - v_{P_{max}} \right) \right]} \tag{4.5c}$$

where κ_R and κ_B (kWh/t) are the energies required per tonne of rocks and balls consumed respectively, κ_F (kWh/t) is the energy required per tonne of fines produced, $v_{P_{max}}$ is the fraction of the mill filled at maximum power draw, and α_{κ_f} accounts for the change in κ_F per change in mill filling. The

equilibrium of the mill is not only upset through variations of the feed size distribution, but also variations in ore hardness. This can be simulated through variation of parameters κ_F and κ_R.

4.1.1.4 Mill load and power draw

The fraction of the mill filled with charge (J_T) is defined as

$$J_T = (x_{mw} + x_{ms} + x_{mr} + x_{mb}) / v_{mill} \tag{4.6}$$

where v_{mill} (m^3) is the total volume of the mill.

The mill power draw is modelled as a quadratic function depending on the total mill charge and the fluidity and density of the slurry in the mill

$$P_{mill} = P_{max} \phi_c^{\alpha_P} (1 - \delta_{P_v} Z_x^2 - 2\delta_{P_c} \delta_{P_v} \delta_{P_s} Z_x Z_r - \delta_{P_s} Z_r^2) \tag{4.7}$$

where P_{max} (kW) is the maximum mill power draw, α_P is the fractional power reduction per fractional reduction from critical mill speed, δ_{P_v} is the power change parameter for volume of mill filled with charge, δ_{P_s} is the power change parameter for the fraction of solids in the mill, and δ_{P_c} is the cross term for maximum power draw.

The effect of the total charge on mill power is modelled by the empirically defined function $Z_x = \frac{J_T}{v_{P_{max}}} - 1$, and the effect of the solids content on the mill power is modelled by the empirically defined function $Z_r = \frac{\varphi}{\varphi_{P_{max}}} - 1$ where $\varphi_{P_{max}}$ is the rheology factor at maximum mill power draw.

4.1.2 Sump model

The population volume balance of sump hold-ups - water (x_{sw}), solids (x_{ss}), and fines (x_{sf}) - are defined as

$$\dot{x}_{sw} = V_{mwo} - V_{swo} + SFW \tag{4.8a}$$

$$\dot{x}_{ss} = V_{mso} - V_{sso} \tag{4.8b}$$

$$\dot{x}_{sf} = V_{mfo} - V_{sfo} \tag{4.8c}$$

where V_{swo}, V_{sso} and V_{sfo} (m^3/h) are the sump discharge flow-rates of water, solids and fines respectively. It is assumed the slurry in the sump is fully mixed.

The discharge of each state from the sump through the variable speed pump is defined as

$$V_{swo} = CFF\frac{x_{sw}}{x_{sw}+x_{ss}} \tag{4.9a}$$

$$V_{sso} = CFF\frac{x_{ss}}{x_{sw}+x_{ss}} \tag{4.9b}$$

$$V_{sfo} = CFF\frac{x_{sf}}{x_{sw}+x_{ss}}. \tag{4.9c}$$

The volume of the sump filled with slurry ($SVOL$) (m^3) and the cyclone feed density (CFD) (t/m^3) are defined as

$$SVOL = x_{ss}+x_{sw} \tag{4.10}$$

$$CFD = \frac{\rho_W V_{swo}+\rho_O V_{sso}}{V_{swo}+V_{sso}} = \frac{\rho_W x_{sw}+\rho_O x_{ss}}{x_{sw}+x_{ss}} \tag{4.11}$$

where ρ_W is the density of water.

4.1.3 Hydrocyclone model

4.1.3.1 Underflow and overflow

Static non-linear models in the form of efficiency curves are often used to model classification units in minerals processing (Nageswararao, Wiseman and Napier-Munn 2004). The non-linear static cyclone model presented here aims to model the product size and density by taking the effects of angular velocity of the particle inside the cyclone, the slurry density, and slurry viscosity into account. The underflow of coarse material (V_{ccu}) is modelled as

$$V_{ccu} = (V_{sso}-V_{sfo})\left(1-C_1\exp\left(\frac{-CFF}{\varepsilon_c}\right)\right)\left(1-\left(\frac{F_i}{C_2}\right)^{C_3}\right)\left(1-P_i^{C_4}\right) \tag{4.12}$$

where $F_i = \frac{V_{sso}}{CFF}$ is the fraction solids in the cyclone feed, $P_i = \frac{V_{sfo}}{V_{sso}}$ is the fraction fines in the feed solids, ε_c (m^3/h) relates to the coarse split, C_1 relates to the split at low-flows when the centrifugal force on particles is relatively small, C_2 normalizes the fraction solids in the feed according to the upper limit for the packing fraction of solid particles, and C_3 and C_4 adjusts the sharpness of the dependency on F_i and P_i.

To determine the amount of water and fines accompanying the coarse underflow, the fraction of solids in the underflow (F_u) must be determined. This is modelled as

$$F_u = C_5 - (C_5 - F_i)\exp\left(-V_{ccu}/(\alpha_{su}\varepsilon_c)\right) \tag{4.13}$$

where C_5 is the approximate maximum packing fraction, and α_{su} relates to the fraction solids in the underflow.

Therefore, the cyclone underflow flow-rates in (4.1) are defined as

$$V_{cwu} = \frac{V_{swo}\left(V_{ccu} - F_u V_{ccu}\right)}{F_u V_{swo} + F_u V_{sfo} - V_{sfo}} \tag{4.14a}$$

$$V_{cfu} = \frac{V_{sfo}\left(V_{ccu} - F_u V_{ccu}\right)}{F_u V_{swo} + F_u V_{sfo} - V_{sfo}} \tag{4.14b}$$

$$V_{csu} = V_{ccu} + V_{cfu}. \tag{4.14c}$$

These equations follow from the assumption that the fines are not influenced by centrifugal forces. This implies the ratio of fines to water in the overflow, underflow and feed is equal, and that the fraction of solids in the underflow can be written as $F_u = \frac{V_{csu}}{V_{csu}+V_{cwu}}$. Consequently, the cyclone water overflow flow-rate (V_{cwo}), solids overflow flow-rate (V_{cso}) and fines overflow flow-rate (V_{cfo}) can be calculated using a flow balance around the cyclone.

4.1.3.2 Product quality and throughput

The product quality is defined as the fraction of fines to solids in the cyclone overflow, and is represented by the particle size estimate (PSE). The product throughput (TP) is defined as the mass flow of solids in the cyclone overflow.

$$PSE = \frac{V_{cfo}}{V_{cso}} \tag{4.15}$$

$$TP = \rho_O V_{cso} \tag{4.16}$$

4.2 OUTPUT TRACKING USING MODEL PREDICTIVE STATIC PROGRAMMING

4.2.1 Algorithm derivation

The MPSP control technique for output tracking is discussed next. The state dynamics and output equation of a general discrete non-linear system can be written as

$$\begin{aligned} X_{k+1} &= F_k(X_k, U_k) \\ Y_k &= H_k(X_k, U_k) \end{aligned} \tag{4.17}$$

where $X \in \mathbb{R}^n$, $U \in \mathbb{R}^m$, $Y \in \mathbb{R}^p$ represent the states, the input and the output of the system respectively, and k are time steps.

The primary objective of output tracking by means of MPSP is to find an input projection U_k for time steps 1 to N so that the output Y_k goes to the desired output value Y_k^* for time steps 1 to N, i.e. $Y_k \rightarrow Y_k^*$ $\forall\, k = 1, 2, ..., N$. It is important to note that the output Y_k is a function of both the states X_k and the input U_k of the system. The MPSP algorithm predicts the output for N time steps and calculates inputs for N time steps. Compared to MPC, N represents both the prediction and control horizon for MPSP.

For the control technique presented here, it is necessary to start with a "guess" initial input. Obviously the method to obtain a good estimate or intelligent guess of the initial input is problem specific. Because the optimal input will not necessarily be achieved by the guessed input, the input must be improved by an iterative process where i is the iteration index which increases until the algorithm converges. Convergence can be measured as $\frac{\|Y_k^i - Y_k^*\|}{\|Y_k^*\|} < \varepsilon_k$, $\forall\, k = 1, 2, ..., N$, where Y_k^* is the desired output and ε_k is a user defined tolerance limit on the output error.

The system shown in (4.17) can now be written as

$$\begin{aligned} X_{k+1}^i &= F_k\left(X_k^i, U_k^i\right) \\ Y_k^i &= H_k\left(X_k^i, U_k^i\right). \end{aligned} \tag{4.18}$$

The relationship of variables between consecutive iterations i and $i+1$ at time step k are

$$Y_k^{i+1} = Y_k^i + \Delta Y_k^i \tag{4.19a}$$

$$X_k^{i+1} = X_k^i + \Delta X_k^i \tag{4.19b}$$

$$U_k^{i+1} = U_k^i + \Delta U_k^i. \tag{4.19c}$$

The output Y_k^{i+1} at time step k and iteration $(i+1)$ can be expanded by Taylor series expansion, retaining only first order terms

$$\begin{aligned} Y_k^{i+1} &= H_k\left(X_k^{i+1}, U_k^{i+1}\right) \\ &= H_k\left(X_k^i + \Delta X_k^i, U_k^i + \Delta U_k^i\right) \\ &\approx Y_k^i + \left[\frac{\partial H_k}{\partial X_k}\right]\Delta X_k^i + \left[\frac{\partial H_k}{\partial U_k}\right]\Delta U_k^i. \end{aligned} \tag{4.20}$$

Combining (4.20) and the expression for the outputs in (4.19a), it is possible to write

$$\begin{aligned} \Delta Y_k^i &= Y_k^{i+1} - Y_k^i \\ &\approx \left[\frac{\partial H_k}{\partial X_k}\right]\Delta X_k^i + \left[\frac{\partial H_k}{\partial U_k}\right]\Delta U_k^i \end{aligned} \tag{4.21}$$

where ΔY_k^i is the error in the output at time k and iteration i.

The state X_{k+1}^{i+1} at time step $(k+1)$ and iteration $(i+1)$ can be expanded by Taylor series expansion retaining only first order terms

$$\begin{aligned} X_{k+1}^{i+1} &= F_k\left(X_k^{i+1}, U_k^{i+1}\right) \\ &= F_k\left(X_k^i + \Delta X_k^i, U_k^i + \Delta U_k^i\right) \\ &\approx F\left(X_k^i, U_k^i\right) + \left[\frac{\partial F_k}{\partial X_k}\right]\Delta X_k^i + \left[\frac{\partial F_k}{\partial U_k}\right]\Delta U_k^i \\ &\approx X_{k+1}^i + \left[\frac{\partial F_k}{\partial X_k}\right]\Delta X_k^i + \left[\frac{\partial F_k}{\partial U_k}\right]\Delta U_k^i. \end{aligned} \tag{4.22}$$

Combining (4.22) and the expression for states in (4.19b), it is possible to write

$$\begin{aligned} \Delta X_{k+1}^i &= X_{k+1}^{i+1} - X_{k+1}^i \\ &\approx \left[\frac{\partial F_k}{\partial X_k}\right]\Delta X_k^i + \left[\frac{\partial F_k}{\partial U_k}\right]\Delta U_k^i \end{aligned} \tag{4.23}$$

where ΔX_k^i is the error in the state and ΔU_k^i is the error in the input solution at time step k and iteration i. If small input deviations ($\Delta U_k^i = dU_k^i$), small state deviations ($\Delta X_k^i = dX_k^i$), and small output errors are assumed ($\Delta Y_k^i = dY_k^i$), the output error dY_k^i in (4.21) can be written in terms of the state and input error of (4.23) as

$$\begin{aligned} dY_k^i &= \left[\frac{\partial H_k}{\partial X_k}\right] dX_k^i + \left[\frac{\partial H_k}{\partial U_k}\right] dU_k^i \\ &= \left[\frac{\partial H_k}{\partial X_k}\right]\left[\frac{\partial F_{k-1}}{\partial X_{k-1}}\right] dX_{k-1}^i + \left[\frac{\partial H_k}{\partial X_k}\right]\left[\frac{\partial F_{k-1}}{\partial U_{k-1}}\right] dU_{k-1}^i + \left[\frac{\partial H_k}{\partial U_k}\right] dU_k^i. \end{aligned} \tag{4.24}$$

The state error dX^i_{k-1} in (4.24) can be expanded further in terms of dX^i_{k-2} and dU^i_{k-2}. And the state error dX^i_{k-2} can be expanded further in terms of dX^i_{k-3} and dU^i_{k-3}, and so on. This expansion procedure can continue until state error dX^i_1 (where $k = 1$) is reached. Finally,

$$dY^i_k = \left[A^k\right]^i dX^i_1 + \left[B^k_1\right]^i dU^i_1 + \left[B^k_2\right]^i dU^i_2 + \ldots + \left[B^k_{k-1}\right]^i dU^i_{k-1} + \left[B^k_k\right]^i dU^i_k \tag{4.25}$$

where

$$\begin{aligned} \left[A^k\right]^i &= \left[\frac{\partial H_k}{\partial X_k}\right]\left[\frac{\partial F_{k-1}}{\partial X_{k-1}}\right]\left[\frac{\partial F_{k-2}}{\partial X_{k-2}}\right]\cdots\left[\frac{\partial F_1}{\partial X_1}\right] \\ \left[B^k_j\right]^i &= \left[\frac{\partial H_k}{\partial X_k}\right]\left[\frac{\partial F_{k-1}}{\partial X_{k-1}}\right]\cdots\left[\frac{\partial F_{j+1}}{\partial X_{j+1}}\right]\left[\frac{\partial F_j}{\partial U_j}\right] \\ \left[B^k_k\right]^i &= \left[\frac{\partial H_k}{\partial U_k}\right]. \end{aligned} \tag{4.26}$$

If it is assumed that with full-state feedback the initial condition of the system is known, i.e. X_1 is known, the error $dX^i_1 = X^{i+1}_1 - X^i_1$ has to be zero, i.e. $dX_1 = 0$. Therefore, the error in the output in (4.25) reduces to

$$dY^i_k = \sum_{j=1}^{k} \left[B^k_j\right]^i dU^i_j. \tag{4.27}$$

Note that for the derivation of (4.27) the input variables at each time step are independent of the previous values of the states and/or inputs. The input variables are seen as decision variables and independent decisions can be made at every point in time. During the implementation of the algorithm, the entire input projection is computed, but only the first input move is performed. For the next time step the algorithm repeats, calculates a new input trajectory and again only performs the first input move of the new trajectory. Feedback is implemented via the cost function, described later in this section.

Equation (4.27) represent the output sensitivity at time step k with respect to change in the input at all time steps prior to and including k. It is intuitively clear that the effect of input changes at future time steps will not change the output vector at the current time step. Therefore, $\left[B^k_j\right]^i$ can be defined for all $k = 1,2,\ldots,N$ and $j = 1,2,\ldots,N$. In order to reduce the computational requirements of the algorithm, $\left[B^k_j\right]^i$ can be computed recursively.

$$\left.\begin{aligned} \left[\phi^k_k\right]^i &= I_{n\times n} \\ \left[\phi^k_j\right]^i &= \left[\phi^k_{j+1}\right]^i\left[\frac{\partial F_j}{\partial X_j}\right] \\ \left[B^k_j\right]^i &= \left[\frac{\partial H_k}{\partial X_k}\right]\left[\phi^k_{j+1}\right]^i\left[\frac{\partial F_j}{\partial U_j}\right] \end{aligned}\right\} \quad \forall j < k$$

$$\begin{aligned} \left[B^k_j\right]^i &= \left[\frac{\partial H_k}{\partial U_k}\right] && \forall j = k \\ \left[B^k_j\right]^i &= [0]_{p\times m} && \forall j > k \end{aligned} \tag{4.28}$$

The primary objective of the control technique can be defined by the following cost function

$$\begin{aligned} J^i &= \tfrac{1}{2}\sum_{k=1}^{N}\left(Y_k^{i+1}-Y_k^*\right)^T W_k\left(Y_k^{i+1}-Y_k^*\right)+\tfrac{1}{2}\sum_{k=1}^{N}\left(U_k^{i+1}-U_k^i\right)^T R_k\left(U_k^{i+1}-U_k^i\right) \\ &= \tfrac{1}{2}\sum_{k=1}^{N}\left(Y_k^i+dY_k^i-Y_k^*\right)^T W_k\left(Y_k^i+dY_k^i-Y_k^*\right)+\tfrac{1}{2}\sum_{k=1}^{N}\left(dU_k^i\right)^T R_k\left(dU_k^i\right) \\ &= \tfrac{1}{2}\sum_{k=1}^{N}\left(dY_k^i-dY_k^{*i}\right)^T W_k\left(dY_k^i-dY_k^{*i}\right)+\tfrac{1}{2}\sum_{k=1}^{N}\left(dU_k^i\right)^T R_k\left(dU_k^i\right) \end{aligned} \tag{4.29}$$

where $dY_k^{*i}=Y_k^i-Y_k^*$, and W_k and R_k are the output and input weighting matrices respectively. Using (4.27), the cost function can be written in terms of the input error dU_k such that

$$J^i = \tfrac{1}{2}\sum_{k=1}^{N}\beta^T W_k\beta+\tfrac{1}{2}\sum_{k=1}^{N}\left(dU_k^i\right)^T R_k\left(dU_k^i\right) \tag{4.30}$$

where

$$\beta = \sum_{j=1}^{k}\left[B_j^k\right]^i dU_j^i - dY_k^{*i}. \tag{4.31}$$

The objective is to minimize the cost function J in (4.30) for $dU_1, dU_2, ..., dU_N$, which requires the calculation of the partial derivatives $\frac{\partial J}{\partial(dU_1)}$, $\frac{\partial J}{\partial(dU_l)}$, and $\frac{\partial J}{\partial(dU_N)}$. (The iteration index i is dropped throughout the rest of this section for the sake of simplicity.) The equation corresponding to $\frac{\partial J}{\partial(dU_z)}=0$ can be simplified to

$$\frac{\partial J}{\partial(dU_z)} = \sum_{k=1}^{N}\left(B_z^{kT}W_k\sum_{j=1}^{k}B_j^k dU_j\right)-\sum_{k=1}^{N}B_z^{kT}W_k dY_k^*+R_z dU_z. \tag{4.32}$$

The first term in (4.32) can be simplified further such that

$$\begin{aligned} \sum_{k=1}^{N}\left(B_z^{kT}W_k\sum_{j=1}^{k}B_j^k dU_j\right) &= \sum_{k=1}^{N}\left(B_z^{kT}W_kB_1^k dU_1+B_z^{kT}W_kB_2^k dU_2+...+B_z^{kT}W_kB_k^k dU_k\right) \\ &= \left(B_z^{1T}W_1B_1^1 dU_1\right)+\left(B_z^{2T}W_2B_1^2 dU_1+B_z^{2T}W_2B_2^2 dU_2\right)+...+ \\ &\quad \left(B_z^{NT}W_NB_1^N dU_1+B_z^{NT}W_NB_2^N dU_2+...+B_z^{NT}W_NB_N^N dU_N\right) \\ &= \sum_{l=1}^{N}B_z^{lT}W_lB_1^l dU_1+\sum_{l=2}^{N}B_z^{lT}W_lB_2^l dU_2+...+B_z^{NT}W_NB_{N-1}^N dU_N \\ &= C_{z1}dU_1+C_{z2}dU_2+...+C_{zN}dU_N. \end{aligned} \tag{4.33}$$

From the simplification above, matrix $C\in\mathbb{R}^{N\times N}$ is defined as

$$C_{ej}=\sum_{l=j}^{N}\left(B_e^l\right)^T W_lB_j^l \tag{4.34}$$

for $e=1,...,N$ and $j=1,...,N$. Thus, $\frac{\partial J}{\partial(dU_z)}=0$ can now be written as

$$\sum_{k=1}^{N}B_z^{kT}W_k dY_k^* = C_{z1}dU_1+C_{z2}dU_2+...+C_{zN}dU_N+R_z dU_z. \tag{4.35}$$

Compiling all the equations for all times steps, the system of equations can be written as

$$[dU_e]=\left[C_{ej}+\delta_{ej}R_e\right]^{-1}[b_e] \tag{4.36}$$

where δ_{ej} is the Kronecker-delta function and vector $b \in \mathbb{R}^{N\times 1}$ is defined for $e = 1,...,N$ as

$$b_e = \sum_{k=1}^{N} B_e^{kT} W_k dY_k^*. \tag{4.37}$$

Finally, the updated input at time step $k = 1,...,N$ is

$$U_k^{i+1} = U_k^i + dU_k^i. \tag{4.38}$$

Because output tracking using MPSP is a relatively new development, issues such as convergence guarantees and the consolidation of input, state, and output equality, inequality, and rate constraints remain open for exploration. A possible approach to address state constraints is shown in Bhitre and Padhi (2014) where slack variables can be used to handle state variable inequality constraints. However, the technique developed by Bhitre and Padhi (2014) is not for the type of system nor the type of cost function considered here.

4.2.2 General procedure

The general procedure to implement the receding horizon MPSP control algorithm is described below, and depicted in Fig. 4.1.

1. Start the iteration procedure of the MPSP algorithm by estimating an initial input trajectory U_k^1, $\forall k = 1,2...N$. Initialize the iteration index as $i = 1$.

2. Use the known initial condition X_1 and input projection U_k^i to propagate the system dynamics in (4.18). Obtain the state trajectory X_k^i, $\forall k = 1,2...N$.

3. From the state trajectory X_k^i determine the output trajectory Y_k^i. Use the desired output trajectory Y_k^* to calculate $dY_k^i = Y_k^i - Y_k^*$, $\forall k = 1,2...N$.

4. Using X_k^i and U_k^i for all $k = 1,2,...,N$, calculate the matrices shown in (4.34) and the result vector shown in (4.37).

5. Compute the input deviation dU_k^i using (4.36). Update the input for the i-th iteration with (4.38), and apply box constraints to the input.

6. Terminate the algorithm if the output error is smaller than the user-defined tolerance value, i.e. $\frac{\|Y_k^i - Y_k^*\|}{\|Y_k^*\|} < \varepsilon_Y$, $\forall k = 1,...,N$, or if the input projection converged, i.e. $\frac{\|U_k^{i+1} - U_k^i\|_\infty}{\|U_k^i\|_\infty} < \varepsilon_U$, $\forall k = 1,...,N$. If either of these conditions are met for $i \geq 1$, then use U_k^i as the optimal input projection. Otherwise, increase the iteration index i and return to step 2.

4.3 NON-LINEAR MPC

Given the system described by (4.17), the aim of non-linear MPC can be described as

$$\min_U J(U, X_0). \tag{4.39}$$

The controller cost function is defined as

$$J = \frac{1}{2}\sum_{k=1}^{N_P} (Y_k - Y_k^*)^T W_k (Y_k - Y_k^*) + \frac{1}{2}\sum_{k=1}^{N_C} (U_{k+1} - U_k)^T R_k (U_{k+1} - U_k) \tag{4.40}$$

where N_C is the control horizon, and N_P is the prediction horizon. The inputs are constrained between $U_{lb} < U < U_{ub}$ where U_{lb} and U_{ub} are the lower and upper bounds for input U respectively.

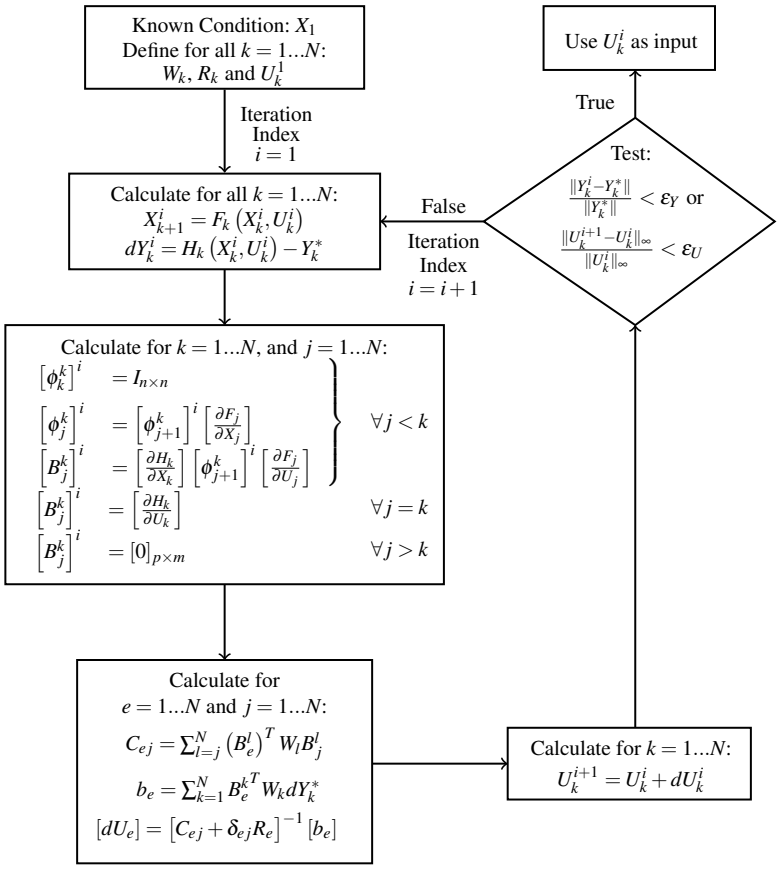

Figure 4.1. MPSP procedure.

When comparing the cost function J above to the cost function for MPSP in (4.29), there is a difference how the input U_k is evaluated. In (4.29) the difference between the input projections for consecutive iterations is evaluated (i.e. $U_k^{i+1} - U_k^i$), whereas in (4.40) the change in the control between time steps is evaluated (i.e. $U_{k+1} - U_k$). The effect of the difference in the cost function formulations can be reduced by increasing the ratio between matrix R and W. If R is much smaller than W, the contribution by the change in the input to the cost function will be much less than the contribution by the deviation of the output from set-point to the cost function.

The problem described above is a constrained minimization problem and can be solved using the *fmincon* function in MATLAB[1]. The minimization technique used by *fmincon* to solve (4.40) was chosen as *sequential quadratic programming*. A description of *sequential quadratic programming* can be found in Grüne and Pannek (2011). The principal idea is the formulation of a quadratic sub-problem based on the quadratic approximation of the Lagrangian function. An approximation of the Hessian of the Lagrangian function using a quasi-Newton updating method is made at each major iteration. This is used to generate the quadratic programming sub-problem whose solution is used to form a search direction for a line search procedure.

[1]MATLAB^{TM} is a registered trademark of The Mathworks Inc.

Table 4.3. Operating point of the milling circuit

Variable	Nominal	Min	Max	Unit
		Input		
CFF	374	200	450	[m^3/h]
MIW	4.64	0	20	[m^3/h]
MFB	5.68	0	10	[t/h]
MFO	65.2	0	100	[t/h]
SFW	140	0	300	[m^3/h]
		Output		
J_T	0.33	0.25	0.45	[-]
$SVOL$	10.0	1.0	20.0	[m^3]
PSE	0.67	0.5	0.8	[-]

4.4 SIMULATION

Using the grinding mill circuit as control problem, the simulation investigates the effect of modelling errors on the MPSP algorithm, its ability to reject noise and large disturbances, and its computational efficiency. The same control problem is solved using NMPC to serve as a comparison between the two control techniques.

4.4.1 Simulation environment

The parameter values, the operating point of the circuit and the initial states can be viewed in Tables 4.2, 4.3, and 4.4 respectively. The data was taken from the sampling campaign of the industrial grinding mill circuit described in Le Roux *et al.* (2013b). The state, input and output vectors are defined as

$$X = [x_{mw}, x_{ms}, x_{mf}, x_{mr}, x_{mb}, x_{sw}, x_{ss}, x_{sf}]^T \tag{4.41a}$$

$$U = [MFO,\ SFW,\ CFF]^T \tag{4.41b}$$

$$Y = [J_T,\ SVOL,\ PSE]^T \tag{4.41c}$$

4.4.1.1 General conditions

The grinding mill circuit was simulated for both controllers, MPSP and NMPC, with the same general conditions:

Table 4.4. Initial states for mill and sump

State	Value	Unit	State	Value	Unit
Mill States			Sump States		
x_{mw}	4.63	[m^3]	x_{sw}	6.86	[m^3]
x_{ms}	4.65	[m^3]	x_{ss}	3.14	[m^3]
x_{mf}	0.96	[m^3]	x_{sf}	0.65	[m^3]
x_{mr}	1.99	[m^3]			
x_{mb}	8.23	[m^3]			

- Full-state feedback is assumed. This is a significant assumption as the states in the mill and the sump cannot be measured directly and need to be estimated. As seen from Wei and Craig (2009b), the measurements available in industrial grinding mill circuit are limited. Various attempts have been made to estimate the states and parameters of the plant, which can then be used for feedback control (Apelt *et al.* 2002a, Olivier *et al.* 2012, Le Roux, Craig and Padhi 2013a, Le Roux *et al.* 2016a).

- A sampling time of $T_s = 10$ s is used.

- A simulation time of 4 h, i.e. 1440 time sampling points, is used.

- The ball feed-rate MFB is kept as a constant ratio of 8% of MFO in an attempt to keep the volume of balls in the mill constant.

- The mill water inlet MIW is a constant ratio of 7% of MFO.

- Model-plant-mismatch between the controller and the plant is achieved by maintaining all the model parameters constant for the controller, but varying the following plant parameters every 3 minutes according to the respective uncertainties shown in Tables 4.2: α_f, α_r, α_{su}, ε_c, κ_B, κ_F, κ_R. Each uncertainty follows a uniform distribution around the nominal value of the parameter to produce large changes in the parameter. A uniform distribution was chosen instead of a normal distribution so that the model-plant-mismatch rejection capabilities of the controllers are clearly visible from the simulation results.

- A constant disturbance in the mill feed size distribution is simulated through a step increase in α_r by 50% of its nominal value. This step is applied between $t = 1.2$ h and $t = 2.8$ h, and is added to the continual variation of α_r every 3 minutes.

- A constant disturbance in the ore hardness is simulated through a step increase in κ_F by 50% of its nominal value. This change is applied between $t = 2.2$ h and $t = 3.8$ h, and is added to the continual variation of ϕ_f every 3 minutes.

- The input U is hard-constrained for both MPSP and NMPC between the limits shown in Table 4.3.

4.4.1.2 Simulation scenarios

To evaluate the noise and disturbance rejection of the controllers, two scenarios are simulated:

1. For the first set of simulations, the milling circuit experience parameter variations and disturbances, but no measurement noise is added to the measured states.

2. The same parameter variations and disturbances are used for the second set of simulations, but now measurement noise with a normal distribution of $\mathcal{N}\left(0,(0.01X_0)^2\right)$ is added to the measured states. Because large and fast unexpected changes to the volume of material in the circuit are not expected, the standard deviation of the noise is kept small.

4.4.1.3 Controller weights

Both controllers made use of the same W and R weighting matrices. The PSE is regarded as the most important output variable to control as this variable determines performance of the milling circuit. Therefore, the W weighting matrix for the output variables was determined such that a 1% deviation from set-point for PSE will produce an error in the cost function equal to a 5% deviation of J_T from set-point and equal to a 20% change in $SVOL$ from set-point, i.e.

$$W_1\left(5\%J_{T_{SP}}\right)^2 = W_2\left(20\%SVOL_{SP}\right)^2 = W_3\left(1\%PSE_{SP}\right)^2 \tag{4.42}$$

Of the three weighting variables, W_2 will be the smallest. Thus, choosing $W_2 = 1$, the output weighting matrix is defined as

$$W = 10^4\,\mathrm{diag}([1.47,\ 0.0001,\ 8.91]) \tag{4.43}$$

The R weighting matrix for the input variables was determined such that 2% changes of half the ranges of MFO, SFW, and CFF will produce the same error in the cost function. The R matrix was scaled to produce 1% of the error compared to the W matrix, i.e.

$$100R_1\left(\frac{2\%MFO_{range}}{2}\right)^2 = W_1\left(5\%J_{T_{SP}}\right)^2 \tag{4.44}$$

and

$$R_1\left(\frac{2\%MFO_{range}}{2}\right)^2 = R_2\left(\frac{2\%SFW_{range}}{2}\right)^2 = R_3\left(\frac{2\%CFF_{range}}{2}\right)^2 \tag{4.45}$$

Therefore, the input weighting matrix is

$$R = 10^{-3}\,\mathrm{diag}([10,\ 4.4,\ 6.4]) \tag{4.46}$$

4.4.2 MPSP and NMPC implementation details

The MPSP and NMPC algorithms are simulated for a control horizon $T_C = 0.1$ h. In the case of NMPC the prediction horizon is set equal to the control horizon. For MPSP the horizon of prediction is by definition the same as the horizon of control.

Both MPSP and NMPC are applied as receding horizon controllers, i.e. the control is calculated from time t_0 to $t_0 + T_C$ where T_C is the fixed control time and t_0 is the current time. Thus, the input trajectory is always $N_C = T_C/T_s$ sampling instances long, where T_s is the sampling time. The time sampling points can be expressed as $\{t_1, t_2, ..., t_{N_C}\} = \{t_0, t_0 + T_s, ..., t_0 + N_C T_s\}$.

When the controller is initiated, i.e. $t_0 = 0$ s, the initial states of the system are provided as well as an initial input trajectory of N_C sampling instances long. The initial input trajectory is not optimal and has to be improved iteratively by the MPSP or NMPC algorithm. Once the algorithm determined a new input trajectory for all the time sampling points when $t_1 = t_0 = 0$ s, the input at $t_1 = 0$ s is implemented and the system moves to the next time step. The time is now at $t_1 = T_s$ and the MPSP or NMPC algorithm repeats. The time series was

$$\{t_1, t_2, ..., t_{N_C}\} = \{0, T_s, ..., N_C T_s\}$$

and is now

$$\{t_1, t_2, ..., t_{N_C}\} = \{T_s, 2T_s, ..., (N_C + 1)T_s\}.$$

A new input trajectory of N_C sampling instances has to be defined before the control algorithm can start again. However, the initial input trajectory for the first minimization routine when $t_1 = 0$ s cannot be used for the next minimization routine when $t_1 = T_s$. The input trajectory for the first minimization routine when $t_1 = 0$ s was only defined until time $t_{N_C} = N_C T_s$. This input trajectory does not define an input for $t_{N_C+1} = (N_C + 1)T_s$ when $t_1 = 0$ s. Therefore, the input trajectory for the second minimization routine requires the definition of an input value for the final time step at $t_{N_C} = (N_C + 1)T_s$ when $t_1 = T_s$. The input trajectory for the second minimization routine at $t_1 = T_s$ is obtained by shifting the input

trajectory calculated during the first minimization routine at $t_1 = 0$ s one sampling instant to the left and equating the input at t_{N_C} to the input at $t_{N_C} - T_s$.

Termination of the MPSP algorithm occurs if all of the following conditions below are met for the three outputs

$$\begin{aligned} \| Y(1)_k^i - Y(1)_k^* \| / \| Y(1)_k^* \| &< 0.05 \\ \| Y(2)_k^i - Y(2)_k^* \| / \| Y(2)_k^* \| &< 0.1 \\ \| Y(3)_k^i - Y(3)_k^* \| / \| Y(3)_k^* \| &< 0.001. \end{aligned} \tag{4.47}$$

or if all of the following conditions below are met for the three inputs

$$\begin{aligned} \| U(1)_k^{i+1} - U(1)_k^* \|_\infty / \| U(1)_k^* \|_\infty &< 0.01 \\ \| U(2)_k^{i+1} - U(2)_k^* \|_\infty / \| U(2)_k^* \|_\infty &< 0.01 \\ \| U(3)_k^{i+1} - U(3)_k^* \|_\infty / \| U(3)_k^* \|_\infty &< 0.01 \end{aligned} \tag{4.48}$$

If these conditions are not met after 10 iterations, the algorithm terminates automatically.

Termination of the NMPC algorithm occurs if the minimization algorithm reached a feasible minimum for the cost function in (4.40), or if the cost function values is less than 0.1, or if 10 iterations were

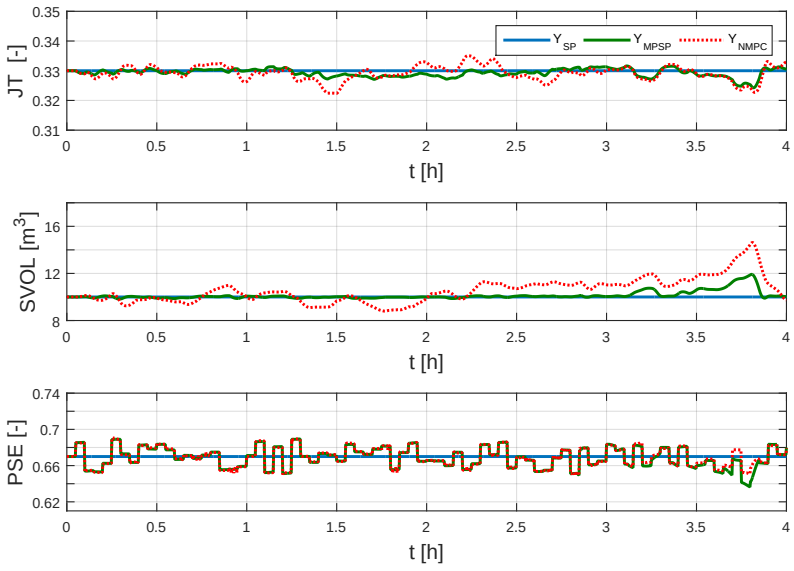

Figure 4.2. Output of the plant when no measurement noise is added to the states, i.e. $X + 0$. [Top: mill total charge fraction (J_T). Middle: sump slurry volume ($SVOL$). Bottom: particle size estimate (PSE). Legend: Y_{SP} is the desired set-point, Y_{MPSP} is the output from the MPSP controller ($T_C = 0.1$ [h]), Y_{NMPC} is the output from the NMPC controller ($T_C = 0.1$ [h]).]

completed.

Finally, the partial derivatives of (4.17) necessary for the MPSP algorithm were explicit functions obtained through symbolic differentiation.

4.4.3 Results

The results of the two simulation scenarios discussed in Section 4.4.1 are shown in Figs. 4.2 to 4.7. To distinguish between the simulations cases, '$X+0$' indicates the case where no measurement noise is added to the states, and '$X+v$' indicates the case where measurement noise is added to the states. Figs. 4.2 and 4.3 show the output of the milling circuit when there is no measurement noise and when there is measurement noise added to the states respectively. Figs. 4.4 and 4.5 show the input to the milling circuit when there is no measurement noise and when there is measurement noise added to the states respectively. Fig. 4.6 shows *PSE* zoomed in between 2 h and 2.5 h for both simulation cases. Fig. 4.7 shows the variation of the parameters every 3 minutes, and also shows the constant disturbances in α_r and κ_F. Fig. 4.8 shows the frequency of the number of iterations per time step.

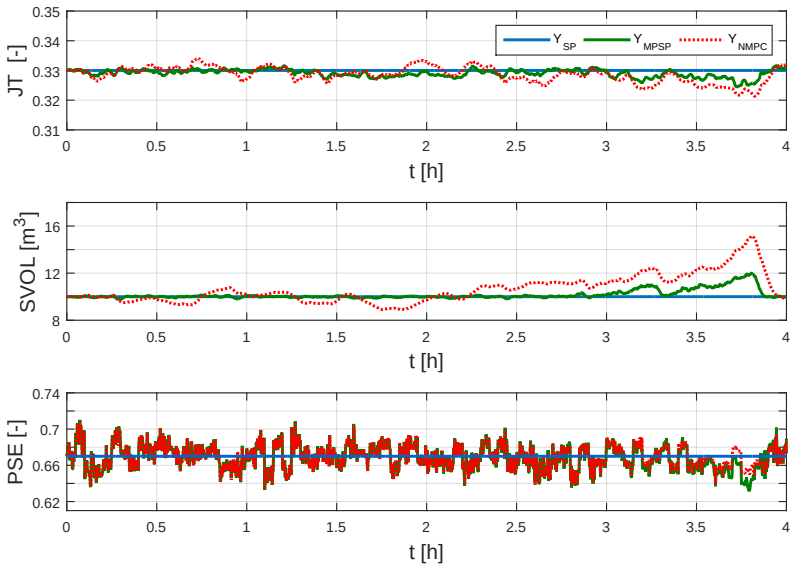

Figure 4.3. Output of the plant when measurement noise is added to the states, i.e. $X+v$. [Top: mill total charge fraction (J_T). Middle: sump slurry volume ($SVOL$). Bottom: particle size estimate (PSE). Legend: Y_{SP} is the desired set-point, Y_{MPSP} is the output from the MPSP controller ($T_C = 0.1$ [h]), Y_{NMPC} is the output from the NMPC controller ($T_C = 0.1$ [h]).]

4.5 DISCUSSION

Table 4.5 shows the normalized root mean squared error between the output of the controllers and the desired set-point. The NMRSE was calculated as

$$NRMSE = \frac{1}{\bar{\lambda}_{SP}} \sqrt{\frac{\sum^{N} (\hat{\lambda} - \lambda_{SP})^2}{N}}$$

where λ_{SP} is the desired set-point, $\bar{\lambda}_{SP}$ is the mean of the set-point over the period, $\hat{\lambda}$ is the process signal, and N is the number of data points. It is interesting to note that the MPSP controller achieves better output regulation than the NMPC controller, especially with regards to $SVOL$. The trends the outputs follow for the NMPC and MPSP controllers are fairly similar, although there is some difference in the trends for J_T. The large deviation of the outputs from set-point after 3 h occurs because CFF is constrained to its maximum allowable rate of 450 m^3/h, as shown in the plots of the inputs in Figs. 4.4 and 4.5.

The measurement noise added to the states appears to have the greatest effect on PSE at the cyclone overflow. This is shown in more detail in Fig. 4.6 where the top plot clearly shows the effect of the

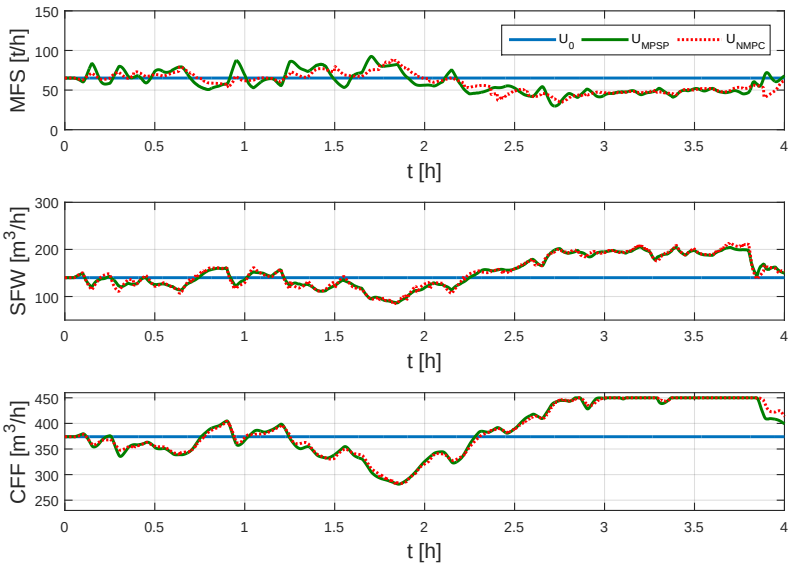

Figure 4.4. Inputs determined by the controllers when no measurement noise is added to the states, i.e. $X + 0$. [Top: mill feed ore (MFO). Middle: sump feed water (SFW). Bottom: cyclone feed flow-rate (CFF). Legend: U_0 is the original operating point of the plant, U_{MPSP} is the input from the MPSP controller ($T_C = 0.1$ [h]), U_{NMPC} is the input from the NMPC controller ($T_C = 0.1$ [h]).]

parameter variation every 3 minutes and the bottom plot shows the effect of the measurement noise added to the states. Because of the integrating effect of the charge in the mill and the charge in the sump, the effect of the high frequency measurement noise added to the states is low-pass filtered for outputs J_T and $SVOL$. However, PSE is calculated using an algebraic function, and the small variations in the state have a significant effect on its value. Since the measurement noise added to the mill states is filtered by the sump, which acts as a buffer between the mill and the cyclone, the noisy states which

Table 4.5. Normalized root mean squared error between desired set-points and outputs for both controllers. ($(X+0)$ - No measurement noise added to states. $(X+\nu)$ - Measurement noise added to states.)

		J_T	$SVOL$	PSE
$X+0$	MPSP	0.46%	3.8%	1.7%
	NMPC	0.77%	12 %	1.6%
$X+\nu$	MPSP	0.49%	4.4%	2.0%
	NMPC	0.89%	14%	1.8%

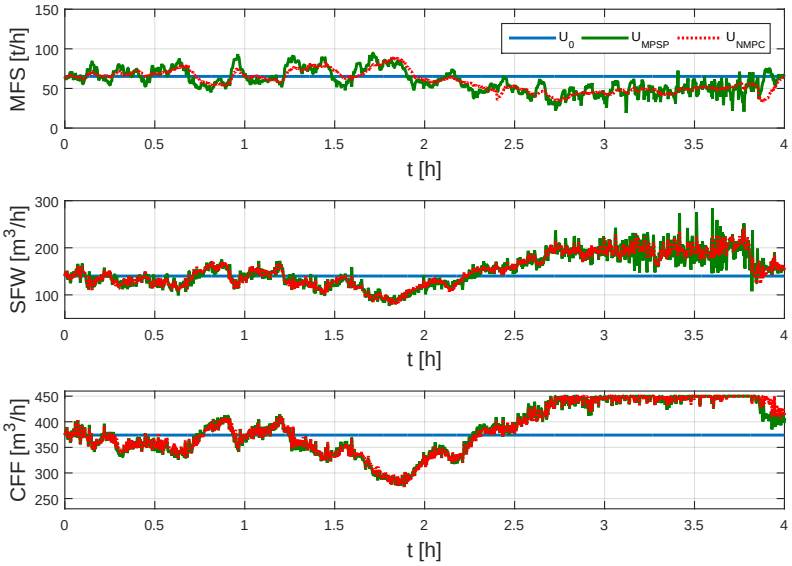

Figure 4.5. Inputs determined by the controllers when measurement noise is added to the states i.e. $X+\nu$. [Top: mill feed solids (MFO). Middle: sump feed water (SFW). Bottom: cyclone feed flow-rate (CFF). Legend: U_0 is original operating point of the plant, U_{MPSP} is the input from the MPSP controller ($T_C = 0.1$ [h]), U_{NMPC} is the input from the NMPC controller ($T_C = 0.1$ [h]).]

contribute most to the variations in *PSE* are x_{sw}, x_{ss} and x_{sf} respectively. Of specific importance is the noise added to x_{sf}, since the volume of fines in the sump is the most significant contributor to *PSE*, as shown in (4.15). What is apparent from Fig. 4.6 is that both controllers struggle to reject measurement noise added to the states.

The model-plant mismatch created by varying the plant parameters every 3 minutes does not appear to

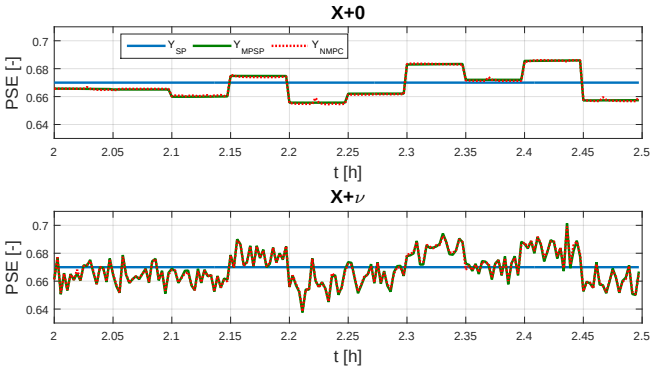

Figure 4.6. A zoomed in plot of (*PSE*) between 2 h and 2.5 h for both simulation cases. The top plot clearly shows the effect of the parameter variation every 3 minutes. For the bottom plot, the noise added to the states dominate the plot.

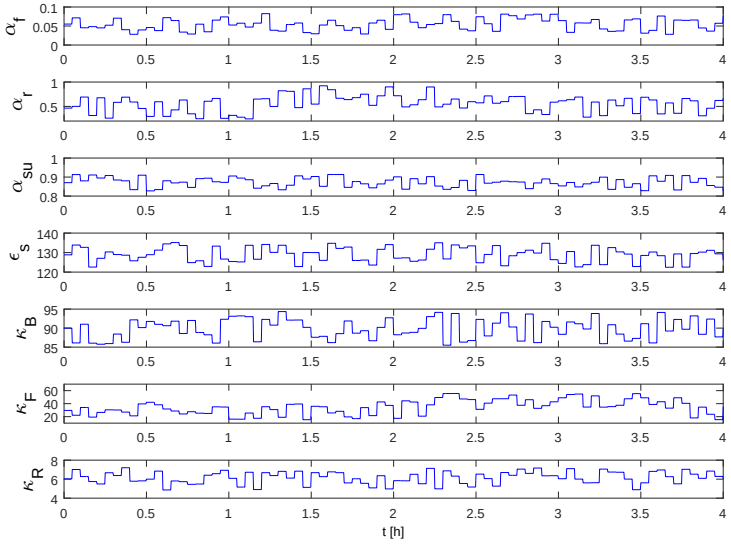

Figure 4.7. The variation of parameters α_f, α_r, $\alpha_s u$, ε_c, κ_B, κ_F and κ_R every 3 minutes (0.1 h) according to their respective uncertainties shown in Tables 4.2. The step disturbances in α_r between 1.2 h and 2.8 h and κ_F between 2.2 and 3.8 h can be seen in the graphs of α_r and κ_F respectively.

have a detrimental effect on overall plant performance. The mismatch effect can be seen most clearly in the top plot of Fig. 4.6. Both controllers are able to maintain an acceptable level of plant performance, but neither controller can fully reject the mismatch.

The step disturbance between 1.2 h and 2.8 h in α_r, as shown in Fig. 4.7, does not seem to have a significant impact on the overall performance of the milling circuit. No significant change in the plant's inputs can be seen to compensate for this disturbance. Another contributing factor that may possibly diminish the effect of this disturbance can be the variation of κ_R.

The effect of the step disturbance between 2.2 h and 3.8 h in κ_F can be seen most clearly in the use of CFF by both controllers. An increase in this parameter simulates a case where the ore hardened and it takes longer for the ore to grind sufficiently fine. In order to maintain the required PSE, it is necessary for CFF to increase. However, an increase in CFF will result in a decrease of $SVOL$. The decrease in $SVOL$ is negated by increasing the flow of SFW. Because more energy is required to break the ore, it takes longer to break. As shown in Figs. 4.4 and 4.5, MFO decreases slightly to maintain a constant J_T. Because CFF is constrained after approximately 3 h, as shown in Figs. 4.4 and 4.5, PSE cannot

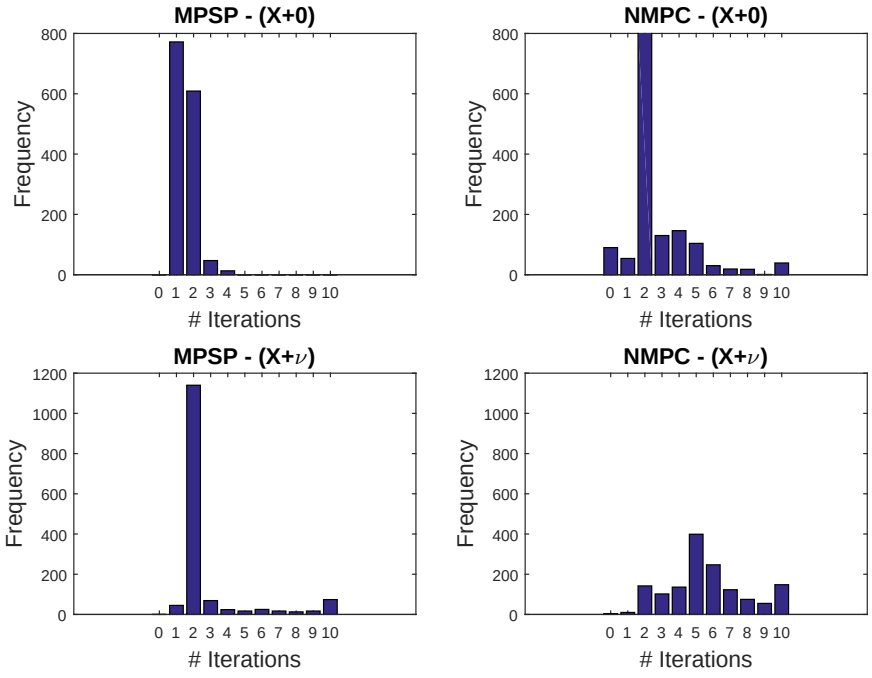

Figure 4.8. Algorithm iterations frequency. [$(X+0)$ - no noise added to states. $(X+v)$ - noise added to states.]

be maintained at set-point, as shown in Figs. 4.2 and 4.3.

Fig. 4.8 shows the frequency of the number of iterations per time step needed by both the MPSP and NMPC minimization algorithms to reach a solution. It should be remembered that the MPSP and NMPC routines were limited to a maximum of 10 iterations. As seen from Figs. 4.8, for the simulation scenarios considered in this paper, 2 iterations of the MPSP routine is usually sufficient to find an optimal solution. When noise is added to the states, the MPSP algorithm may require a few more iterations to achieve a feasible solution. On the other hand, the NMPC algorithm usually achieves convergence within 3 iterations if no noise is added to the states, and between 3 and 6 iterations if noise is added to the states.

It is regarded as unfair to compare the computational time for the custom programmed MPSP routine to the NMPC routine implemented with the *fmincon* function of the Optimization Toolbox of MATLAB. The custom programmed MPSP routine does not call as many subroutines and error handling routines as *fmincon*. However, for interest sake the average computational time required for one iteration of the MPSP routine was 0.23 s. The average computational time for the *fmincon* function to complete one iteration was 2.1 s. Simulations were carried out on a 64-bit system with 8GB RAM and an Intel Core i7-3450M CPU @ 3.00 GHz in MATLAB R2015a. Obviously the computational time of both routines can be decreased, but it is encouraging to note that the large number of matrix operations for the MPSP routine is handled quickly and effectively.

4.6 CONCLUSION

Output tracking using MPSP was successfully applied to a non-linear model of a single-stage closed grinding mill circuit. The performance of the proposed MPSP controller was evaluated against the performance of a standard constrained NMPC controller applied to the same plant for the same conditions. The aim of this work is not to compare the mathematical details of each minimization algorithm, but rather to show the control abilities of MPSP in the presence of noise, model-plant mismatch, disturbances and input box constraints.

Results indicate that the performance of the MPSP controller compares favourably to the performance of an NMPC controller. Compared to NMPC, MPSP achieved improved output regulation in the

presence of model-plant mismatch, disturbances and measurement noise. Even if the MPSP algorithm is limited to two iterations per time step, it is still capable of controlling the plant with adequate accuracy. The advantage of MPSP is that the computational burden is decreased by converting the dynamic optimization problem to a low-dimensional static optimization problem, calculating the sensitivity matrices recursively and using a closed form expression to update the control. Although the prediction and control horizons are equal in MPSP, this does not lead to substantially increased computational time. If these horizons are decreased further the computational time should also decrease, but at the cost of control performance. Further improvements to the computational time of MPSP can be achieved by using improved matrix operation programming techniques for performing matrix inverses and multiplication. Future work for MPSP will involve the application of equality and inequality constraints for states, inputs and outputs in the algorithm formulation, as well as creating a framework for a robust MPSP controller.

MPSP shows promise as a suitable option for non-linear model-based optimal control for output tracking in large industrial processes, especially if computational time and complexity is a limiting factor for the real-time application of a model-based optimal controller.

Because of the limited number of real-time measurements available on industrial circuits, full state feedback, as used above for the MPSP and NMPC controllers, is rarely possible. A common method of MPC feedback is a comparison between the measured output and the model prediction at time k to generate a disturbance estimate. This disturbance term is then added to the output prediction over the entire prediction horizon when formulating the MPC objective function. The implicit assumption is that the disturbance estimate is due to an additive step disturbance which persists in the output for the entire prediction horizon. Although this constant disturbance error model can accurately model setpoint changes which enter the feedback loop as step disturbances, approximate slowly varying disturbances, and provide zero offset for step changes in setpoints, it remains sensitive to random fluctuations in the output. In the case of stable processes, the constant disturbance model provides integral action for the controller, but for integrating and unstable processes the constant disturbance model fails because the estimator contains the unstable poles of the process (Meadows and Rawlings 1997, Qin and Badgwell 2003).

The disadvantages of a constant disturbance model for MPC feedback can easily be addressed by updating the controller model with state and parameter estimates from a state observer (Olivier and

Craig 2013, Le Roux *et al.* 2016a). However, in the case of grinding mill circuits, only a limited number of states and parameters can be realistically estimated from measurements commonly found at industrial circuits. The next chapter investigates which states and parameters can be realistically estimated from measurements at the inflow and outflow of the mill. Furthermore, an observer model with states and parameters linearly observable from mill measurements is developed.

CHAPTER 5 STATE AND PARAMETER ESTIMATION FOR A GRINDING MILL

The aim of this chapter is to develop an observer for use in model-based control strategies of grinding mill circuits (Le Roux *et al.* 2016a, Cortinovis, Mercangöz, Mathur, Poland and Blaumann 2013). An observer model is developed for a SAG mill with states and parameters that are linearly observable from mill inflow, discharge, and total volumetric filling measurements. A proof of observability is provided to indicate which measurements are required for the model to provide a reliable estimation. A simulation study using an EKF is presented to illustrate the effectiveness of the observer.

The chapter is organized as shown below:

1. Section 5.1 discusses the non-linear observer model used to describe the grinding mill.

2. Section 5.2 describes the observability analysis of the non-linear observer model, and the model reduction to obtain a model with states which are linearly observable.

3. Section 5.3 gives a brief description of the design of the EKF.

4. Section 5.4 provides a simulation study for the observer.

5. Section 5.5 discusses the results.

6. Section 5.6 concludes the chapter.

5.1 OBSERVER MODEL FOR A GRINDING MILL

As depicted in Fig. 5.1, only the SAG mill in the single-stage closed grinding circuit described in Section 2.1.1 is considered in this chapter. The variables of interest for the SAG mill are shown in Table 5.1. As discussed in Section 2.1.2, P_{mill} and J_T are commonly measured variables, whereas Q and ρ_Q are not generally included as real-time measured variables on industrial plants. To illustrate the benefits to be gained from including Q and ρ_Q measurement instrumentation on industrial circuits, it is assumed measurements of Q and ρ_Q are available.

This section describes how the observer model is developed. The modelling approach is similar to the mill model of Le Roux *et al.* (2013b) described in Section 4.1.1. However, in this case, use is made of the breakage rate modelling results of Hinde and Kalala (2009), and the discharge flow-rate modelling results of Morrell and Stephenson (1996), and Latchireddi and Morrell (2003), to develop the observer model. The aim of the observer is to use the variables listed in Table 5.1 as measured quantities to estimate the mill states, the discharge rate constant, and the ore and ball breakage rates. The nomenclature for the model is given in Table 5.2.

The constituents in the mill are modelled as four volumetric quantities: water (x_w), solids (x_s), rocks (x_r), and balls (x_b). The observer model makes use of only two size classes to describe ore in the mill:

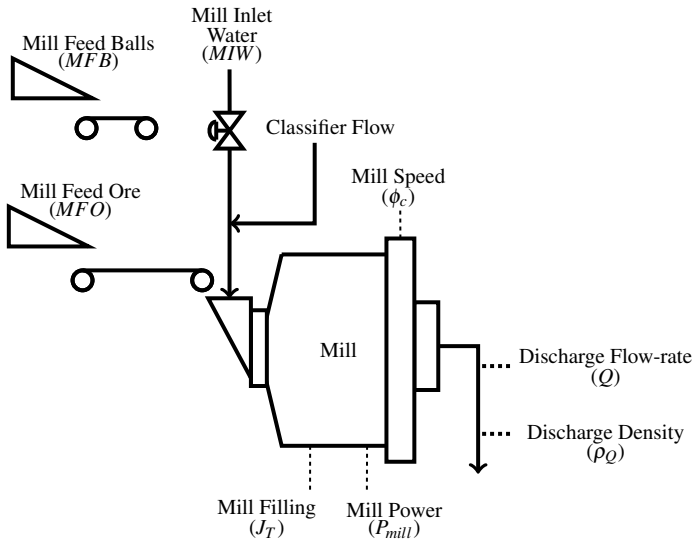

Figure 5.1. A semi-autogenous grinding mill.

solids includes all ore smaller than the end-discharge grate aperture size, and *rocks* all ore larger than the aperture size.

5.1.1 Process dynamics

5.1.1.1 Process feed

Similar to (4.2), the mill feed flow-rates are described as

$$V_{wi} = MIW + V_{cw} \tag{5.1a}$$

$$V_{si} = MFO(1-\alpha_r)/\rho_O + V_{cs} \tag{5.1b}$$

$$V_{ri} = \alpha_r MFO/\rho_O \tag{5.1c}$$

$$V_{bi} = MFB/\rho_B \tag{5.1d}$$

where V_{wi}, V_{si}, V_{ri}, and V_{bi} (m^3/h) are the mill inflow of water, solids, rocks, and balls respectively, and V_{cw} and V_{cs} (m^3/h) are the flow of water and solids returned by the classifier respectively. It is assumed that the flow from the classifier to the mill is known. Parameter α_r, which defines the mass fraction of rocks in MFO, is assumed to be measured as a function of time (Wei and Craig 2009b). The implicit assumption when dividing by ρ_O in (5.1b) and (5.1c) is that the ore is non-porous.

Table 5.1. Description of circuit variables assumed to be measured.

Variable	Unit	Description
MIW	[m^3/h]	Flow-rate of water to the mill
MFO	[t/h]	Feed-rate of ore to the mill
MFB	[t/h]	Feed-rate of steel balls to the mill
J_T	[-]	Fraction of mill volume filled with charge
Q	[m^3/h]	Mill discharge flow-rate
ρ_Q	[t/m^3]	Mill discharge density
P_{mill}	[kW]	Mill power draw

5.1.1.2 Population balance

The population balance used to describe the kinetics of the states defined above is

$$\dot{x}_w = V_{wi} - V_{wo} \tag{5.2a}$$

$$\dot{x}_s = V_{si} - V_{so} + RC \tag{5.2b}$$

$$\dot{x}_r = V_{ri} - RC \tag{5.2c}$$

$$\dot{x}_b = V_{bi} - BC \tag{5.2d}$$

where V_{wo} and V_{so} (m^3/h) are the discharge of water and solids from the mill respectively, and RC and BC (m^3/h) are the consumption of rocks and balls respectively. Because the mill is fitted with an end-discharge grate, no rocks or balls are discharged from the mill. It is assumed the mill is a fully mixed reactor. The rate of ball consumption is considerably slower than for rocks, and its contribution to solids is regarded as negligible.

Table 5.2. Observer Model Nomenclature

Parm	Unit	Description
α_r	[-]	Fraction rock in the feed ore
ρ_B	[t/m^3]	Density of steel balls
ρ_O	[t/m^3]	Density of feed ore
ρ_W	[t/m^3]	Density of water
η	[$h^{-1}m^{-3}$]	Discharge rate per volume of slurry
K_b	[1/h]	Ball abrasion rate
K_r	[1/h]	Rock abrasion rate
v_{mill}	[m^3]	Mill volume
x_b	[m^3]	Volume of balls in the mill
x_r	[m^3]	Volume of rocks in the mill
x_s	[m^3]	Volume of solids in the mill
x_w	[m^3]	Volume of water in the mill

5.1.1.3 Breakage rates

The cumulative rates modelling approach assumes only one function is necessary to describe the grinding kinetics. The cumulative breakage rate function is defined as the rate per unit mass that a given species coarser than a given size breaks to below that size (Le Roux and Craig 2013). This is an advantage over other population balance models which require two functions, a breakage rate and an appearance function, to describe grinding kinetics (Whiten 1974). The cumulative breakage rates modelling approach was used by Austin, Sutherland and Gottlieb (1993) to model the steady-state behaviour and by Amestica, Gonzalez, Barria, Magne, Menacho and Castro (1993) and Amestica *et al.* (1996) to model the dynamic behaviour of SAG mills. A disadvantage of this approach is that the cumulative rate of breakage of ore above a given size s_i is assumed to be unaffected by the grinding environment and the detailed structure of the size distribution above s_i. Empirical relationships are required to relate the parameters of the cumulative breakage rate function to variations in the milling environment. However, more sophisticated models face similar problems where the parameters of both the breakage rate and breakage distribution function vary according to changes in the grinding environment (Hinde and Kalala 2009). The cumulative breakage rate function remains constant if the ball filling level and the charge level remain relatively constant (Amestica *et al.* 1993). A validation study of the cumulative rates model was conducted by Salazar *et al.* (2009), and a model predictive controller using the cumulative rates model was investigated in simulation by Salazar *et al.* (2014).

Similar to the cumulative rates modelling approach, the consumption of rocks (RC) and balls (BC) in the population balance of (5.2b) to (5.2d) are described as

$$RC = x_r K_r \tag{5.3a}$$

$$BC = x_b K_b \tag{5.3b}$$

where K_r and K_b (1/h) are the abrasion rates of rocks and balls respectively.

A relatively constant rock abrasion rate K_r can be achieved through a high x_b (as in the case of a ball mill), but the heavy balls increase the power required to turn the mill and consequently increase the energy costs. The ball abrasion rate K_b depends on the ore characteristics, the mill liner type, the ball material, x_r, and x_b. A high x_b increases K_b as there is more ball-ball and ball-liner contact rather than ball-ore contact. Although a low x_b reduces K_b, it also reduces the grinding ability of the mill. For a

very high mill rotational rate the balls may collide with exposed liners causing unnecessary liner wear and a higher K_b.

5.1.1.4 Mill discharge

The mill discharge model for the observer is adapted from the model presented in Morrell and Stephenson (1996), where the discharge of charge from the mill through the end-discharge grate is viewed as a product of two mechanisms: the fluid transport through the grate, and the solids classification by the grate which differentiates between ground particles either returning to the milling chamber for further grinding or becoming part of the mill discharge stream. In the case of $i = 1, 2, ..., N$ ore size classes, the discharge rate (d_i) (h^{-1}) of the mill charge is approximated as (Morrell 2004)

$$\begin{aligned} d_i &= d_0 \qquad\qquad ; \quad s_i \leq s_m \\ d_i &= d_0 \frac{\ln s_i - \ln s_g}{\ln s_m - \ln s_g} \quad ; \quad s_m < s_i \leq s_g \\ d_i &= 0 \qquad\qquad ; \quad s_i > s_g, \end{aligned} \tag{5.4}$$

where s_i (mm) represents the particle size classes, d_0 (h^{-1}) is the specific discharge rate for water and ore up to particle size s_m (mm) (i.e. slurry), and s_g (mm) is the effective mesh size of the grate above which discharge is zero. Since rocks and balls are larger than s_g, they have a discharge rate of 0 h^{-1}.

To determine d_0, a function relating slurry hold-up to slurry flow (i.e. flow of particles smaller than s_m exhibiting the same flow characteristics as water) out of the mill is required. This function should account for whether the slurry flow occurs via the grinding media or via a slurry pool. The slurry flowing through a single grate aperture depends on the following factors: area of the aperture, depth of the aperture below the free surface of the slurry, gravity and centrifugal forces, and slurry viscosity. By analysing pilot and industrial mills, Morrell and Stephenson (1996) expressed the relationship between slurry flow-rate and hold-up for the case where slurry flow occurs via the grinding media and for the case where slurry flow occurs via the slurry pool. Slurry flow via the grinding media Q_m (m^3/h) is expressed as

$$Q_m = k_m J_{pm}^2 \lambda^{2.5} D_m^{0.5} A \phi_c^{-1.38} \quad ; \quad J_p \leq J_{max}, \tag{5.5}$$

where k_m ($m^{0.5}/h$) is a constant, J_{pm} is the net fractional slurry hold-up in the grinding media, D_m (m) is the mill diameter, A (m^2) is the total open area of the grate apertures, ϕ_c is the fraction of the critical mill speed, J_p is the net fraction of the mill volume filled with slurry hold-up in the grinding

media plus the pool zone, $J_{max} = 0.5J_T - J_{po}$ is the maximum net fractional slurry hold-up within the interstices of the grinding media, $J_{po} = 0.33(1 - \bar{r}_a)$ is the fractional "dead" slurry hold-up within the mill (contained between the mill shell and the outer most grate aperture), and $\bar{r}_a$ (m) is the radial position of the outermost row of grate apertures as a fraction of the mill radius r_m. The mean relative radial position of the grate apertures is defined as $\lambda = \frac{\sum r_i a_i}{r_m \sum a_i}$ where a_i is the open area of all holes at a radial position r_i. Slurry flow via the slurry pool Q_t (m^3/h) is expressed as

$$Q_t = k_t J_{pt} \lambda^2 D_m^{0.5} A \quad ; \quad J_p > J_{max} \quad ; \quad J_{pt} = J_p - J_{max}, \tag{5.6}$$

where J_{pt} is the net fractional hold-up of slurry in the slurry pool, and k_t (m$^{0.5}$/h) is a constant.

It is worth noting the inverse relationship between ϕ_c and Q_m in (5.5). A possible reason for this relationship is the increase in the dynamic porosity (void fraction) of the charge as the mill speed increases (Latchireddi and Morrell 2003). Also, the grinding media thrown from the charge shoulder overshoots the charge toe because of the higher speed. As a result of the overshoot the number of high impact breakage events reduces and consequently the fines contributing to the mill slurry reduce. Morrell and Stephenson (1996) assumed the viscosity effects would be captured by the constants k_m and k_t without altering the form of (5.5) and (5.6).

Solids between sizes s_m and s_g also exit the mill and contribute approximately 5-15% to the volumetric flow-rate depending on the size of the grates. To predict the total flow-rate of slurry out of the mill Q, the predictions for Q_m and Q_t need to be increased to account for the additional amount of coarse material. Therefore

$$Q = k_g(Q_m + Q_t), \tag{5.7}$$

where k_g is a positive dimensionless factor to account for coarse material. The value of k_g varies depending on the grate aperture size. Morrell and Stephenson (1996) provide guidelines on the choice of k_g.

In the inferential measurement work of Apelt *et al.* (2002a) it is assumed that no slurry pooling occurs in the case of a large open area (A), a high relative radial position of the open area (λ), and a high relative radial position of the outermost apertures ($\bar{r}_a$) in the end-discharge grate. For this study it was assumed that the discharge flow is only through the grinding media, i.e. $Q = k_g Q_m$. Therefore, assuming no slurry pooling, Q can be approximated as (Kojovic, Powell, Bailey and Drinkwater 2011)

$$Q = k_g k_m \lambda^{2.5} D_m^{0.5} A \phi_c^{-1.38} J_{pm}^2. \tag{5.8}$$

As shown in (5.8), Q is quadratically proportional to J_{pm} if there is no slurry pool. Thus, in terms of the four states of the observer defined (x_w, x_s, x_r, and x_b), it is possible to express Q as

$$Q = \eta \left(x_w + x_s\right)^2 \tag{5.9}$$

where $(x_w + x_s)$ represents the total slurry hold-up in the mill, and η ($\mathrm{h}^{-1}\mathrm{m}^{-3}$) is the discharge rate per volume of slurry. Since only two size classes are used for the observer model, one size which discharges completely and one which remains inside the mill, it is implicitly assumed in (5.9) that $s_g = s_m$ in (5.4). Therefore, the discharge of the water (V_{wo}) and solids (V_{so}) in (5.2a) and (5.2b) can be expressed as

$$V_{wo} = \eta \left(x_w + x_s\right) x_w \tag{5.10a}$$

$$V_{so} = \eta \left(x_w + x_s\right) x_s. \tag{5.10b}$$

5.1.2 Process output

For this study, it is assumed that measurements of J_T, Q and ρ_Q are available. The implications of measuring these variables are discussed in Section 2.1.2. These quantities are modelled as

$$J_T = \frac{x_w + x_s + x_r + x_b}{v_{mill}} \tag{5.11a}$$

$$Q = \eta \left(x_w + x_s\right)^2 \tag{5.11b}$$

$$\rho_Q = \frac{\rho_O x_s + \rho_W x_w}{x_s + x_w}. \tag{5.11c}$$

The fourth measured output listed in Table 5.1 is P_{mill} (kW), which is defined by Apelt *et al.* (2001) as

$$P_{mill} = P_{NL} + k_P P_C, \tag{5.12}$$

where P_{NL} (kW) is the no-load power (empty mill power draw), P_C (kW) is the mill power draw attributed to the mill contents, and k_P is a lumped power draw parameter to account for heat losses due to internal friction, energy for attrition and abrasion breakage and rotation of grinding media, plus inaccuracies associated with the assumptions and measurements of the charge shape and motion Napier-Munn *et al.* (2005).

Apelt *et al.* (2001) models P_C as an empirical function of J_T and the mill charge density (ρ_C)

$$\rho_C = \frac{\rho_b x_b + \rho_o \left(x_r + x_s\right) + \rho_w x_w}{x_b + x_r + x_s + x_w}. \tag{5.13}$$

Ideally ρ_C could be inferred from the measurement of P_{mill} using the power draw model in Apelt *et al.* (2001). However, to use the model, parameter k_P in (5.12) must be fitted to process data. This fitting process requires ρ_C to be known. Therefore, the observer model does not make use of P_{mill} as an output equation as it only introduces additional parameters to estimate. The same holds true for other models of P_{mill}, such as for example the models in Austin (1990) and Le Roux *et al.* (2013b).

5.2 OBSERVABILITY OF STATES AND PARAMETERS

5.2.1 Background

A multi-input-multi-output control-affine nonlinear state-space model with $\dim(x) = n$ and $\dim(y) = m$ can be written as

$$\begin{aligned} \dot{x} &= f(x) + g(x)u \\ y &= h(x). \end{aligned} \tag{5.14}$$

The system in (5.14) is said to be locally (weakly) observable at x_0 if there exists a neighbourhood X_0 of x_0 such that for every x_1 which is an element of the neighbourhood $X_1 \subset X_0$ of x_0 the indistinguishability of the states x_0 and x_1 implies that $x_0 = x_1$. The two states x_1 and x_0 are said to be indistinguishable if for every admissible input u the output y of (5.14) for the initial state x_0 and for the initial state x_1 is identical. If the system satisfies the so called observability rank condition, i.e. the observability codistribution of x_0 (Hermann and Krener 1977)

$$d\mathcal{O} = \text{span}\left\{\mathrm{d}h_j, \mathrm{d}L_f h_j, \ldots, \mathrm{d}L_f^{n-1} h_j\right\};\ j = 1 \ldots m \tag{5.15}$$

has dimension n at x_0, then the system is locally (weakly) observable. Note, $L_f^k h_j$ refers to the k-th repeated Lie derivative of the scalar function $h_j(x)$ along the vector field $f(x)$, and d is the exterior derivative (Doyle and Henson 1997). In the linear case, the observability codistribution corresponds to the observability matrix $\mathcal{O}^T = \left[C^T, A^T C^T, \ldots, (A^{n-1})^T C^T\right]$ where $C = \frac{\partial h}{\partial x}|_{x=x_0}$ and $A = \frac{\partial}{\partial x}\left(f(x) + g(x)u\right)|_{x=x_0,\ u=u_0}$.

5.2.2 Analysis of observer model

For the observer model of the grinding mill, it is assumed that the parameters η, K_r and K_b are unknown constants, although in practice these parameters may vary slowly. Thus, the observer model described

in Section 5.1 can be written in the form of (5.14), such that

$$\dot{x} = f_O(x) + g_O(x)\,u = \begin{bmatrix} -\eta\,(x_w + x_s)\,x_w \\ -\eta\,(x_w + x_s)\,x_s + x_r K_r \\ -x_r K_r \\ -x_b K_b \\ 0_{3\times 1} \end{bmatrix} + \begin{bmatrix} I_{4\times 4} \\ 0_{3\times 4} \end{bmatrix} u \tag{5.16a}$$

$$y = h_O(x) \qquad = [J_T, Q, \rho_Q]^T \tag{5.16b}$$

where $x = [x_w, x_s, x_r, x_b, \eta, K_r, K_b]^T$, $u = [V_{wi}, V_{si}, V_{ri}, V_{bi}]^T$ and $y = h_O(x)$ is given by (5.11). (The subscript O refers to *Observer*.)

For the system in (5.16), the dimension of the observability codistribution $d\mathcal{O}$ was determined using Maple[1]. The dimension of $d\mathcal{O}$ at a generic point x_0 is 7, which implies that the nonlinear system is locally (weakly) observable. Thus, a non-linear observer such as a moving horizon estimator (MHE) could possibly estimate the unknown states and parameters. However, it is necessary to correctly assume the time-varying nature of the parameters for the MHE to estimate the true state and parameter values. A longer time horizon for the MHE reduces the validity of modelling the parameters as constants, but a shorter time horizon may not include sufficient system dynamics for the observer to estimate the unknown states and parameters.

Linearisation of (5.16) results in the A and C matrices

$$A = \begin{bmatrix} -\eta\,(2x_w + x_s) & -\eta x_w & 0 & 0 & -(x_w + x_s)\,x_w & 0 & 0 \\ -\eta x_s & -\eta\,(x_w + 2x_s) & K_r & 0 & -(x_w + x_s)\,x_s & x_r & 0 \\ 0 & 0 & -K_r & 0 & 0 & -x_r & 0 \\ 0 & 0 & 0 & -K_b & 0 & 0 & -x_b \\ 0_{3\times 1} & 0_{3\times 1} & 0_{3\times 1} & 0_{3\times 1} & 0_{3\times 1} & 0_{3\times 1} & 0_{3\times 1} \end{bmatrix} \tag{5.17a}$$

$$C = \begin{bmatrix} \frac{1}{v_{mill}} & \frac{1}{v_{mill}} & \frac{1}{v_{mill}} & \frac{1}{v_{mill}} & 0 & 0_{1\times 2} \\ 2\eta\,(x_w + x_s) & 2\eta\,(x_w + x_s) & 0 & 0 & (x_w + x_s)^2 & 0_{1\times 2} \\ \frac{\rho_W - \rho_Q}{x_w + x_s} & \frac{\rho_O - \rho_Q}{x_w + x_s} & 0 & 0 & 0 & 0_{1\times 2} \end{bmatrix}. \tag{5.17b}$$

The observability matrix $\mathcal{O}$ formed from (5.17) has rank 5. From an analysis of the eigenvalues and eigenvectors of the matrix A it can be seen that the three unknown parameters (η, K_r, K_b) each contribute an integral mode to the linearised system. Because of this repeated mode, two of the

[1] Maple^{TM} is a trademark of Waterloo Maple Inc.

three parameters need to be chosen in the linearised model for the other parameter to be linearly observable.

In an attempt to attain linear observability of the system, the time derivatives of (5.16b) can be used as additional measurements. However, the addition of $\dot{J}_T$, $\dot{Q}$, or $\dot{\rho}_Q$, or all of these derivatives only increases the rank of the observability matrix $\mathcal{O}$ from 5 to 6. To achieve full column rank, the measurement ρ_C needs to be used along with $\dot{Q}$, or $\dot{\rho}_Q$, or both (Le Roux, Steinboeck, Kugi and Craig 2016c). However, direct measurement of ρ_C is rarely possible. If ρ_C is estimated from P_{mill}, additional unknown parameters are introduced which negates any benefit of using ρ_C as an inferred measured variable. (For further details on the observability analysis, refer to the Appendix.)

5.2.3 Model reduction and linear observability

5.2.3.1 Reduced model

To achieve linear observability, the model in (5.16) is reduced based on the assumption that the dynamics of the slurry (x_w and x_s) is much faster than the dynamics of the grinding media (x_r and x_b). Therefore,

$$\dot{x} = f_{RM}(x) + g_{RM}(x)\,u = \begin{bmatrix} -\eta\,(x_w + x_s)\,x_w \\ -\eta\,(x_w + x_s)\,x_s + \chi \\ 0_{3\times 1} \end{bmatrix} + \begin{bmatrix} I_{2\times 2} \\ 0_{3\times 2} \end{bmatrix} u \tag{5.18a}$$

$$y = h_{RM}(x,u) = \begin{bmatrix} \frac{x_w + x_s + x_{rb}}{v_{mill}} \\ \eta\,(x_w + x_s)^2 \\ \frac{\rho_O x_s + \rho_W x_w}{x_s + x_w} \\ \frac{(\rho_O - \rho_W)(\chi x_w + x_w V_{si} - x_s V_{wi})}{(x_s + x_w)^2} \end{bmatrix} \tag{5.18b}$$

where $x = [x_w, x_s, x_{rb}, \eta, \chi]^T$, $u = [V_{wi}, V_{si}]^T$, and $y = [J_T, Q, \rho_Q, \dot{\rho}_Q]^T$. (The subscript *RM* refers to *Reduced Model*.) The state x_{rb} (m^3) represents all grinding media in the mill (sum of rocks and balls) which is assumed to stay relatively constant compared to x_w and x_s, and the state χ (m^3/h) represents the accumulation of solids. The output vector in (5.11) is extended in (5.18b) with the addition of $\dot{\rho}_q$.

5.2.3.2 Linear observability

The A and C matrices for the system in (5.18) are

$$A = \begin{bmatrix} -\eta(2x_w + x_s) & -\eta x_w & 0 & -(x_w + x_s)x_w & 0 \\ -\eta x_s & -\eta(x_w + 2x_s) & 0 & -(x_w + x_s)x_s & 1 \\ 0_{3\times1} & 0_{3\times1} & 0_{3\times1} & 0_{3\times1} & 0_{3\times1} \end{bmatrix} \tag{5.19a}$$

$$C = \begin{bmatrix} \frac{1}{v_{mill}} & \frac{1}{v_{mill}} & \frac{1}{v_{mill}} & 0 & 0 \\ 2\eta(x_w + x_s) & 2\eta(x_w + x_s) & 0 & (x_w + x_s)^2 & 0 \\ \frac{\rho_W - \rho_Q}{x_w + x_s} & \frac{\rho_O - \rho_Q}{x_w + x_s} & 0 & 0 & 0 \\ \frac{(\rho_O - \rho_W)(\chi + V_{si})}{(x_w + x_s)^2} - \frac{2\dot{\rho}_Q}{x_w + x_s} & \frac{(\rho_W - \rho_O)V_{wi}}{(x_w + x_s)^2} - \frac{2\dot{\rho}_Q}{x_w + x_s} & 0 & 0 & \frac{(\rho_O - \rho_W)x_w}{(x_w + x_s)^2} \end{bmatrix}. \tag{5.19b}$$

The observability matrix $\mathcal{O}$ of the pair (C, A) has full column rank. Therefore, all states and parameters are observable from the system outputs. However, at steady-state, $\dot{\rho}_Q$ will be equal to zero and the observability matrix $\mathcal{O}$ will no longer have full column rank. (The determinant of the first 5 rows and columns is $\det(\mathcal{O}_{1..5,1..5}) = (\rho_O - \rho_W)\dot{\rho}_Q / v_{mill}^2$ which reduces to zero at steady-state.) For a reasonable value of $\dot{\rho}_Q$ it is necessary to continuously excite the system.

As seen in (5.18b), the derivative of ρ_Q is used as a fourth measurement. This is necessary to achieve linear observability. If $\dot{J}_T$ is used instead of $\dot{\rho}_Q$ in (5.18b), the observability matrix $\mathcal{O}$ does not have full column rank. Although $\dot{Q}$ could be used to achieve full column rank, it is a function of $\dot{\eta}$ which is assumed to be equal to zero in (5.18a). Rather than including the assumption that $\dot{\eta} = 0$ in the measurement model, $\dot{\rho}_Q$ is used in (5.18b).

The eigenvalues of A in (5.19a) are

$$\lambda = \{-2\eta(x_w + x_s), -\eta(x_w + x_s), 0, 0, 0\} \tag{5.20}$$

and the associated eigenvectors are

$$T = \begin{bmatrix} \frac{x_w}{x_s} & -1 & \frac{-x_w}{2\eta(x_w + x_s)^2} & \frac{-x_w}{2\eta} & 0 \\ 1 & 1 & \frac{x_s + 2x_w}{2\eta(x_w + x_s)^2} & \frac{-x_s}{2\eta} & 0 \\ 0 & 0 & 0 & 0 & 1 \\ 0 & 0 & 0 & 1 & 0 \\ 0 & 0 & 1 & 0 & 0 \end{bmatrix}. \tag{5.21}$$

The output pole matrix $Y_\lambda = CT$ is

$$Y_\lambda = \begin{bmatrix} \frac{x_w+x_s}{v_{mill}x_s} & 0 & \frac{1}{2\eta(x_w+x_s)v_{mill}} & \frac{-x_w-x_s}{2\eta v_{mill}} & \frac{1}{v_{mill}} \\ \frac{2\eta(x_w+x_s)^2}{x_s} & 0 & 1 & 0 & 0 \\ 0 & \frac{\rho_O-\rho_W}{x_w+x_s} & \frac{x_w(\rho_O+\rho_W)}{\eta(x_w+x_s)^3} & 0 & 0 \\ \frac{(\rho_W-\rho_O)\dot{\rho}_Q}{x_s} & \frac{(\rho_W-\rho_O)(\chi+V_{si}+V_{wi})}{(x_w+x_s)^2} & \frac{(\rho_W-\rho_O)\left(x_w\left(3\chi+3V_{si}+2V_{wi}-2\eta(x_w+x_s)^2\right)-V_{wi}x_s\right)}{2\eta(x_w+x_s)^4} & \frac{\dot{\rho}_Q}{2\eta} & 0 \end{bmatrix} \tag{5.22}$$

Through the state transformation $x = Tz$, with x as in (5.18a), T as in (5.21), and the transformed state z, it is seen that the three repeated eigenvalues $\lambda_3 = \lambda_4 = \lambda_5 = 0$ are associated with the state x_{rb} and the parameters η and χ. Collecting the eigenvectors associated with the repeated eigenvalues in the matrix $T_{\lambda_{3..5}}$ (i.e. the last three columns in (5.21)), and the corresponding output pole vectors in the matrix $Y_{\lambda_{3..5}}$ (i.e. the last three rows in (5.22)), shows that the number of observable states corresponding to eigenvalue $\lambda_i = 0$ is (Skogestad and Postlethwaite 2005)

$$\text{rank}(T_{\lambda_{3..5}}) - \text{rank}(Y_{\lambda_{3..5}}) = 3 - 3 = 0.$$

This corresponds to the result from evaluating the rank of the observability matrix $\mathcal{O}$. The state x_{rb} and the parameters η and χ are observable through the integrating mode. The states x_w and x_s are observable through the fast and slow modes.

5.3 OBSERVER DESIGN

The trapezoidal rule is used to discretize the reduced observer model presented in continuous-time form in (5.18). A discrete EKF is used as the non-linear estimator (Simon 2006). The system and measurement equations are

$$\begin{aligned} x_k &= F_{k-1}(x_{k-1}, u_{k-1}, w_{k-1}) \\ y_k &= H_k(x_k, u_k, v_k) \\ w_k &\sim (0, Q_k)\ ;\ v_k \sim (0, R_k) \end{aligned} \tag{5.23}$$

where the process noise w_k is white noise with covariance $Q_k > 0$ and the measurement noise v_k is white noise with covariance $R_k > 0$.

Between each measurement, the state estimate $\hat{x}_k$ and the estimation-error covariance matrix P_k is propagated according to the known non-linear dynamics of the system:

$$\begin{aligned} \hat{x}_k^- &= F_{k-1}(\hat{x}_{k-1}^+, u_{k-1}, 0) \\ P_k^- &= T_{k-1}P_{k-1}^+T_{k-1}^T + L_{k-1}Q_{k-1}L_{k-1}^T \end{aligned} \tag{5.24}$$

where $T_{k-1} = \frac{\partial F_{k-1}}{\partial x_{k-1}} \mid_{\hat{x}^+_{k-1},u_{k-1},0}$ and $L_{k-1} = \frac{\partial F_{k-1}}{\partial w_{k-1}} \mid_{\hat{x}^+_{k-1},u_{k-1},0}$. The state estimate and its covariance is updated through

$$\begin{aligned} K_k &= P_k^- S_k^T \left(S_k P_k^- S_k^T + R_k\right)^{-1} \\ \hat{x}_k^+ &= \hat{x}_k^- + K_k \left[y_k - H_k\left(\hat{x}_k^-, u_k, 0\right)\right] \\ P_k^+ &= \left(I - K_k S_k\right) P_k^- \end{aligned} \tag{5.25}$$

where $S_k = \frac{\partial H_k}{\partial x} \mid_{\hat{x}_k^-,u_k,0}$.

Since the trapezoidal rule is used to discretize the system, matrices L_k and T_k are defined as

$$\begin{aligned} T_{k-1} &= \left[I - \tfrac{T_s}{2}\tfrac{\partial f_{RM}}{\partial x} \mid_{\hat{x}_k^-,u_k,0}\right]^{-1} \cdot \left[I + \tfrac{T_s}{2}\tfrac{\partial f_{RM}}{\partial x} \mid_{\hat{x}^+_{k-1},u_{k-1},0}\right] \\ L_{k-1} &= \tfrac{T_s}{2}\left[I - \tfrac{T_s}{2}\tfrac{\partial f_{RM}}{\partial x} \mid_{\hat{x}_k^-,u_k,0}\right]^{-1} \end{aligned} \tag{5.26}$$

where T_s is the time step between samples.

5.4 SIMULATION

5.4.1 Simulation setup

The aim of the simulation is to test the effectiveness of the reduced observer model to be used in a state and parameter estimation scheme. The simulation setup is depicted in Fig. 5.2. The plant, a SAG mill with an end-discharge grate, is represented by the continuous-time dynamic non-linear model of Le Roux *et al.* (2013b) as described in Section 4.1.1. However, in this chapter, the power-draw is given by the model of Apelt *et al.* (2001). This representation of the mill is used to simulate the system and to generate fictitious measurement data. The noisy measurement data is filtered using a Savitzky-Golay filter, which is also used to determine the derivative $\dot{\rho}_Q$ (Savitzky and Golay 1964). A discrete EKF using the reduced observer model in (5.18) is used as the non-linear estimator.

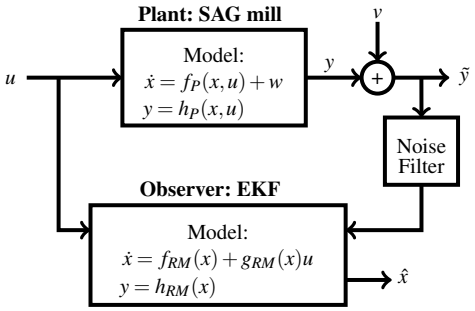

Figure 5.2. Simulation setup.

5.4.1.1 Plant model

The plant model divides the ore into the same two size classes as used in the observer model. Therefore, the mill inflow flow-rates are the same as in (5.1), and the population balance of the model is the same as in (5.2). The mill discharge flow-rates for water and solids are defined as in (4.3a) and (4.3b), and the rock consumption (RC) and ball consumption (BC) for the plant model are defined as in (4.5a) and (4.5b).

The mill power draw model described in Apelt *et al.* (2001) is used to define P_{mill}. The mill parameters and variables necessary to calculate the mill power draw is depicted in Fig. 5.3. P_{mill} in (5.12) is described in terms of $P_N L$ and P_C. The latter can be written as

$$P_C = P_{cyl} + P_{cone} \tag{5.27}$$

where P_{cone} is the power draw resulting from material in the conical feed end section and P_{cyl} is the power draw resulting from material in the cylindrical section of the mill. These are expressed as

$$\begin{aligned} P_{cyl} =& \pi g L_m \omega r_m \rho_C \frac{2r_m^3 - 3zr_m^2 r_i + r_i^3(3z-2)}{3(r_m - zr_i)} (\sin\theta_S - \sin\theta_T) + \\ & L_m \omega^3 r_m^3 \pi^3 \rho_C \frac{(r_m - zr_i)^4 - (zr_i - r_i)^4}{(r_m - zr_i)^3} \end{aligned} \tag{5.28a}$$

$$\begin{aligned} P_{cone} =& \frac{\pi g L_c \omega \rho_C}{3(r_m - r_t)} \left(r_m^4 - 4r_m r_i^3 + 3r_i^4\right) \cdot (\sin\theta_S - \sin\theta_T) + \\ & \frac{2\pi^3 L_c \omega^3 \rho_C}{5(r_m - r_t)} \left(r_m^5 - 5r_m r_i^4 + 4r_i^5\right) \end{aligned} \tag{5.28b}$$

where g (m/s^2) is the acceleration constant, $\omega = \frac{\phi_c}{2\pi}\sqrt{\frac{g}{r_m}}$ (Hz) is the rotational rate of the mill, z is a charge velocity profile parameter, r_m (m) is the mill inner radius, r_i (m) is the inner charge radius, r_t

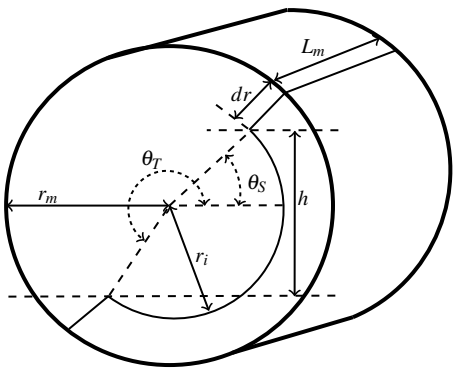

Figure 5.3. Parameters to calculate mill power draw.

(m) is the mill trunnion radius, L_c (m) is the cone length, θ_S (rad) is the charge shoulder angle, and θ_T (rad) is the charge toe angle. The mill charge toe angle θ_T and shoulder angle θ_S are empirically defined as (Napier-Munn *et al.* 2005)

$$\begin{aligned}\theta_T &= 2.5307\,(1.2796 - J_T)\left(1 - e^{-19.42(\phi_{ec}-\phi_c)}\right) + \tfrac{\pi}{2} \\ \theta_S &= \tfrac{\pi}{2} - \left(\theta_T - \tfrac{\pi}{2}\right)\left[(0.3386 + 0.1041\phi_c) + (1.54 - 2.5673\phi_c)\,J_T\right]\end{aligned}$$

where $\phi_{ec} = 0.35\,(3.364 - J_T)$ is the experimentally determined fraction of critical mill speed at which centrifuging is fully established. The empirical relations for z and r_i are

$$\begin{aligned}z &= (1 - J_T)^{0.4532} \\ r_i &= r_m \cdot \left(1 - \tfrac{2\pi\beta J_T}{2\pi - \theta_T + \theta_S}\right)\end{aligned}$$

where $\beta = \frac{t_c}{t_c + t_{ff}}$ is the fraction of the charge that is active. To calculate β, empirical relations are defined for the mean travel time of particles in the mill from the charge toe to the charge shoulder (t_c), the mean travel time of particles in free fall from the charge shoulder to the charge toe (t_{ff}), and the mean radial position of the mill charge $\bar{r}$.

$$\begin{aligned}t_c &= \tfrac{2\pi - \theta_T + \theta_S}{\pi\omega} \\ t_{ff} &= \left(\tfrac{2\bar{r}\cdot(\sin\theta_S - \sin\theta_T)}{g}\right)^{0.5} \\ \bar{r} &\approx \tfrac{r_m}{2} \cdot \left(1 + \left(1 - \tfrac{2\pi J_T}{2\pi - \theta_T + \theta_S}\right)^{0.5}\right)\end{aligned}$$

Finally, the plant model is written as

$$\dot{x} = f_P(x,u) = \begin{bmatrix} V_{wi} - \varphi d_H x_w \left(\frac{x_w}{x_s + x_w}\right) \\ V_{si} - \varphi d_H x_w \left(\frac{x_s}{x_s + x_w}\right) + \frac{\varphi P_{mill} x_r}{\rho_O \kappa_r (x_r + x_s)} \\ V_{ri} - \frac{\varphi P_{mill} x_r}{\rho_O \kappa_r (x_r + x_s)} \\ V_{bi} - \frac{\varphi P_{mill} x_b}{\kappa_b [\rho_O (x_r + x_s) + \rho_B x_b]} \end{bmatrix} \tag{5.29a}$$

$$y = h_P(x,u) = \begin{bmatrix} \frac{x_w + x_s + x_r + x_b}{v_{mill}} \\ \varphi d_H x_w \\ \frac{\rho_O x_s + \rho_W x_w}{x_s + x_w} \end{bmatrix} \tag{5.29b}$$

where $y = [J_T, Q, \rho_Q]^T$. (The subscript P refers to the plant.)

5.4.2 Simulation environment

Table 5.3 shows the plant model parameter values and Table 5.4 shows the considered initial conditions. The data is for an industrial single-stage closed grinding mill circuit as in Le Roux *et al.* (2013b).

5.4.2.1 Plant and observer

The general simulation environment for the plant and observer is described below:

- The plant is integrated using the fourth order Runge-Kutta method at a rate of $T_s = 2$ s. The full simulation time is 8 h.

- Measurements are sampled at a rate of $T_s = 2$ s.

Table 5.3. Model parameter values.

Parameter	Value	Unit	Description
α_r	0.47	[-]	Fraction of rock in feed ore
d_H	88	[1/h]	Constant mill discharge parameter
D_m	4.07	[m]	Mill inside diameter ($D_m = 2r_m$)
ε_{sv}	0.6	[-]	Max fraction solids by volume of slurry at zero slurry flow
ϕ_c	0.72	[-]	Fraction of critical mill speed
g	9.8	[m^2/s]	Gravity constant
κ_B	90	[kWh/t]	Energy required per tonne of steel balls consumed
κ_R	6.72	[kWh/t]	Energy required per tonne of rocks consumed
k_P	0.97	[-]	Power draw fitting parameter
L_c	0	[m]	Mill cone length
L_m	4.54	[m]	Mill cylinder length
P_{NL}	93.73	[kW]	Mill power at zero load
ρ_B	7.85	[t/m^3]	Steel ball density
ρ_O	3.2	[t/m^3]	Ore density
ρ_W	1	[t/m^3]	Water density
r_t	0.46	[m]	Mill feed trunnion radius
V_{cs}	96.9	[m^3/h]	Flow of classifier solids to mill
V_{cw}	112	[m^3/h]	Flow of classifier water to mill
v_{mill}	59.12	[m^3]	Mill volume

- There is no feedback controller for the mill.

- The plant is excited by sinusoidally varying input MIW with a period of $T_{MIW} = 12$ minutes and an amplitude of 8 m^3/h around its nominal operating condition. Since the amplitude is greater than the nominal condition, the boundary $MIW \geq 0$ m^3/h is applied.

- To show the ability of the observer to track changes in x_s, and x_{rb}, inputs MFO and MFB are varied. Input MFO is sinusoidally varied at a period of $T_{MFO} = 4$ h and an amplitude of 10 t/h. Step changes at intervals of 2 h are applied to MFB where the size of step changes are chosen from the uniform distribution $\mathcal{U} \sim (-1, 1)$ (t/h).

- Disturbances in the feed-ore size-distribution and the feed-ore hardness are simulated by varying α_r and κ_r around their nominal values.

  – A change in feed size distribution is simulated by applying step-changes to α_r at intervals of 1.5 h starting at $t = 2.5$ h. The size of step-changes are randomly selected from the uniform

Table 5.4. Initial operating conditions.

Variable	Value	σ	Unit
Inputs and Outputs			
MIW	4.64	-	[m^3/h]
MFO	65.2	-	[t/h]
MFB	5.68	-	[t/h]
J_T	0.33	0.006	[-]
Q	234	5	[m^3/h]
ρ_Q	2.10	0.02	[t/m^3]
Plant Initial States			
x_b	8.23	0.04	[m^3]
x_r	1.88	0.01	[m^3]
x_s	4.65	0.02	[m^3]
x_w	4.63	0.02	[m^3]

distribution $\mathcal{U}(-0.14, 0.14)$. It is assumed measurement instrumentation is available to measure α_r at the input of the plant (Wei and Craig 2009b).

– A change in feed ore hardness is simulated by applying step-changes to κ_r at intervals of 1.5 h starting at $t = 1.5$ h. The size of step-changes are randomly selected from the uniform distribution $\mathcal{U}(-2, 2)$ (kWh/t). This parameter is not measured.

- Fig. 5.4 shows the inputs and disturbances to the plant.

For the plant, only the mill simulated. The sump and cyclone is removed from the circuit. However, since the data used as basis for the simulation of the mill is for a closed grinding mill circuit, the closed circuit underflow to the mill must be accounted for. The cyclone underflow at the operating point provided by Le Roux *et al.* (2013b) is regarded as a constant in the simulations below. This enables a simulation environment for the mill which is reasonably consistent with the data used as reference. As seen in Fig. 5.4, the simulated inflow of water to the mill is the sum of MIW and a constant cyclone water underflow (V_{cw} in Table 5.3).

The sinusoidal variation of MIW and MFO causes a sinusoidal variation in the mill discharge flow-rate. This variation in Q can be absorbed by the sump, if the sump volume is large enough to accommodate this variation. Therefore, a sinusoidal variation in MIW will not necessarily translate to a sinusoidal variation in CFF, and consequently a sinusoidal variation in the cyclone cut. Should the variational trends of MIW and MFO translate to similar variational trends in the cyclone underflow and overflow, it should not affect the observer. Variations in the cyclone underflow flow-rate and density will contribute to the dynamics in the mill outputs used by the observer to estimate the unknown states and parameters. However, care should still be taken to ensure the variations in MIW and MFO does not cause the mill to operate outside its operational constraints.

5.4.2.2 Simulation scenarios

For the observer initialisation, the initial state estimate and the state estimate covariance matrix are

$$\hat{x}_0 = \left[3.5\ \mathrm{m}^3,\ 4\ \mathrm{m}^3,\ 9\ \mathrm{m}^3,\ 3\ \mathrm{h}^{-1}\mathrm{m}^{-3},\ 10\ \mathrm{m}^3\mathrm{h}^{-1}\right]^T \tag{5.30}$$

$$P_0 = \left(\mathrm{diag}\left[2\ \mathrm{m}^3,\ 2\ \mathrm{m}^3,\ 2\ \mathrm{m}^3,\ 2\ \mathrm{h}^{-1}\mathrm{m}^{-3},\ 2\ \mathrm{m}^3\mathrm{h}^{-1}\right]\right)^2. \tag{5.31}$$

On industrial mills, the mill states are generally estimated through expensive and arduous sampling campaigns. Since these campaigns are conducted infrequently, and assume a steady-state of operation, it is doubtful if accurate estimate of the states are always readily available. Therefore, $\hat{x}_0$ is chosen relatively far from the true initial state provided in Table 5.4, and P_0 is chosen relatively large as little confidence is placed in the initial estimate.

Two simulation scenarios in terms of measurement noise and process noise are considered:

1. No measurement noise or process noise is added. Since perfect measurements of the outputs in (5.29b) as well as the derivative of ρ_Q is assumed, R_k in (5.23) is chosen small.

   $$R_k = 10^{-4} \times \left(\mathrm{diag}\left[1,\ 1\ \mathrm{m}^3\mathrm{h}^{-1},\ 1\ \mathrm{tm}^{-3},\ 1\ \mathrm{tm}^{-3}\mathrm{h}^{-1}\right]\right)^2$$

   The covariance matrix Q_k is used as a tuning matrix for the EKF and is specified by trail-and-error.

   $$Q_k = 10^{-1} \times \left(\mathrm{diag}\left[0.2\ \mathrm{m}^3,\ 0.5\ \mathrm{m}^3,\ 1\ \mathrm{m}^3,\ 0.8\ \mathrm{h}^{-1}\mathrm{m}^{-3},\ 2\ \mathrm{m}^3\mathrm{h}^{-1}\right]\right)^2$$

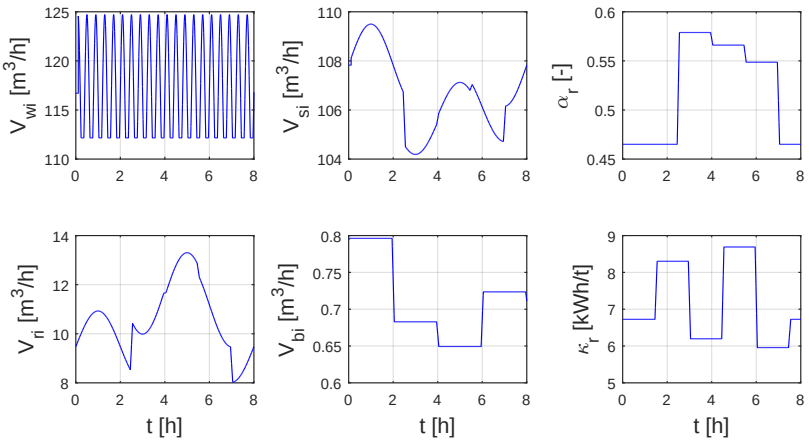

Figure 5.4. Inputs and disturbances for simulation scenarios.

2. Measurement noise (v) with a normal distribution of $\mathcal{N}\left(0, \sigma_v^2\right)$ is added to the outputs of the plant. The absolute values of the standard deviations of the measurement noise is shown in the second last column of Table 5.4. The covariance matrix R_k for the EKF aligns with the covariance of the measurement noise added to the plant outputs (Schneider and Georgakis 2013). A high covariance is assigned to the measurement of $\dot{\rho}_Q$ as this measurement is highly sensitive to the noise on ρ_Q.

$$R_k = \left(\text{diag}\left[0.006,\ 5\ \text{m}^3\text{h}^{-1},\ 0.02\ \text{tm}^{-3},\ 1.0\ \text{tm}^{-3}\text{h}^{-1}\right]\right)^2$$

Process noise (w) is added to the plant states with a normal distribution of $\mathcal{N}\left(0, \sigma_w^2\right)$. The absolute values of the standard deviations of the process noise is shown in the second last column of Table 5.4.

Similar to the previous simulation scenario, the covariance matrix Q_k is used as a tuning matrix for the EKF and is determined by means of trial-and-error.

$$Q_k = \left(\text{diag}\left[0.1\ \text{m}^3,\ 0.1\ \text{m}^3,\ 0.1\ \text{m}^3,\ 0.2\ \text{h}^{-1}\text{m}^{-3},\ 2\ \text{m}^3\text{h}^{-1}\right]\right)^2$$

For the second simulation scenario where noise is added, the noisy measurements are filtered using a Savitzky-Golay digital filter. The filter smooths data by fitting a frame of F data samples with polynomials of small order N by means of linear least squares. The filter returns a filtered value at the centre of the frame. For real-time applications this means that the value returned by the filter is delayed by half the frame length ($(F+1)/2$). To handle the time delay problem, two consecutive filters are used:

1. The three measurements described in (5.29b) are filtered with a filter configured to fit a polynomial of order 2 using a frame length of $F_1 = 35$ samples.

2. The first order derivative $\dot{\rho}_Q$ is calculated from the delayed filtered ρ_Q data. A Savitzky-Golay filter with an order of 2 and a frame length of $F_2 = 135$ is used.

As depicted in Fig. 5.5, the filtered measurements are delayed by 18 samples from the current sample. Because $\dot{\rho}_Q$ is calculated from the filtered data, another 68 samples delay is introduced. The equivalent delay is 86 samples, i.e. 172 s.

5.5 RESULTS AND DISCUSSION

5.5.1 Simulation scenario 1

The results of the simulation scenario where perfect measurements and no process noise are assumed is shown in Figs. 5.6 and 5.7. As seen from Fig. 5.7, the filter converges within two hours to the correct state value and is able to track the changes in the states. The effect of the disturbances in parameter κ_r in Fig. 5.4, which affects the generation of solids, is clearly visible in the large deviations in χ in Fig. 5.7, which represents the accumulation of solids.

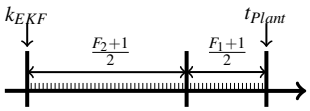

Figure 5.5. Filter implementation and management of phase shift.

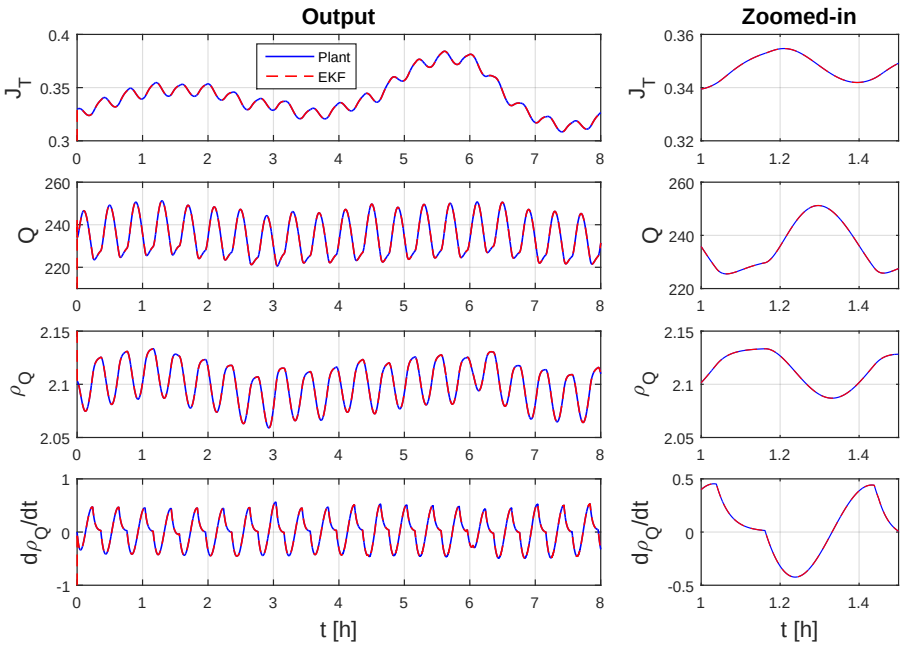

Figure 5.6. Output for Simulation Scenario 1.

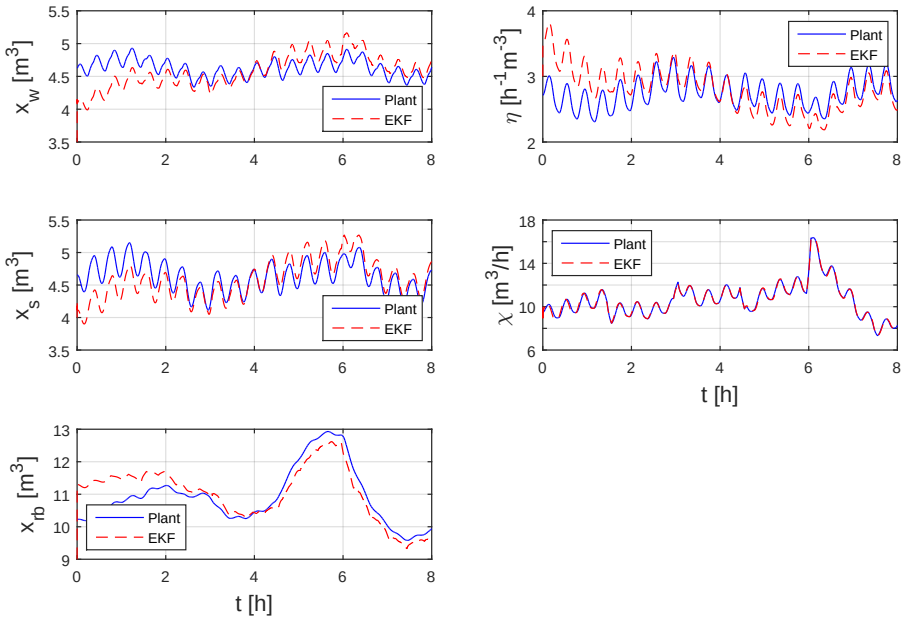

Figure 5.7. States and parameters for Simulation Scenario 1.

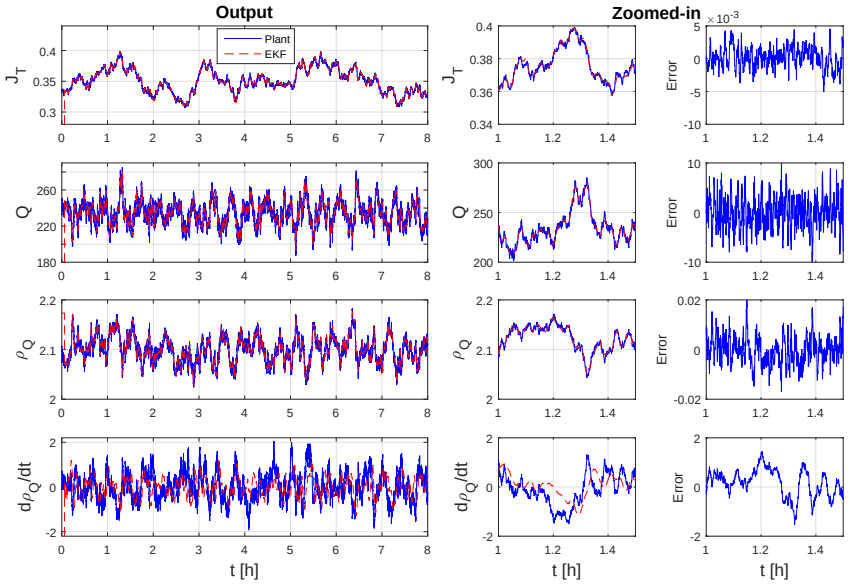

Figure 5.8. Output for Simulation Scenario 2. The error shown in the last column is the difference between the EKF output and the plant output.

5.5.2 Simulation scenario 2

The results of the simulation scenario where measurements are filtered to remove noise and to calculate the derivative of ρ_Q is shown in Figs. 5.8 and 5.9. As seen in Fig. 5.8, the noise on the measurements of J_T, Q and ρ_Q are filtered very well, but the derivative of ρ_Q is not calculated with sufficient accuracy. The error between the filtered value and the plant output is shown in the last column of Fig. 5.8. The error in $\dot{\rho}_Q$ is almost as large as the signal itself.

The normalised root mean squared error between the actual state and the estimated state in Fig. 5.9 is shown in Table 5.5 and calculated as

$$NRMSE = \frac{1}{\bar{\Lambda}}\sqrt{\frac{\Sigma^N(\Lambda-\hat{\Lambda})^2}{M}}$$

where Λ is the process signal, $\bar{\Lambda}$ is the mean of the process signal, $\hat{\Lambda}$ is the estimate of the process signal, and M is the number of data points. Results in Fig. 5.9 and Table 5.5 indicate the EKF filter

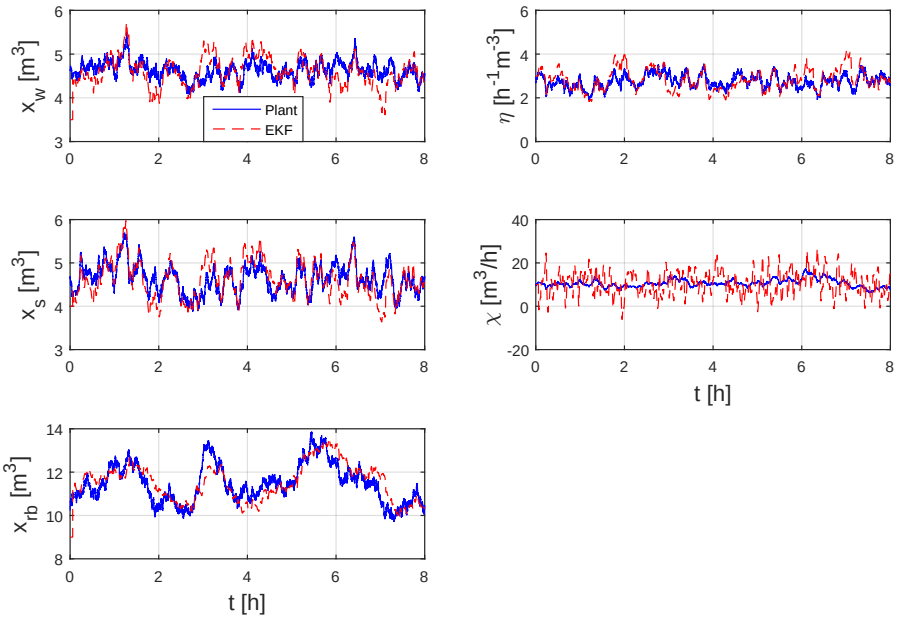

Figure 5.9. States and parameters for Simulation Scenario 2.

Table 5.5. Normalised Root Mean Squared Error

	x_w	x_s	x_{rb}	η	χ
NRMSE	6.66%	6.17%	5.14%	12.9%	53.3%

is able to track x_{rb} with reasonable accuracy, where x_w and x_s are estimated with lower accuracy. Parameters χ and η are used to absorb the uncertainties in the measured data.

5.6 CONCLUSION

The states and parameters of a non-linear grinding mill observer model developed in this chapter are weakly non-linearly observable, although they are not observable in the linearised case. For linear observability, a reduced observer model was developed. This reduced model represents the constituents of the mill using three states: water, solids, and grinding media (sum of rocks and balls). The grinding environment is modelled using two parameters: a discharge rate and an accumulation rate of solids. The measurement used are: the mill filling volume, the discharge rate of the mill, the discharge density of the mill, and the first time derivative of the discharge density.

Milling data is generated from a model different to the observer model. Simulations indicate that with accurate mill discharge measurements it is possible to estimate the system states and parameters using a discrete EKF. The main challenge is to accurately calculate the first time derivative of the mill discharge density.

Since industrial mills rarely include measurement instrumentation at the mill discharge, this work aims to motivate the inclusion of accurate discharge measurements in light of the information about mill inventories to be gained. This would require careful consideration of mill discharge trommel designs to allow sufficient space to install the required instrumentation. Future work involves using the observer to provide state feedback for an advanced process controller for a grinding mill circuit.

CHAPTER 6 CONCLUSION

The aim of this work is to developed a control structure for a single-stage closed grinding mill circuit following the systematic plant-wide control design procedure in Skogestad (2004). It provides a structural approach to resolve essential questions such as which variables should be controlled, which variables should be manipulated, what links should be made between the two, and which set-points are appropriate for the controlled variables. Subsequently, an MPSP controller is developed to implement the regulatory and supervisory aims of the plant-wide control structure. Since the MPSP controller requires state-feedback, an observer is developed with states and parameters which can be estimated from plant measurements.

6.1 PLANT-WIDE CONTROL

The initial step in any control design study is the definition of the economic operational objectives of the mineral processing plant (Hodouin 2011). Because the concentrate produced by the separation process is responsible for the revenue generated by the plant, optimal economic operation occurs when operating at the most profitable region on the concentrate's grade-recovery curve. This region on the curve is determined by the purchase contract between the mineral processing plant and the smelter. Therefore, given the contract stipulations, the net smelter return can be described in terms of the grade and recovery of the separator concentrate (Wills 2006). To optimise the economic return of the mineral processing plant, individual optimisation of the grinding mill circuit and separation circuit may lead to a sub-optimal result (Sosa-Blanco *et al.* 2000). As shown in Chapter 2, the economic operational objectives of the mineral processing plant can be related to the grinding mill circuit by expressing the separator concentrate grade and recovery in terms of the grinding mill circuit's product quality, throughput, and grade (McIvor and Finch 1991, Wei and Craig 2009a). Optimisation of the economic

objective can therefore be done in terms of the characteristics of the grinding mill circuit's product characteristics.

Given the description of the economic operational objective of the mineral processing plant in terms of the grinding mill circuit's product quality, throughput, and grade, it is necessary to define a control structure for the grinding mill circuit to achieve these economic goals. As discussed in Chapter 3, the top-down analysis provides a control structure to address steady-state operation, whereas the bottom-up analysis develops a control structure to address dynamic operation.

For the top-down analysis, the operational economic objective developed in Chapter 2 can be used to formulate a scalar cost function for the grinding mill circuit. Although there are six dynamic degrees of freedom available - mill ore feed-rate, mill inlet water flow-rate, mill ball feed-rate, sump feed water flow-rate, cyclone feed flow-rate, and mill rotational speed - there are only five steady-state degrees of freedom available to achieve the operating point determined by optimisation of the cost function. This is because the sump slurry volume has no economic steady-state effect.

Once the cost function is defined, it is necessary to formulate the constraint function which defines the range of optimal steady-state operating conditions of the circuit. Since optimal steady-state operation for grinding mill circuits is primarily determined by the operating performance of the mill, the mill performance indicators - mill power draw, mill throughput, and mill grind - are used to define the optimal steady-state operation. The mill performance indicators can be described as functions of the mill filling and the mill rotational speed. These relations are called grindcurves (Van der Westhuizen and Powell 2006, Powell *et al.* 2009). Although the mill performance indicators show a parabolic relation to mill filling, the peaks for the indicators occur at different mill fillings. Consequently, if a mill operates at maximum mill power draw, this does not necessarily guarantee optimal grind and maximum mill throughput. For closed circuit operation, the grindcurves are developed assuming the cyclone maintains a consistent cut-size and water recovery to underflow (Craig *et al.* 1992). This can be achieved if the cyclone feed flow-rate has sufficient range of operation, and the cyclone's capacity is not exceeded (Botha, Craig and Roux 2015). Therefore, the grinding mill circuit's product throughput and quality can be defined as constant functions of the mill performance indicators. Since the grinding mill circuit's product throughput and quality can be defined as functions of the mill filling and mill rotational speed by means of the mill performance indicators, the cost function is optimised with respect to the mill filling and the mill rotational speed. Therefore, the main economic controlled variable is the mill

filling (Borell *et al.* 1996), and the mill rotational speed is the throughput manipulator of the grinding mill circuit. If the grinding mill does not have a variable speed drive to alter the mill's rotational speed, one degree of freedom is removed. In this case, independent control of the circuit's throughput and the circuit's product quality is no longer feasible (Viklund *et al.* 2006, Bauer and Craig 2008, Le Roux *et al.* 2016a).

In light of the top-down analysis, the pairing shown below between controlled and manipulated variables for regulatory control is suggested in the bottom-up analysis:

- The mill rotational speed is used to set the desired circuit product throughput.
- The mill ore feed-rate is used to control the mill filling.
- The cyclone feed flow-rate is used to reject disturbances on the circuit product quality.
- The mill inlet water flow-rate is used to maintain a consistent mill slurry density.
- The mill ball feed-rate is used to maintain a consistent mill ball filling.
- The sump feed water flow-rate is used to control the sump slurry volume.

Because of the significant advantages offered by MPC over PID control for grinding mill circuits (Pomerleau *et al.* 2000, Remes *et al.* 2010), an MPC controller is suggested for the regulatory and supervisory layer. The optimisation layer specifies set-points for the mill filling and the mill rotational speed based on optimisation of the cost function. The grindcurves act as equality constraints for the optimisation.

6.2 MODEL PREDICTIVE STATIC PROGRAMMING

One of the main impediments to applying non-linear process control for regulatory and supervisory control, is the computational burden associated with minimising the non-linear controller objective function (Coetzee *et al.* 2010, Wolf and Marquardt 2016). To address this issue, Chapter 4 develops

an MPSP controller capable of achieving the regulatory and supervisory control goals described in the plant-wide analysis. The advantage of the MPSP controller is that the computational burden is decreased by converting the dynamic optimization problem to a low-dimensional static optimization problem, calculating the sensitivity matrices recursively and using a closed form expression to update the control.

When applied in simulation to a non-linear model of a single-stage closed grinding mill circuit, comparison of the performance of the MPSP controller to a regular NMPC controller indicated that MPSP achieved improved output regulation in the presence of model-plant mismatch, disturbances and measurement noise. Although the prediction and control horizons are equal in MPSP, computational time was significantly reduced. MPSP is presented as a suitable option for non-linear model-based optimal control for output tracking in large industrial processes, especially if computational time and complexity is a limiting factor for real-time applications.

6.3 STATE AND PARAMETER ESTIMATION

The difficulty with applying non-linear model-based control such as MPSP or NMPC to grinding mill circuits, is the estimation of the states for state feedback. Because of the limited number of real-time measurements available on industrial circuits (Wei and Craig 2009b), full state feedback is rarely possible. To reject model-plant mismatch and disturbances, it is important for states and parameters to be estimated correctly.

Chapter 5 develops a non-linear observer model with states and parameters which are non-linearly (weakly) observable from measurements of the mill filling, mill discharge flow-rate and the mill discharge density. However, the states of the linearised model are not observable. Although a non-linear observer such as MHE is a preferable solution, it requires the correct modelling of the time-varying nature of the parameters. The ore breakage rate and the ball breakage rate vary according to unmeasured changes in ore hardness and grinding conditions in the mill, but is modelled as constants by the model. This approximation is valid over a short period, especially when compared to the quick dynamics of the water and solids over the same period. But for longer periods the approximation cannot hold. The discharge rate parameter used for the observer model is also modelled as a constant. As seen from (5.5), which is used as basis to model the discharge, the discharge rate parameter lumps

together factors such as the mill diameter, grate aperture open area, mill speed, and the relative radial position of grate apertures. Since these factors remain constant, the assumption that this parameter remains constant is valid only if the mill speed remains constant. For a mill with varying speed, the change in mill discharge can be modelled using the relation between discharge and speed shown in (5.5). Therefore, if a long time horizon is used for MHE, the validity of assuming constant ore and ball breakage reduces, but a shorter time horizon may not contain sufficient process dynamics for MHE to provide reasonable estimates.

The non-linear observer model is reduced so that the states and parameters are linearly observable from measurements of the mill filling, mill discharge flow-rate, the mill discharge density, and the time derivative of the mill discharge density. The states included in the model are the mill water hold-up, the mill solids hold-up and the mill grinding media hold-up. The parameters include the discharge rate per volume of slurry, and the accumulation rate of solids. A linear observer, such as an EKF, can provide one-step-ahead prediction for the states and parameters. Therefore, the validity of approximating the grinding media as constant over each approximation step holds.

A simulation study was conducted where milling data is generated from a model different to the observer model. The observer model is then incorporated in an EKF observer to estimate the states and parameters. As expected, with no measurement noise, all states and parameters are estimated correctly. In the case of noisy measurements, the EKF filter is able to track the grinding media hold-up with reasonable accuracy, and the water and solids hold-ups with less accuracy. The parameters absorb the uncertainties in the measured data.

Although industrial circuits are not designed to include flow and density measurement instrumentation at the discharge trommel of the grinding mill, this work shows that mill inventories can be estimated with reasonable accuracy if these measurements are made. This would require careful consideration of the mill discharge trommel design to allow sufficient space to install the required instrumentation.

6.4 FUTURE WORK

6.4.1 Plant-wide Control

The plant-wide control strategy views the mineral processing plant as the combination of a comminution circuit and a separation circuit. In this study, the operation of the separation circuit, which is assumed to be a flotation circuit, is not included in the plant-wide strategy. It is assumed the flotation circuit maintains a consistent relationship between the comminution product quality and the separator concentrate recovery. This assumption is used by Munoz and Cipriano (1999), Sosa-Blanco *et al.* (2000), and Wei and Craig (2009a) to define the control objectives of the comminution circuit to optimise the economic performance of the mineral processing plant. Yet, for a truly plant-wide control strategy, the dynamics and operation of the flotation circuit should also be considered. Given the large number of variables available to influence the flotation's circuits performance, and the complex non-linear interactions of the process, modelling the process remains challenging (Seppälä *et al.* 2016). Therefore, including the flotation circuit in a plant-wide control strategy of a mineral processing plant is not a trivial task (Shean and Cilliers 2011, Bergh and Yianatos 2011).

A simulation study of the plant-wide control strategy, which is not done in this thesis, will assist to determine the economic benefit the plant-wide control strategy can provide to a mineral processing plant. For such a study, a simulation platform capable of reproducing the steady-state operating conditions specified by the grindcurves, while accurately representing the dynamics of the plant, is required. This enables consideration of the economic impact of common disturbances such as variations in ore hardness (Bueno, Kojovic, Powell and Shi 2013), ore composition (Shi and Napier-Munn 2002, Tungpalan, Manlapig, Andrusiewicz, Keeney, Wightman and Edraki 2015), and ore size distribution (Morrell and Valery 2001).

A simulation platform for analysis of the plant-wide control strategy requires adequate process unit models. The SAG mill model of Le Roux *et al.* (2013b) presented in Section 4.1, is adequate to capture the dynamics of the mill around a specific operating condition, but is not suited to capture the range of steady-state operating conditions specified by the grindcurves in Section 3.1.2. Although detailed phenomenological models of SAG mills are available (Valery and Morrell 1995, Morrell 2004, Hinde and Kalala 2009, Salazar *et al.* 2009), it is not clear if these models can reproduce the grindcurves

as they do not predict breakage kinetics changes for large variations in operating conditions. The model parameters are generally fitted to a specific steady-state operating condition through laborious sampling campaign and laboratory test work. Therefore, similar to Le Roux *et al.* (2013b), the available fundamental models are limited to specific operating conditions. Although a parameter update scheme can be developed to ensure a model is suitable over a wider range of conditions, it is not clear how this should be done. DEM simulations may provide further options as to how breakage kinetics can be adapted to accommodate wider operating regions (Delaney, Cleary, Morrison, Cummins and Loveday 2013).

Depending on the industrial test data used during parameter fitting, fundamental hydrocyclone models are applicable over fairly wide operating regions. However, similarly to mills, significant sampling campaign work is required to use these models for simulation purposes, as the model parameters are dependent on the type of ore being processed and the range of operating conditions considered (Nageswararao *et al.* 2004, Narasimha, Mainza, Holtham, Powell and Brennan 2014).

The net smelter return described in Section 2.3.1 assumes a single metal component. However, mineral processing plants often produce a concentrate with a variety of metals. The value of each metal can easily be added to the net smelter return calculation, but the incorporation of each metal component in a simulation model is not trivial. Multi-component models can be used (Hinde and Kalala 2009), but this significantly increases parameter estimation efforts. Additional modelling effort is also required for the separator concentrate to account for the different grade and recovery relationships for each metal type (Sosa-Blanco *et al.* 2000).

If it is known that a plant will soon process ore with a significant change in mineralogical characteristics, a feed-forward controller can be used to ensure the grinding environment is suitably changed to meet the new breakage requirements. This requires dynamic models which considers how important mineralogical characteristics of the ore influence the plant's performance (Tungpalan *et al.* 2015). For example, the ore mineralogy influences the rheology of the slurry created by the ore which in turn influences breakage characteristics (Shi and Napier-Munn 2002). However, quantifying the effect of slurry rheology on milling performance remains a challenge (Bazin and B-Chapleau 2005). Alternatively, if sufficient sampling campaign data is available, mineralogical changes can be empirically related to the breakage functions (Bueno *et al.* 2013).

Since the grindcurves are quasi-static curves, a steady-state operating condition is represented at each point along the curve. It is assumed the grinding conditions remain the same as one moves along the curve, i.e. the ore and the mill characteristics remain unchanged at each point along the curve. However, as seen from the grindcurves in Craig *et al.* (1992) and Van der Westhuizen and Powell (2006) fitted to industrial data, there is an inherent uncertainty and variance in the grindcurves. This is not to say there are no distinct relationships between the mill's performance indicators and the mill's filling and speed, only that a degree of uncertainty should be accounted for when the grindcurves are used as equality constraints in the optimisation of the economic objective function.

6.4.2 Model Predictive Static Programming

Although the MPSP controller is well suited to meet the regulatory and supervisory control aims, the algorithm does not explicitly include state constraints. A slack-variable approach, where a constrained optimisation problem is transformed into an unconstrained optimisation problem (Jacobson and Lele 1969), is used by Bhitre and Padhi (2014) to allow state constraints for finite horizon MPSP problems. Alternatively, since the sensitivity matrices calculated in the MPSP algorithm are explicit functions of the process states, constraints could potentially be applied directly to the sensitivity matrices.

A limitation of the MPSP simulation environment is that the same model is used to represent the plant and to develop the controller. For linear MPC studies, a non-linear model is often used to represent the plant, and the controller is developed from the linear version of the model (Pomerleau *et al.* 2000, Ramasamy *et al.* 2005, Le Roux and Craig 2013). This provides a degree of model-plant mismatch between the true plant and the time-invariant model developed from process data (Craig and MacLeod 1995, Chen *et al.* 2007). However, given the inherent non-linearity of the plant, the models used by linear MPC for grinding mill circuits require frequent parameter updates.

Since non-linear models of grinding mill circuits describe a larger range of operation compared to linear models, it is preferable to use non-linear models in advanced process controllers. In the non-linear MPC simulations studies for grinding mill circuits of Coetzee *et al.* (2010) and Salazar *et al.* (2014), where the same model is used to represent the plant and develop the controller, model-plant mismatch

is introduced by varying the parameters of the plant. This is a relatively simple method to evaluate the characteristics of the control strategy, and is also followed in this thesis.

For industrial applications, model-plant mismatch is expected as the model used for control rarely captures all the process dynamics. Other than varying parameters in a single model as mentioned above, inherent model-plant mismatch can be created in simulation if the plant is modelled in a different manner compared to the model used for control. Variations in modelling the grinding mill circuit can be introduced with respect to size classes (Le Roux and Craig 2013), ore breakage (Apelt, Asprey and Thornhill 2002b, Hinde and Kalala 2009), mill power draw (Austin 1990, Apelt *et al.* 2001), slurry discharge (Latchireddi and Morrell 2003), sump mixing, and cyclone classification (Nageswararao *et al.* 2004, Narasimha *et al.* 2014).

6.4.3 State and Parameter Estimation of Grinding Mill Conditions

The reduced observer model was developed to include only states and parameters which can be reasonably estimated from limited measurements. The main difficulty remains accurate calculation of the derivative of the discharge density, especially if there is not sufficient variation in the density. Therefore, to observe the states and parameters, a degree of plant excitation is required. For industrial applications, where the aim is to maintain steady-state operation, excitation is unwelcome. However, the process noise may be sufficient excitation for the states and parameters to be estimated. If this is not sufficient, acceptable excitation conditions for accurate estimation needs to be specified.

The EKF observer assumes time-invariant process noise characteristics. However, for varying process dynamics and operating conditions, the noise statistics are time-varying. Since fixed noise statistics can lead to deteriorating filter performance, a more systematic approach should be considered to select and update the noise statistics. Valappil and Georgakis (2000) present two approaches to estimate the process noise covariance on-line. Assuming the non-linear process model uncertainty is quantified by a parameter covariance matrix, the first approach linearly approximates the dependence of the model predictions on the model parameters. The second approach, which considers the non-linear dependence of model predictions on parameters, involves Monte Carlo simulations. The difficulty with this approach is that the parameter error covariance matrix may change over time, or may be unknown. Alternatively, Bavdekar, Deshpande and Patwardhan (2011) propose two methods for constructing the

maximum likelihood estimates of process and measurement noise covariance matrices from operating data. For disturbances modelled as either structured or unstructured noise, the first approach minimises the negative of the log likelihood function associated with the innovation sequence generated by the EKF. The second approach, which extends the expectation-maximisation algorithm of Dempster, Laird and Rubin (1977), uses the joint likelihood function of all available data to compute the next iterate of the decision variables for the optimisation problem. As an alternative to the EKF observer, constrained unscented Kalman filters (Teixeira, Torres, Aguirre and Bernstein 2010) or particle filters (Zhao, Huang and Liu 2014, Olivier *et al.* 2012) can also be considered to improve the observer's performance (Psiaki 2013).

Although the model used to generate fictitious plant data is different to the observer model, both models assume a sharp cut between rocks not passing through the discharge screen and solids remaining in the mill. For further simulation studies, more ore size classes can be used such that the discharge rate of size classes is given by the log-linear relationship in (5.4). Additionally, the observer presented in this study assumes the discharge grate is such that no slurry pooling occurs. The discharge of slurry is only via the grinding media, as modelled in (5.5). The observer can potentially be extended to identify slurry pooling conditions, using the discharge via the slurry pool as modelled in (5.6).

This work motivates the inclusion of discharge density and flow-rate measurement instrumentation at mill. However, the mill's discharge density and flow-rate can potentially be estimated using a flow-balance at the sump, where flow-rate and density measurement instrumentation is easier to include (Le Roux *et al.* 2016a). This assumes that the sump is not also fed by unmeasured spillage or underflow from other process units. Since the time derivative of the sump volume is required to estimate the mill's discharge flow-rate (Le Roux and Craig 2016), this can potentially introduce significant noise and uncertainty in the estimates. Therefore, the accuracy of the measurement instrumentation at the sump needs to be specified such that the observer at the sump can provide sufficiently accurate information to the observer at the mill.

The observer should be tested on a real circuit, as the aim is to produce a tool which can be readily applied in industry. A pilot-plant, with adequate density, flow and mill filling measurements, provides a good test platform. The challenge at the pilot-plant is to track the mill's constituents for validation against the estimates provided by the observer. Tracking the constituents independent of the observer requires careful sampling campaign planning (Napier-Munn *et al.* 2005). A further challenge is to

use the observer as part of a model-based control loop (Le Roux *et al.* 2016a). As an expansion of the observer model, it would be interesting to note what further information could be estimated if the particle size at the mill discharge is measured.

REFERENCES

Amestica, R., Gonzalez, G. D., Barria, J., Magne, L., Menacho, J. and Castro, O. (1993). A SAG mill circuit dynamic simulator based on a simplified mechanistic model, *Proc. XVIII Int. Mineral Processing Congress*, Sydney, Australia, pp. 117-129.

Amestica, R., Gonzalez, G. D., Menacho, J. and Barria, J. (1996). A mechanistic state equation model for semiautogenous mills, *Int. J. Mineral Process.* **44-45**: 349–360.

Apelt, T. A. and Thornhill, N. F. (2009). Inferential measurement of SAG mill parameters V: MPC simulation, *Minerals Eng.* **22**: 1045–1052.

Apelt, T. A., Asprey, S. P. and Thornhill, N. F. (2001). Inferential measurement of SAG mill parameters, *Minerals Eng.* **14**(6): 575–591.

Apelt, T. A., Asprey, S. P. and Thornhill, N. F. (2002a). Inferential measurement of SAG mill parameters II: State estimation, *Minerals Eng.* **15**: 1043–1053.

Apelt, T. A., Asprey, S. P. and Thornhill, N. F. (2002b). Inferential measurement of SAG mill parameters III: Inferential models, *Minerals Eng.* **15**: 1055–1071.

Austin, L. G. (1990). Mill power equation for SAG mills, *Minerals Metallurgical Process.* **7**(1): 57–63.

Austin, L. G., Sutherland, D. N. and Gottlieb, P. (1993). An analysis of SAG mill grinding and liberation tests, *Minerals Eng.* **6**(5): 491–507.

Bauer, M. and Craig, I. K. (2008). Economic assessment of advanced process control - A survey and framework, *J. Process Control* **18**(1): 2–18.

Bavdekar, V. A., Deshpande, A. P. and Patwardhan, S. C. (2011). Identification of process and measurement noise covariance for state and parameter estimation using extended Kalman filter, *J. Process Control* **21**: 585–601.

Bazin, C. and B-Chapleau, C. (2005). The difficulty associated with measuring slurry rheological properties and linking them to grinding mill performance, *Int. J. Mineral Process.* **76**: 93–99.

Bemporad, A., Borrelli, F. and Morari, M. (2002a). Model predictive control based on linear programming - the explicit solution, *IEEE Trans. Automatic Control* **47**(12): 1974–1985.

Bemporad, A., Morari, M., Dua, V. and Pistikopoulos, E. N. (2002b). The explicit linear quadratic regulator for constrained systems, *Automatica* **38**: 3–20.

Bergh, L. G. and Yianatos, J. B. (2011). The long way toward multivariate predictive control of flotation processes, *J. Process Control* **21**: 226–234.

Bhitre, N. G. and Padhi, R. (2014). State constrained Model Predictive Static Programming: A slack variable approach, *Proc. 3rd Int. IFAC Conf. Advances Control Optimization Dynamical Systems*, Kanpur, India, pp. 832-839, doi: 10.3182/20140313-3-IN-3024.00175.

Borell, M., Backstrom, P. and Soderberg, L. (1996). Supervisory control of autogenous grinding circuits, *Int. J. Mineral Process.* **44-45**: 337–348.

Botha, S., Craig, I. K. and Roux, J. D. L. (2015). Switching cyclones to increase product particle size range for ore milling circuits, *Proc. 4th IFAC Workshop Mining Mineral Metal Processing*, Oulu, Finland, pp. 92-97, doi: 10.1016/j.ifacol.2015.10.084.

Bouche, C., Brandt, C., Broussaud, A. and Drunick, W. (2005). Advanced control of grinding controllers in South Africa, *Minerals Eng.* **18**: 866–876.

Bueno, M. P., Kojovic, T., Powell, M. S. and Shi, F. N. (2013). Multi-component AG/SAG mill model, *Minerals Eng.* **43-44**: 12–21.

Chawla, C., Sarmah, P. and Padhi, R. (2010). Supoptimal re-entry guidance of a reusable launch vehicle using pitch plane maneuver, *Aerospace Science Tech.* **14**: 377–386.

Chen, X., Li, Q. and Fei, S. (2008). Constrained model predictive control in ball mill grinding process, *Powder Tech.* **186**(1): 31–39.

Chen, X., Zhai, J., Li, S. and Li, Q. (2007). Application of model predictive control in ball mill grinding circuit, *Minerals Eng.* **20**(11): 1099–1108.

Coetzee, L. C., Craig, I. K. and Kerrigan, E. C. (2010). Robust nonlinear model predictive control of a run-of-mine ore milling circuit, *IEEE Trans. Control Syst. Technol.* **18**(1): 222–229.

Cortinovis, A., Mercangöz, M., Mathur, T., Poland, J. and Blaumann, M. (2013). Nonlinear coal mill modeling and its application to model predictive control, *Control Eng. Practice* **21**: 308–320.

Craig, I., Aldrich, C., Braatz, R., Cuzzola, F., Domlan, E., Engell, S., Hahn, J., Havlena, V., Horch, A., Huang, B., Khanbaghi, M., Konstantellos, A., Marquardt, W., McAvoy, T., Parisini, T., Pistikopoulos, S., Samad, T., Skogestad, S., Thornhill, N. and Yu, J. (2011). The impact of control technology: Control in the process industries. www.ieeecss.org. Last accessed on 2015-11-18.

Craig, I. K. and Henning, R. G. D. (2000). Evaluation of advanced industrial control projects: a framework for determining economic benefits, *Control Eng. Practice* **8**: 769–780.

Craig, I. K. and Koch, I. (2003). Experimental design for economic performance evaluation of industrial controllers, *Control Eng. Practice* **11**: 56–66.

Craig, I. K. and MacLeod, I. M. (1995). Specification framework for robust control of a run-of-mine ore milling circuit, *Control Eng. Practice* **3**(5): 621–630.

Craig, I. K. and MacLeod, I. M. (1996). Robust controller design and implementation for a run-of-mine ore milling circuit, *Control Eng. Practice* **4**(1): 1–12.

Craig, I. K., Hulbert, D. G., Metzner, G. and Moult, S. P. (1992). Optimized multivariable control of an industrial run-of-mine milling circuit., *J. South African Inst. Mining and Metallurgy* **92**: 169–176.

Cramer, L. A. (2008). What is your PGM concentrate worth?, *Proc. 3rd Int. Platinum Conf. - Platinum in Transformation, SAIMM, Sun City, South Africa*, pp. 387–394.

Darby, M. L. and Nikolaou, M. (2012). MPC: Current practice and challenges, *Control Eng. Practice* **20**: 328–342.

De Oliveira, N. M. C. and Biegler, L. T. (1995). An extension of Newton-type algorithms for non-linear process control, *Automatica* **31**(2): 281–286.

Delaney, G. W., Cleary, P. W., Morrison, R. D., Cummins, S. and Loveday, B. (2013). Predicting breakage and the evolution of rock size and shape distributions in AG and SAG mills using DEM, *Minerals Eng.* **50-51**: 132–139.

Dempster, A. P., Laird, N. M. and Rubin, D. (1977). Maximum likelihood from incomplete data via the EM algorithm, *J. R. Stat. Soc. B* **3**: 1–38.

Desbiens, A., Hodouin, D., Najim, K. and Flament, F. (1994). Long-range predictive control of a rougher flotation unit, *Minerals Eng.* **7**(1): 21–37.

Desbiens, A., Najim, K., Pomerleau, A. and Hodouin, D. (1997). Adaptive control - practical aspects and application to a grinding circuit, *Optimal Control Applications Methods* **18**: 29–47.

Dochain, D., Marquardt, W., Won, S., Malik, O., Kinnaert, M. and Lunze, J. (2008). Monitoring and control of process and power systems: Adapting to environmental challenges, increasing competitivity and challenging customer and consumer demands, *Proc. 17th IFAC World Congress*, Seoul, Korea, pp. 7160-7171, doi: 10.3182/20080706-5-KR-1001.3660.

Downs, J. J. and Skogestad, S. (2011). An industrial and academic perspective on plantwide control, *Annual Reviews Control* **35**: 99–110.

Downs, J. J. and Vogel, E. F. (1993). A plant-wide industrial process control problem, *Computers Chem. Eng.* **17**(3): 245–255.

Doyle, III, F. J. and Henson, M. A. (1997). Nonlinear process control, Prentice-Hall, Inc., Upper Saddle River, NJ, USA, chapter Nonlinear Systems Theory, pp. 111–147.

Edwards, R., Vien, A. and Perry, R. (2002). *Mineral Processing Plant Design, Practice, and Control Proceedings*, Society Mining Metallurgy Exploration, chapter Strategies for the instrumentation and control of grinding circuits, pp. 2130–2151.

Foss, A. S. (1973). Critique of chemical process control theory, *AIChE Journal* **19**: 209–214.

Grüne, L. and Pannek, J. (2011). *Nonlinear Model Predictive Control, Theory and Algorithms*, Springer-Verlag.

Gupta, A. and Yan, D. S. (2006). *Mineral Processing Design and Operation: An Introduction*, Elsevier B. V., The Boulevard, Langford Lane, Kidlington, Oxford OX5 1GB, UK.

Halbe, D. and Smolik, T. J. (2002). *Mineral processing plant design, practice, and control proceedings*, Society Mining Metallurgy Exploration, chapter Process operating costs with applications in mine planning and risk analysis, pp. 326–345.

Halbe, O., Raja, R. G. and Padhi, R. (2014). Robust re-entry guidance of a reusable launch vehicle using Model Predictive Static Programming, *J. Guidance Control Dynamics* **37**(1): 134–148.

Herbst, J. A. and Pate, W. T. (1999). Object components for comminution system softsensor design, *Powder Tech.* **105**: 424–429.

Herbst, J. A., Pate, W. T. and Oblad, A. E. (1992). Model-based control of mineral processing operations, *Powder Tech.* **69**: 21–23.

Herbst, J. S. and Pate, W. T. (1996). On-line estimation of charge volumes in semi-autogenous and autogenous grinding mills, *Proc. SAG 1996, Vancouver, B.C., Canada*, pp. 817–827.

Herbst, J. S., Pate, W. T. and Oblad, A. E. (1989). Experiences in the use of model-based expert control systems in autogenous and semi-autogenous grinding circuits, *Proc. SAG 1989, Vancouver, B.C., Canada*, pp. 669–686.

Hermann, R. and Krener, A. J. (1977). Nonlinear controllability and observability, *IEEE Trans. Automatic Control* **AC-22**(5): 728–740.

Hinde, A. L. and Kalala, J. T. (2009). The application of a simplified approach to modelling tumbling mills, stirred media mills and HPGR's, *Minerals Eng.* **22**(7-8): 633–641.

Hodouin, D. (2011). Methods for automatic control, observation and optimization in mineral processing plants, *J. Process Control* **21**(2): 211–225.

Hodouin, D., Jämsä-Jounela, S. L., Carvalho, M. T. and Bergh, L. G. (2001). State-of-the-art and challenges in Mineral Processing Control, *Control Eng. Practice* **9**(9): 995–1005.

Hulbert, D. G., Craig, I. K., Coetzee, M. L. and Tudor, D. (1990). Multivariable control of a run-of-mine milling circuit, *J. South African Inst. Mining and Metallurgy* **90**(7): 173–181.

Jacobson, D. H. and Lele, M. M. (1969). A transformation technique for optimal control problems with a state variable inequality constraint, *IEEE Trans. Automatic Control* **AC-14**(5): 457–464.

Joe, E. G. (1979). Energy consumption in Canadian mills, *CIM Bulletin* **72**: 147–151.

Joshi, G. and Padhi, R. (2013). Formation flying of small satellites using suboptimal MPSP guidance, *Proc. American Control Conf.*, Washington, DC, United States, pp. 1584-1589, doi: 10.1109/ACC.2013.6580061.

Kestenbaum, A., Shinnar, R. and Thau, F. E. (1976). Design concepts for process control, *Ind. Eng. Chem. Proc. Des. Dev.* **15**(1): 2–13.

King, R. P. (2001). *Modeling and Simulation of Mineral Processing Systems*, Butterworth-Heinemann, Linacre House, Jordan Hill, Oxford OX2 8DP.

Kojovic, T., Powell, M. S., Bailey, C. and Drinkwater, D. (2011). Upgrading the JK SAG mill model, *Proc. SAG 2011, Vancouver, B.C., Canada*, pp. 1–20.

Kouramas, K. I., Panos, C., Faisca, N. P. and Pistikopoulos, E. N. (2013). An algorithm for robust explicit/multi-parametric model predictive control, *Automatica* **49**: 381–389.

Larsson, T. and Skogestad, S. (2000). Plantwide control - A review and a new design procedure, *Modeling Identification Control* **21**(4): 209–240.

Latchireddi, S. and Morrell, S. (2003). Slurry flow in mills: grate-only discharge mechanism (Part-1), *Minerals Eng.* **16**: 625–633.

Laurila, H., Karesvuori, J. and Tiili, O. (2002). *Mineral processing plant design, practice, and control proceedings*, Society Mining Metallurgy Exploration, chapter Strategies for instrumentation and control of flotation circuits, pp. 2174–2195.

Le Roux, J. D. and Craig, I. K. (2013). Reducing the number of size classes in a cumulative rates model used for process control of a grinding mill circuit, *Powder Tech.* **246**: 169–181.

Le Roux, J. D. and Craig, I. K. (2016). State and parameter identifiability of a nonlinear grinding mill circuit model, *Proc. 17th IFAC Symposium Mining Mineral Metal Processing*, Vienna, Austria. (Accepted.).

Le Roux, J. D., Craig, I. K. and Padhi, R. (2013a). State and parameter estimation for a grinding mill circuit from operational input-output data, *Proc. 10th IFAC Symposium Dynamics Control Process Systems*, Mumbai, India, pp. 178-183, doi: 10.3182/20131218-3-IN-2045.00046.

Le Roux, J. D., Craig, I. K., Hulbert, D. G. and Hinde, A. L. (2013b). Analysis and validation of a run-of-mine ore grinding mill circuit model for process control, *Minerals Eng.* **43-44**: 121–134.

Le Roux, J. D., Olivier, L. E., Naidoo, M. A., Padhi, R. and Craig, I. K. (2016a). Throughput and product quality control for a grinding mill circuit using non-linear MPC, *J. Process Control* **42**: 35–50.

Le Roux, J. D., Padhi, R. and Craig, I. K. (2014). Optimal control of grinding mill circuit using model predictive static programming: A new nonlinear MPC paradigm, *J. Process Control* **24**: 29–40.

Le Roux, J. D., Skogestad, S. and Craig, I. K. (2016b). Plant-wide control of grinding mill circuits: Top-down analysis, *Proc. 17th IFAC Symposium Mining Mineral Metal Processing*, Vienna, Austria. (Accepted.).

Le Roux, J. D., Steinboeck, A., Kugi, A. and Craig, I. K. (2016c). Nonlinear observability of grinding mill conditions, *Proc. 17th IFAC Symposium Mining Mineral Metal Processing*, Vienna, Austria. (Accepted.).

Lestage, R., Pomerleau, A. and Hodouin, D. (2002). Constrained real-time optimization of a grinding circuit using steady-state linear programming supervisory control, *Powder Tech.* **124**(3): 254–263.

Li, W. and Biegler, L. T. (1989). Multistep, Newton-type control strategies for constrained, nonlinear processes, *Chem. Eng. Research Design* **67**(6): 562–577.

Luyben, M. L., Tyreus, B. D. and Luyben, W. L. (1997). Plantwide control design procedure, *AIChE Journal* **43**(12): 3161–3174.

Maity, A., Oza, H. B. and Padhi, R. (2013). Generalized model predictive static programming and its application to 3D impact angle constrained guidance of air-to-surface missiles, *Proc. American Control Conf.*, Washington, DC., United States.

Matthews, B. and Craig, I. K. (2013). Demand side management of a run-of-mine ore milling circuit, *Control Eng. Practice* **21**: 759–768.

McIvor, R. and Finch, J. (1991). A guide to interfacing of plant grinding and flotation operations, *Minerals Eng.* **4**(1): 9–23.

Meadows, E. S. and Rawlings, J. B. (1997). Nonlinear process control, Prentice-Hall, Inc., Upper Saddle River, NJ, USA, chapter Model Predictive Control, pp. 233–310.

Minasidis, V., Skogestad, S. and Kaistha, N. (2015). Simple rules for economic plantwide control, *Proc. 12th Int. Symposium Process Systems Eng. and 25th European Symposium Computer Aided Process Eng.*, Copenhagen, Denmark, pp. 397-402, doi: 10.3182/20131218-3-IN-2045.00103.

Mishra, B. K. (2003a). A review of computer simulation of tumbling mills by the discrete element method: Part I - contact mechanics, *Int. J. Mineral Process.* **71**(1-4): 73–93.

Mishra, B. K. (2003b). A review of computer simulation of tumbling mills by the discrete element method: Part II - practical applications, *Int. J. Mineral Process.* **71**(1-4): 95–112.

Morari, M., Arkun, Y. and Stephanopoulos, G. (1980). Studies in the synthesis of control sstructure for chemical processes - Part 1: Formulation of the problem. Decomposition and classification tasks. Analysis of the optimising control structures., *AIChE Journal* **26**(2): 220–232.

Morrell, S. (2004). A new autogenous and semi-autogenous mill model for scale-up, design and optimisation, *Minerals Eng.* **17**(3): 437–445.

Morrell, S. and Stephenson, I. (1996). Slurry discharge capacity of autogenous and semi-autogenous mills and the effect of grate design, *Int. J. Mineral Process.* **46**: 53–72.

Morrell, S. and Valery, W. (2001). Influence of feed size on AG/SAG mill performance, *Proc. SAG 2001, Vancouver, B.C., Canada*, pp. 203–214.

Morrison, R. D., Shi, F. N. and Whyte, R. (2007). Modelling of incremental rock breakage by impact - for use in DEM models, *Minerals Eng.* **20**: 303–309.

Munoz, C. and Cipriano, A. (1999). An integrated system for supervision and economic optimal control of mineral processing plants, *Minerals Eng.* **12**(6): 627–643.

Nageswararao, K., Wiseman, D. M. and Napier-Munn, T. J. (2004). Two empirical hydrocyclone models revisited, *Minerals Eng.* **17**(5): 671–687.

Napier-Munn, T. J., Morrell, S., Morrison, R. D. and Kojovic, T. (2005). *Mineral Communition Circuits: Their Operation and Optimisation*, 3rd edn, JKMRC Monograph Series in Mining and Mineral Processing, Isles Road, Indooroopilly, Queensland 4068, Australia.

Narasimha, M., Mainza, A., Holtham, P. N., Powell, M. S. and Brennan, M. S. (2014). A semi-mechanistic model of hydrocyclones - Developed from industrial data and inputs from CFD, *Int. J. Mineral Process.* **133**: 1–12.

Ng, C. S. and Stephanopoulos, G. (1996). Synthesis of control systems for chemical plants, *Computers Chem. Eng.* **20**(Suppl. 2): S999–S1004.

Niemi, A. J., Tian, L. and Ylinen, R. (1997). Model predictive control for grinding systems, *Control Eng. Practice* **5**(2): 271–278.

Olivier, L. E. and Craig, I. K. (2013). Model-plant mismatch detection and model update for a run-of-mine ore milling circuit under model predictive control, *J. Process Control* **23**(2): 100–107.

Olivier, L. E., Huang, B. and Craig, I. K. (2012). Dual particle filters for state and parameter estimation with application to a run-of-mine ore mill, *J. Process Control* **22**(4): 710–717.

Oza, H. B. and Padhi, R. (2012). Impact-angle-constrained suboptimal model predictive static programming guidance of air-to-ground missiles, *J. Guidance Control Dynamics* **35**(1): 153–164.

Padhi, R. and Kothari, M. (2009). Model predictive static programming: A computationally efficient technique for suboptimal control design, *Int. J. Innovative Computing Information Control* **5**(2): 399–411.

Pannocchia, G., Rawlings, J. B. and Wright, S. J. (2007). Fast large-scale model predictive control by partial enumeration, *Automatica* **43**(5): 852–860.

Pomerleau, A., Hodouin, D., Desbiens, A. and Gagnon, E. (2000). A survey of grinding circuit control methods: from decentralized PID controllers to multivariable predictive controllers, *Powder Tech.* **108**(2-3): 103–115.

Powell, M. S. and Mainza, A. N. (2006). Extended grinding curves are essential to the comparison of milling performance, *Minerals Eng.* **19**: 1487–1494.

Powell, M. S. and Morrison, R. D. (2007). The future of comminution modelling, *Int. J. Mineral Process.* **84**(1-4): 228–239.

Powell, M. S., van der Westhuizen, A. P. and Mainza, A. N. (2009). Applying grindcurves to mill operation and optimisation, *Minerals Eng.* **22**(7-8): 625–632.

Psiaki, M. L. (2013). The blind tricyclist problem and a comparative study of nonlinear filters, *IEEE Control Systems Magazine* pp. 40–54.

Putz, E. and Cipriano, A. (2015). Hybrid model predictive control for flotation plants, *Minerals Eng.* **70**: 26–35.

Qin, S. J. and Badgwell, T. A. (2003). A survey of industrial model predictive control technology, *Control Eng. Practice* **11**(7): 733–764.

Ramasamy, M., Narayanan, S. S. and Rao, C. D. P. (2005). Control of ball mill grinding circuit using model predictive control scheme, *J. Process Control* **15**(3): 273–283.

Remes, A., Aaltonen, J. and Koivo, H. (2010). Grinding circuit modeling and simulation of particle size control at Siilinjärvi concentrator, *Int. J. Mineral Process.* **96**(1-4): 70–78.

Rivotti, P. and Pistikopoulos, E. N. (2015). A dynamic programming based approach for explicit model predictive control of hybrid systems, *Computers Chem. Eng.* **72**: 126–144.

Salazar, J. L., Magne, L., Acuña, G. and Cubillos, F. (2009). Dynamic modelling and simulation of semi-autogenous mills, *Minerals Eng.* **22**(1): 70–77.

Salazar, J., Valdez-Gonzalres, H., Vyhmesiter, E. and Cubillos, F. (2014). Model predictive control of semi-autogenous mills, *Minerals Eng.* **64**: 92–96.

Savitzky, A. and Golay, M. J. E. (1964). Smoothing and differentiation of data by simplified least squares procedures, *Analytical Chemistry* **36**(8): 1627–1629.

Sbarbaro, D. and del Villar, R. (2010). *Advanced Control and Supervision of Mineral Processing Plants*, Springer-Verlag London Limited.

Schneider, R. and Georgakis, C. (2013). How to not make the extended Kalman filter fail, *Ind. Eng. Chem. Res.* **52**: 3354–3362.

Scokaert, P. O. M., Mayne, D. Q. and Rawlings, J. B. (1999). Suboptimal model predictive control (Feasibility implies stability), *IEEE Trans. Automatic Control* **44**(3): 648–654.

Seborg, D. E., Edgar, T. F. and Mellichamp, D. A. (2004). *Process Dynamics and Control*, 2nd edn, John Wiley & Sons, Inc.

Seppälä, P., Sorsa, A., Paavola, M., Ruuska, J., Remes, A., Kumar, H., Lamberg, P. and Leiviskä, K. (2016). Development and calibration of a dynamic flotation circuit model, *Minerals Eng.* **96-97**: 168–176.

Shean, B. J. and Cilliers, J. J. (2011). A review of froth flotation control, *Int. J. Mineral Process.* **100**: 57–71.

Shi, F. N. and Napier-Munn, T. J. (2002). Effects of slurry rheology on industrial grinding performance, *Int. J. Mineral Process.* **65**(3-4): 125–140.

Simon, D. J. (2006). *Optimal State Estimation*, John Wiley and Sons, Inc., 111 River Street, Hoboken, NJ 07030, United States.

Skogestad, S. (2004). Control structure design for complete chemical plants, *Computers Chem. Eng.* **28**: 219–234.

Skogestad, S. (2012). *Plantwide Control: Recent Developments and Applications*, John Wiley & Sons Ltd, The Atrium, Southern Gate, Chichester, West Sussex PO19 8SQ, United Kingdom, chapter Economic Plantwide Control, pp. 229–251.

Skogestad, S. and Postlethwaite, I. (2005). *Multivariable Feedback Control: Analysis and Design*, 2nd edn, John Wiley & Sons Ltd, The Atrium, Southern Gate, Chichester, West Sussex PO19 8SQ, England.

Sosa-Blanco, C., Hodouin, D., Bazin, C., Lara-Valenzuele, C. and Salazar, J. (2000). Economic optimisation of a flotation plant through grinding circuit tuning, *Minerals Eng.* **13**(10-11): 999–1018.

Stanley, G. G. (1987). *The extractive metallurgy of gold in South Africa*, Vol. 1, South African Institute of Mining and Metallurgy, Johannesburg.

Stephanopoulos, G. (2014). Laying the foundations: an advisor's perspective, *Computers Chem. Eng.* **70**: 3–10.

Stephanopoulos, G. and Ng, C. (2000). Perspectives on the synthesis of plant-wide control structures, *J. Process Control* **10**: 97–111.

Steyn, C. W. (2011). *Optimisation of a fully autogenous comminution circuit*, Master's thesis, University of Pretoria.

Suichies, M., Leroux, D., Dechert, C. and Trusiak, A. (2000). An implementation of generalized predictive control in a flotation plant, *Control Eng. Practice* **8**: 319–325.

Summers, S., Jones, C. N., Lygeros, J. and Morari, M. (2011). A multiresolution approximation method for fast explicit model predictive control, *IEEE Trans. Automatic Control* **56**(11): 2530–2541.

Teixeira, B. O. S., Torres, L. A. B., Aguirre, L. A. and Bernstein, D. S. (2010). On unscented Kalman filtering with state interval constraints, *J. Process Control* **20**: 45–57.

Trahar, W. J. (1981). A rational interpretation of the role of particle size in flotation, *Int. J. Mineral Process.* **8**: 289–327.

Tungpalan, K., Manlapig, E., Andrusiewicz, M., Keeney, L., Wightman, E. and Edraki, M. (2015). An integrated approach of predicting metallurgical performance relating to variability in deposit characteristics, *Minerals Eng.* **71**: 49–54.

Umeda, T., Kuriyama, T. and Ichidawa, A. (1978). A logical structure for process control system synthesis, *Proc. 7th Int. IFAC World Congress*, Helsinki, Finland.

Valappil, J. and Georgakis, C. (2000). Systematic estimation of state noise statistics for extended Kalman filters, *AIChE Journal* **46**(2): 292–308.

Valery, W. and Morrell, S. (1995). The development of a dynamic model for autogenous and semi-autogenous grinding, *Minerals Eng.* **8**(11): 1285–1297.

Van der Westhuizen, A. and Powell, M. S. (2006). Milling curves as a tool for characterising SAG mill performance, *Proc. SAG 2006, Vancouver, B.C., Canada*, pp. 217–232.

Viklund, T., Albertsson, J., Burstedt, J., Isaksson, M. and Soderlund, J. (2006). Evolution of AG mill control system at Boliden Mineral AB., *Proc. SAG 2006, Vancouver, B.C., Canada*, pp. 311–325.

Wang, Y. and Boyd, S. (2010). Fast model predictive control using online optimization, *IEEE Trans. Control Syst. Technol.* **18**(2): 267–278.

Wei, D. and Craig, I. K. (2009a). Economic performance assessment of two ROM ore milling circuit controllers, *Minerals Eng.* **22**(9-10): 826–839.

Wei, D. and Craig, I. K. (2009b). Grinding mill circuits - A survey of control and economic concerns, *Int. J. Mineral Process.* **90**(1-4): 56–66.

Whiten, W. J. (1974). A matrix theory of communition machines, *Chemical Eng. Sci.* **29**(2): 589–599.

Wills, B. A. (2006). *Wills' Mineral Processing Technology: An Introduction to the Practical Aspects of Ore Treatment and Mineral Recovery*, 7th edn, Butterworth-Heinemann, Linacre House, Jordan Hill, Oxford OX2 8DP, UK.

Wolf, I. J. and Marquardt, W. (2016). Fast NMPC schemes for regulatory and economic NMPC - A review, *J. Process Control* **44**: 162–183.

Yang, J., Li, S., Chen, X. and Li, Q. (2010). Disturbance rejection of ball mill grinding circuits using DOB and MPC, *Powder Tech.* **198**: 219–228.

Zhao, Z., Huang, B. and Liu, F. (2014). Constrained particle filtering methods for state estimation of nonlinear processes, *AIChE Journal* **60**(6): 2072–2082.

APPENDIX A

NON-LINEAR OBSERVABILITY ANALYSIS

This section describes the observability analysis completed in Section 5.2.2 of the non-linear observer model. The non-linear observer model can be written as

$$\begin{aligned}
\dot{x} &= f(x) + g(x)u &&= \begin{bmatrix} -\eta(x_w + x_s)x_w \\ -\eta(x_w + x_s)x_s + x_r K_r \\ -x_r K_r \\ -x_b K_b \\ 0_{3\times 1} \end{bmatrix} + \begin{bmatrix} I_{4\times 4} \\ 0_{3\times 4} \end{bmatrix} u \\
y &= h(x) &&= \begin{bmatrix} \frac{x_w + x_s + x_r + x_b}{v_{mill}} \\ \eta(x_w + x_s)^2 \\ \frac{\rho_O x_s + \rho_W x_w}{x_s + x_w} \end{bmatrix}
\end{aligned}$$

where $x = [x_w, x_s, x_r, x_b, \eta, K_r, K_b]^T$, $u = [V_{wi}, V_{si}, V_{ri}, V_{bi}]^T$ and $y = [J_T, Q, \rho_Q]^T$. It is assumed that the parameters η, K_r and K_b are unknown constants, although in practice these are slow time-varying parameters.

The repeated Lie derivatives of the system output with respect to the system dynamics are collected in a single vector, as shown below.

$$\begin{bmatrix} h \\ L_f h \\ L_f^2 h \end{bmatrix} = \begin{bmatrix} \frac{x_w+x_s+x_r+x_b}{v_{mill}} \\ \eta\left(x_w+x_s\right)^2 \\ \frac{\rho_O x_s+\rho_W x_w}{x_s+x_w} \\ -\frac{\eta(x_s+x_w)^2+K_b x_b}{v_{mill}} \\ -2\eta^2\left(x_s+x_w\right)^3+2\eta K_r x_r\left(x_s+x_w\right) \\ \frac{x_w x_r K_r(\rho_o-\rho_w)}{(x_w+x_s)^2} \\ \frac{2\eta^2(x_s+x_w)^3-2\eta K_r x_r(x_s+x_w)+K_b^2 x_b}{v_{mill}} \\ 6\eta^3\left(x_s+x_w\right)^4-8\eta^2 K_r x_r\left(x_s+x_w\right)^2+2\eta K_r^2 x_r\left(x_r-x_s-x_w\right) \\ \frac{x_w x_r K_r(\rho_o-\rho_w)\left(\eta(x_s+x_w)^2-2K_r x_r-K_r x_s-K_r x_w\right)}{(x_w+x_s)^3} \end{bmatrix}$$

The exterior derivative is applied to obtain the following matrices. Note, for display purposes, the transpose of matrices dh and d$L_f h$ is shown, whereas the transpose of the rows of d$L_f^2 h$ is shown.

$$\mathrm{d}h = \begin{bmatrix} \frac{1}{v_{mill}} & 2\eta\left(x_w+x_s\right) & \frac{\rho_W-\rho_Q}{x_w+x_s} \\ \frac{1}{v_{mill}} & 2\eta\left(x_w+x_s\right) & \frac{\rho_O-\rho_Q}{x_w+x_s} \\ \frac{1}{v_{mill}} & 0 & 0 \\ \frac{1}{v_{mill}} & 0 & 0 \\ 0 & \left(x_w+x_s\right)^2 & 0 \\ 0 & 0 & 0 \\ 0 & 0 & 0 \end{bmatrix}^T$$

$$\mathrm{d}L_f h = \begin{bmatrix} -\frac{2\eta x_s+2\eta x_w}{v_{mill}} & -6\eta^2\left(x_s+x_w\right)^2+2\eta K_r x_r & \frac{x_r K_r(\rho_o-\rho_w)(-x_w+x_s)}{(x_w+x_s)^3} \\ -\frac{2\eta x_s+2\eta x_w}{v_{mill}} & -6\eta^2\left(x_s+x_w\right)^2+2\eta K_r x_r & -\frac{2x_w x_r K_r(\rho_o-\rho_w)}{(x_w+x_s)^3} \\ 0 & 2\eta K_r\left(x_s+x_w\right) & \frac{(\rho_o-\rho_w)x_w K_r}{(x_w+x_s)^2} \\ -\frac{K_b}{v_{mill}} & 0 & 0 \\ -\frac{(x_s+x_w)^2}{v_{mill}} & -4\eta\left(x_s+x_w\right)^3+2K_r x_r\left(x_s+x_w\right) & 0 \\ 0 & 2\eta x_r\left(x_s+x_w\right) & \frac{x_w x_r(\rho_o-\rho_w)}{(x_w+x_s)^2} \\ -\frac{x_b}{v_{mill}} & 0 & 0 \end{bmatrix}^T$$

$$\mathrm{d}L_f^2 h_{1,1..7} = \begin{bmatrix} \frac{6\eta^2(x_s+x_w)^2-2\eta K_r x_r}{v_{mill}} \\ \frac{6\eta^2(x_s+x_w)^2-2\eta K_r x_r}{v_{mill}} \\ \frac{-2\eta(x_w+x_s)K_r}{v_{mill}} \\ \frac{K_b^2}{v_{mill}} \\ \frac{4\eta(x_w+x_s)^3-2K_r x_r(x_w+x_s)}{v_{mill}} \\ \frac{-2x_r\eta(x_w+x_s)}{v_{mill}} \\ \frac{2x_b K_b}{v_{mill}} \end{bmatrix}^T$$

$$\mathrm{d}L_f^2 h_{2,1..7} = \begin{bmatrix} 24\eta^3(x_s+x_w)^3 - 16\eta^2 K_r x_r(x_s+x_w) - 2\eta K_r^2 x_r \\ 24\eta^3(x_s+x_w)^3 - 16\eta^2 K_r x_r(x_s+x_w) - 2\eta K_r^2 x_r \\ -8\eta^2 K_r(x_w+x_s)^2 + 2\eta K_r^2(2x_r - x_s - x_w) \\ 0 \\ 18\eta^2(x_s+x_w)^4 - 16\eta K_r x_r(x_s+x_w)^2 + 2K_r^2 x_r(x_r - x_s - x_w) \\ -8\eta^2 x_r(x_s+x_w)^2 + 4\eta K_r x_r(x_r - x_s - x_w) \\ 0 \end{bmatrix}^T$$

$$\mathrm{d}L_f^2 h_{3,1..7} = \begin{bmatrix} \frac{x_r K_r(\rho_o-\rho_w)\left(\eta x_s(x_s+x_w)^2-2K_r x_r(x_s-2x_w)-K_r\left(x_s^2+x_w^2\right)\right)}{(x_w+x_s)^4} \\ \frac{-x_w x_r K_r(\rho_o-\rho_w)\left(\eta(x_s+x_w)^2-2K_r(3x_r+x_s+x_w)\right)}{(x_w+x_s)^4} \\ \frac{x_w(\rho_o-\rho_w)K_r(\eta(x_w+x_s)^2-K_r(4x_r+x_s+x_w)}{(x_w+x_s)^3} \\ 0 \\ \frac{x_w x_r K_r(\rho_o-\rho_w)}{x_w+x_s} \\ \frac{x_w x_r(\rho_o-\rho_w)\left(\eta(x_w+x_s)^2-2K_r(2x_r-x_s-x_w)\right)}{(x_w+x_s)^3} \\ 0 \end{bmatrix}^T$$

Two observability codistributions are defined:

$$d\mathcal{O}_1 = \mathrm{span}\left\{\mathrm{d}h, \mathrm{d}L_f h\right\}$$
$$d\mathcal{O}_2 = \mathrm{span}\left\{\mathrm{d}h, \mathrm{d}L_f h, \mathrm{d}L_f^2 h\right\}.$$

The rank of $d\mathcal{O}_1$, which has 6 rows and 7 columns, is 6. The rank of $d\mathcal{O}_2$, which has 9 rows and 7 columns, is 7. Since full rank is achieved for $d\mathcal{O}_2$, the addition of further Lie derivatives is not necessary. The determinant of the first 7 rows and columns of $d\mathcal{O}_2$ is $\frac{2x_w x_r x_b K_b^2 \eta^2 (x_w+x_s)(\rho_o-\rho_w)^2}{v_{mill}^3}$. Therefore, all 7 system states are locally (weakly) observable from the available measurements.

LINEAR OBSERVABILITY ANALYSIS

This section describes the observability analysis completed in Section 5.2.2 for the linearised observer model. Linearisation of the non-linear observer model gives the following A and C matrices:

$$A = \begin{bmatrix} -\eta(2x_w+x_s) & -\eta x_w & 0 & 0 & -(x_w+x_s)x_w & 0 & 0 \\ -\eta x_s & -\eta(x_w+2x_s) & K_r & 0 & -(x_w+x_s)x_s & x_r & 0 \\ 0 & 0 & -K_r & 0 & 0 & -x_r & 0 \\ 0 & 0 & 0 & -K_b & 0 & 0 & -x_b \\ 0_{3\times1} & 0_{3\times1} & 0_{3\times1} & 0_{3\times1} & 0_{3\times1} & 0_{3\times1} & 0_{3\times1} \end{bmatrix}$$

$$C = \begin{bmatrix} \frac{1}{v_{mill}} & \frac{1}{v_{mill}} & \frac{1}{v_{mill}} & \frac{1}{v_{mill}} & 0 & 0_{1\times2} \\ 2\eta(x_w+x_s) & 2\eta(x_w+x_s) & 0 & 0 & (x_w+x_s)^2 & 0_{1\times2} \\ \frac{\rho_W-\rho_Q}{x_w+x_s} & \frac{\rho_O-\rho_Q}{x_w+x_s} & 0 & 0 & 0 & 0_{1\times2} \end{bmatrix}.$$

The eigenvalues of A are

$$\lambda = \{0,\ 0,\ 0,\ K_r,\ K_b,\ -\eta(x_s+x_w),\ -2\eta(x_s+x_w)\}$$

and the corresponding eigenvectors collected as columns are given by

$$T = \begin{bmatrix} 0 & 0 & -\frac{x_w}{2\eta} & \frac{-\eta x_w K_r}{2\eta^2(x_s+x_w)^2-3\eta K_r(x_s+x_w)+K_r^2} & 0 & -1 & \frac{x_w}{x_s} \\ 0 & 0 & -\frac{x_s}{2\eta} & \frac{K_r(\eta x_s+2\eta x_w-K_r)}{2\eta^2(x_s+x_w)^2-3\eta K_r(x_s+x_w)+K_r^2} & 0 & 1 & 1 \\ 0 & -\frac{x_r}{K_r} & 0 & 1 & 0 & 0 & 0 \\ -\frac{x_b}{K_b} & 0 & 0 & 0 & 1 & 0 & 0 \\ 0 & 0 & 1 & 0 & 0 & 0 & 0 \\ 0 & 1 & 0 & 0 & 0 & 0 & 0 \\ 1 & 0 & 0 & 0 & 0 & 0 & 0 \end{bmatrix}.$$

The output pole matrix $Y_\lambda = CT$ is

$$Y_\lambda = \begin{bmatrix} -\frac{x_b}{v_{mill}K_b} & -\frac{x_r}{v_{mill}K_r} & \frac{-x_w-x_s}{2v_{mill}\eta} & \frac{2\eta(x_w+x_s)}{(2\eta(x_s+x_w)-K_r)v_{mill}} & \frac{1}{v_{mill}} & 0 & \frac{x_w+x_s}{v_{mill}x_s} \\ 0 & 0 & 0 & \frac{2\eta(x_w+x_s)K_r}{2\eta(x_s+x_w)-K_r} & 0 & 0 & \frac{2\eta(x_w+x_s)^2}{x_s} \\ 0 & 0 & 0 & \frac{(\rho_o-\rho_w)x_w K_r}{(\eta(x_s+x_w)-K_r)(x_w+x_s)^2} & 0 & \frac{\rho_o-\rho_w}{x_w+x_s} & 0 \end{bmatrix}.$$

Introduce the new state vector

$$z = T^{-1}x \quad ; \quad x = Tz.$$

Since the eigenvectors are independent, T^{-1} exists. Therefore, the matrix A may be diagonalised as

$$\Lambda = T^{-1}AT = \text{diag}\left[0,\ 0,\ 0,\ K_r,\ K_b,\ -\eta\left(x_s + x_w\right),\ -2\eta\left(x_s + x_w\right)\right]. \tag{.1}$$

The linearised system can now be written as

$$\begin{aligned} \dot{z} &= \Lambda z + T^{-1}Bu \\ y &= CTz \end{aligned} \tag{.2}$$

As seen from the transformed system, the repeated integrating mode ($\lambda = 0$) is associated with the transformed states $z_1 = K_b$, $z_2 = K_r$ and $z_3 = \eta$. These three parameters respectively indicate the rate at which the ball level, the rock level, and the slurry level increases or decreases. It is expected that the three aforementioned parameters are associated with the integrating modes, as levels in tanks represent integrating processes.

As seen from the new output matrix CT, the states z_1, z_2, and z_3 are only visible in the first output measurement J_T. Therefore, if the integrating mode is excited in the system, it is not possible to distinguish the individual contribution of each state (z_1, z_2, and z_3) to the measurement of J_T. Two of the states need to be defined for the third state to be observable. Therefore, only 5 of the 7 states are observable for the linearised system.

This result that the linearised system's parameters and states are not observable is not surprising considering neither the rocks or balls exit the mill. Apart from the measurement J_T, where these states appear as a linear combination, no further information is available. However, the observability analysis of the non-linear system indicates that if sufficient dynamics are visible in the output, and a non-linear observer is used, the individual contribution of the rocks and balls to J_T is distinguishable.

Although a non-linear observer such as MHE is a preferable solution, it requires the correct modelling of the time-varying nature of the parameters. The ore breakage rate and the ball breakage rate vary according to unmeasured changes in ore hardness and grinding conditions in the mill, but is modelled as constants by the model. This approximation is valid over a short period, especially when compared to the quick dynamics of the water and solids over the same period. But for longer periods the approximation cannot hold.

The discharge rate is also modelled as a constant, which is a valid assumption over long periods since this parameter lumps together constant factors such as mill diameter, grate aperture open area, and the

relative radial position of the grate apertures. However, for a mill where the rotational speed changes, the discharge rate needs to account for this variation in speed as shown in (5.5). Therefore, if a long time horizon is used for MHE, the validity of the model reduces with regards to the ore and ball breakage, but a shorter time horizon may not contain sufficient process dynamics for MHE to provide reasonable estimates of the states and parameters.

APPENDIX B

An overview of the work is provided in the slides below.

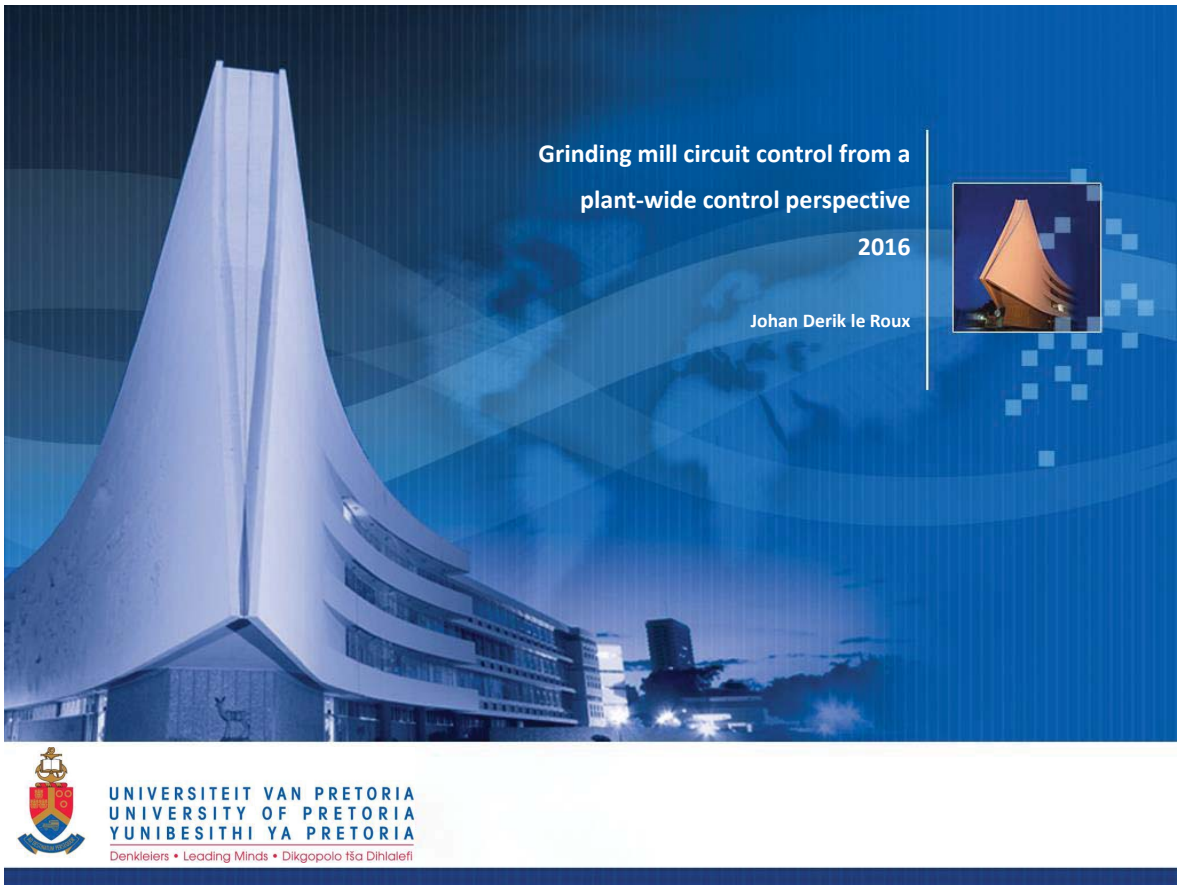

Context

- Mineral processing plant
  - Comminution: liberation of valuable particles from ore
  - Separation: removal of valuable particles from waste
    - Separator concentrate sold to refinery

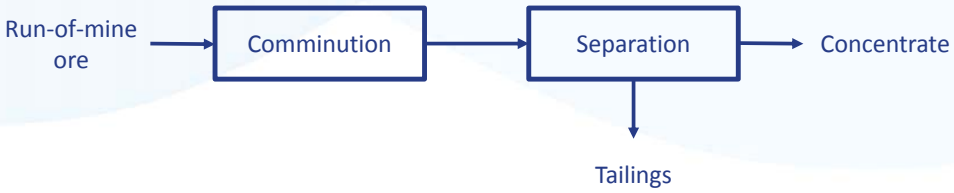

Context

- Mineral processing plant
  - Comminution: liberation of valuable particles from ore
  - Separation: removal of valuable particles from waste
    - Separator concentrate sold to refinery

How should the *comminution circuit* be operated to improve the value of the *separator concentrate*?

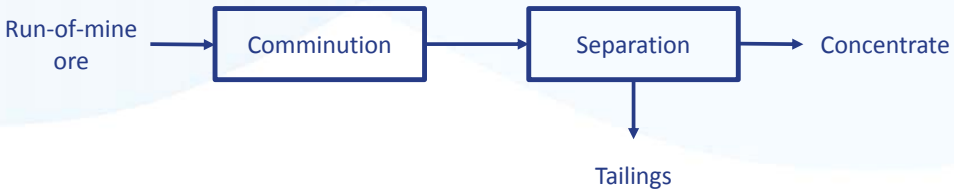

Comminution: Single-stage grinding mill circuit

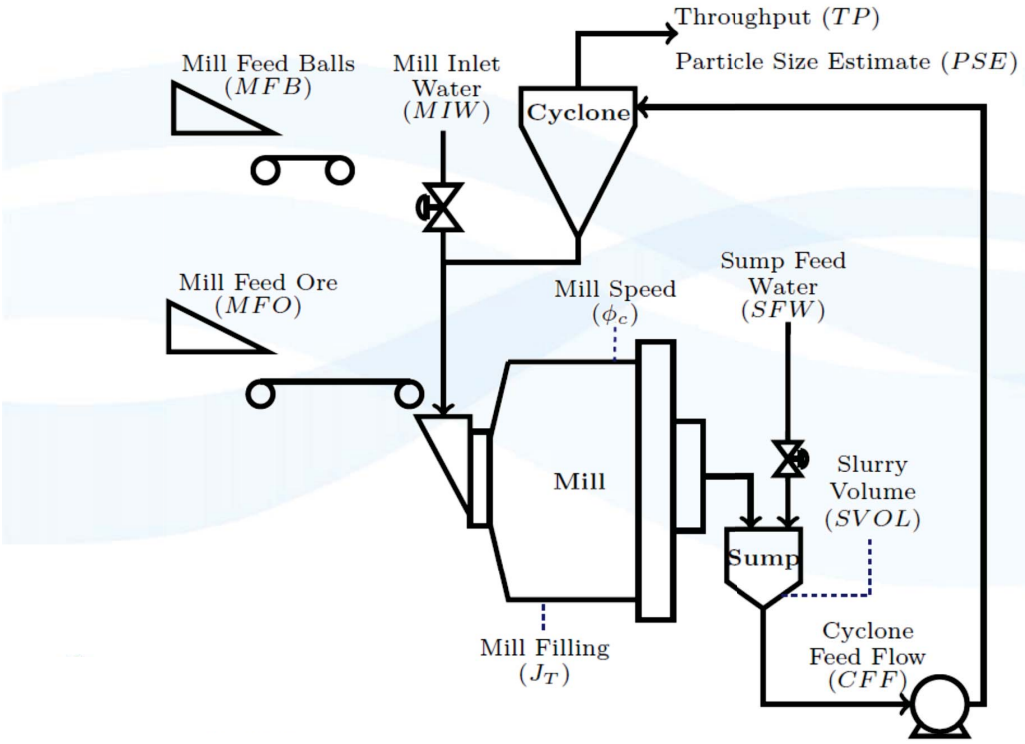

Plant-wide control[1] – Top-down analysis

- Operational economic objective
  - Separator concentrate grade (γ_C) and recovery (Υ) expressed in terms of comminution's product throughput (TP) and quality (PSE)
  - Revenue expressed as function of TP and PSE

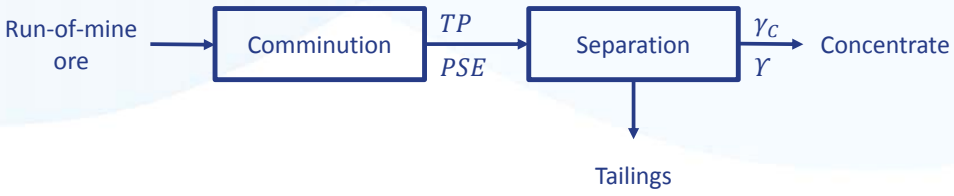

[1] Skogestad, S. (2004). Control structure design for complete chemical plants, Computers Chem. Eng. 28: 219–234.

Plant-wide control[1] – Top-down analysis

- Operational economic objective
  - Separator concentrate grade (γ_C) and recovery (Υ) expressed in terms of comminution's product throughput (TP) and quality (PSE)
  - Revenue expressed as function of TP and PSE

How should the grinding mill circuit's *operating point* be chosen to achieve a specific TP and PSE?

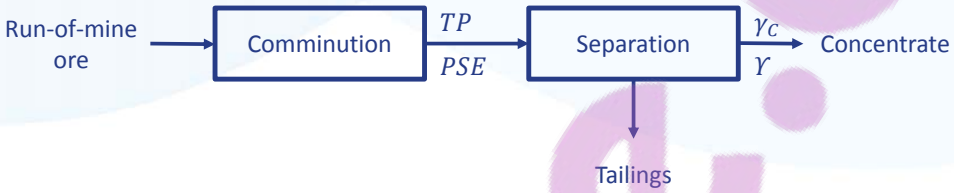

[1] Skogestad, S. (2004). Control structure design for complete chemical plants, Computers Chem. Eng. 28: 219–234.

Plant-wide control – Top-down analysis

- Optimal steady-state operation
  - Grindcurves[2] define mill performance
  - Using grindcurves, both TP and PSE are defined in terms of
    - mill filling (J_T)
    - mill speed (ϕ_C)

[2] Craig, I.K., Hulbert, D.G., Metzner, G., and Moult, S.P. (1992). Optimized multivariable control of an industrial run-of-mine milling circuit. *J. S. Afr. Inst. Min. Metall.*, 92(6), 169-176.

Powell, M.S., van der Westhuizen, A.P., and Mainza, A.N. (2009). Applying grindcurves to mill operation and optimisation. *Minerals Eng.*, 22(7-8), 625-632.

Van der Westhuizen, A. and Powell, M.S. (2006). Milling curves as a tool for characterising SAG mill performance. In *Proceedings of SAG 2006*, Vancouver, B.C., Canada, 217-232.

Plant-wide control – Top-down analysis

- Optimal steady-state operation
  - Grindcurves[2] define mill performance
  - Using grindcurves, both TP and PSE are defined in terms of
    - mill filling (J_T)
    - mill speed (ϕ_C)

Which variables should be *controlled*
to achieve the economic goal, and
which variable should *manipulate throughput*?

[2] Craig, I.K., Hulbert, D.G., Metzner, G., and Moult, S.P. (1992). Optimized multivariable control of an industrial run-of-mine milling circuit. *J. S. Afr. Inst. Min. Metall.*, 92(6), 169-176.

Powell, M.S., van der Westhuizen, A.P., and Mainza, A.N. (2009). Applying grindcurves to mill operation and optimisation. *Minerals Eng.*, 22(7-8), 625-632.

Van der Westhuizen, A. and Powell, M.S. (2006). Milling curves as a tool for characterising SAG mill performance. In *Proceedings of SAG 2006*, Vancouver, B.C., Canada, 217-232.

Plant-wide control – Top-down analysis

Primary controlled variables:
- Product particle size (PSE)
- Throughput (TP)
- Mill filling (J_T)
- Ball filling
- Mill slurry density

Manipulation of throughput:
- Mill speed (ϕ_C)

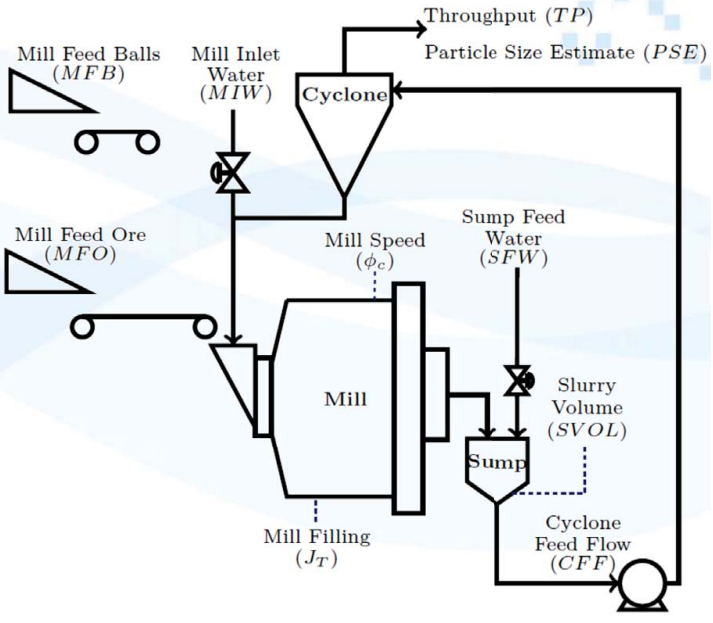

Plant-wide control – Top-down analysis

Primary controlled variables:

- Product particle size (PSE)
- Throughput (TP)
- Mill filling (J_T)
- Ball filling
- Mill slurry density

Manipulation of throughput:

- Mill speed (ϕ_C)

Which *control structure* should be chosen?

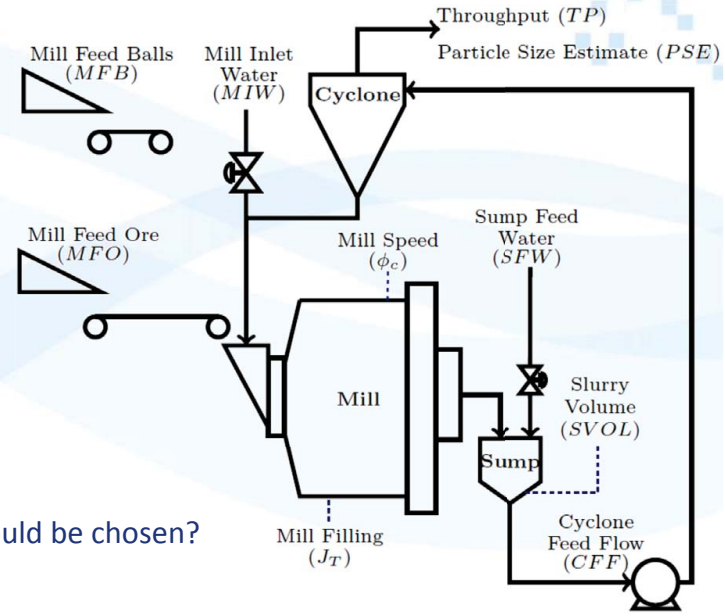

Plant-wide control – Bottom-up analysis
Regulatory layer

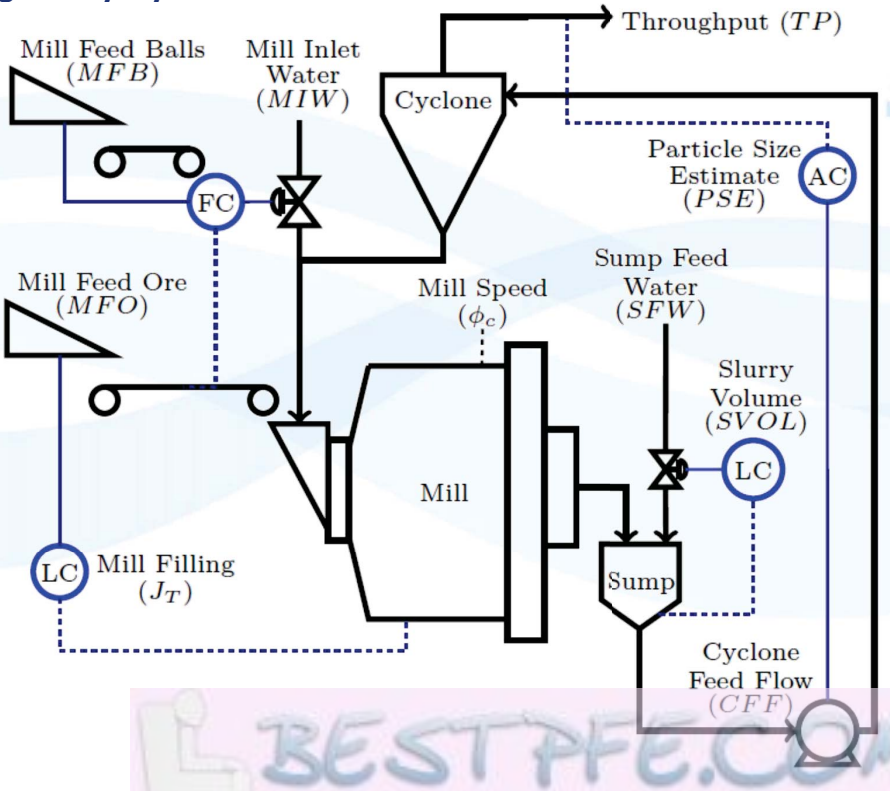

Plant-wide control – Bottom-up analysis
Regulatory layer

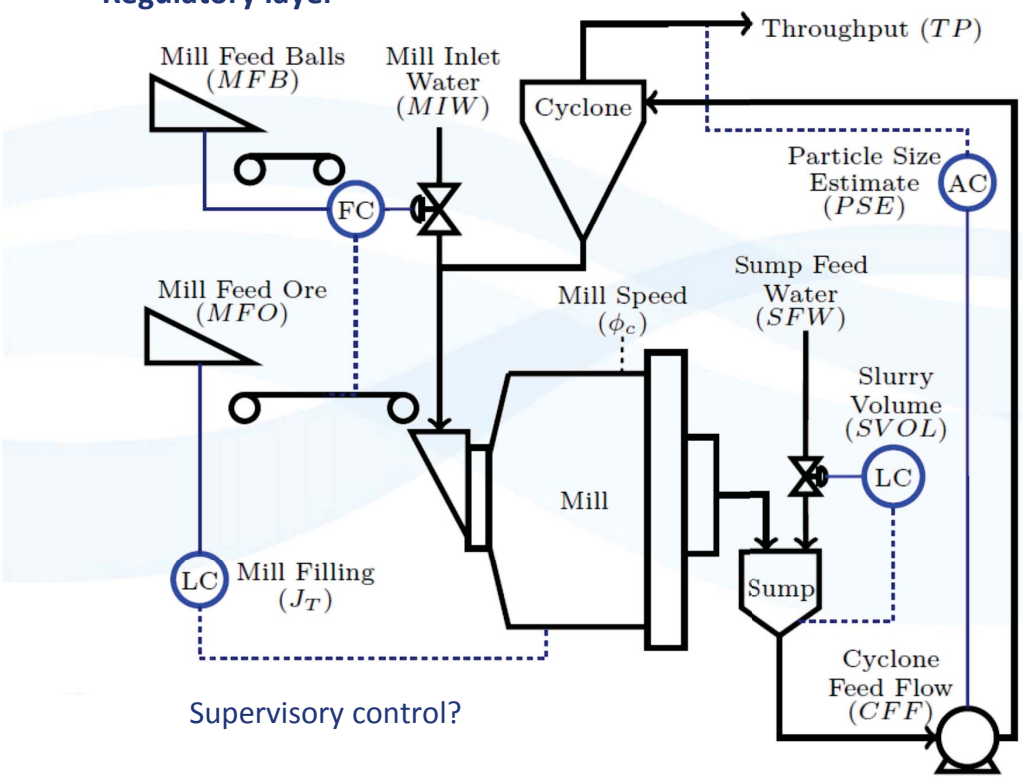

Supervisory control?

Plant-wide control – Bottom-up analysis
Supervisory layer: MPSP

- Challenge is to reduce computational time for NMPC applications[3]
- Model Predictive Static Programming
  - Computational complexity is reduced by
    - Linearising system for every time step[4]
    - Reducing feedback law to an explicit function[5]
  - MPSP achieves similar performance to NMPC when applied to the grinding mill circuit

[3] Coetzee, L. C., Craig, I. K. and Kerrigan, E. C. (2010). Robust nonlinear model predictive control of a run-of-mine ore milling circuit, IEEE Trans. Control Syst. Technol. 18(1): 222–229.

[4] De Oliveira, N. M. C. and Biegler, L. T. (1995). An extension of Newton-type algorithms for non-linear process control, Automatica 31(2): 281–286

[5] Bemporad, A., Borrelli, F. and Morari, M. (2002). Model predictive control based on linear programming - the explicit solution, IEEE Trans. Automatic Control 47(12): 1974–1985.

Plant-wide control – Bottom-up analysis
Supervisory layer: MPSP

- Challenge is to reduce computational time for NMPC applications[3]
- Model Predictive Static Programming
  - Computational complexity is reduced by
    - Linearising system for every time step[4]
    - Reducing feedback law to an explicit function[5]
  - MPSP achieves similar performance to NMPC when applied to the grinding mill circuit

How to achieve state feedback for controller?

[3] Coetzee, L. C., Craig, I. K. and Kerrigan, E. C. (2010). Robust nonlinear model predictive control of a run-of-mine ore milling circuit, IEEE Trans. Control Syst. Technol. 18(1): 222–229.

[4] De Oliveira, N. M. C. and Biegler, L. T. (1995). An extension of Newton-type algorithms for non-linear process control, Automatica 31(2): 281–286

[5] Bemporad, A., Borrelli, F. and Morari, M. (2002). Model predictive control based on linear programming - the explicit solution, IEEE Trans. Automatic Control 47(12): 1974–1985.

Plant-wide control – Bottom-up analysis
Supervisory layer: State Feedback

- Challenge is to estimate hold-ups inside mill
- A non-linear observer model is developed with states observable from linearized system
- An EKF is used to estimate the states and parameters
  - States and parameters:
    - Solids
    - Water
    - Grinding media
    - Discharge rate
    - Solids accumulation rate
  - Measurements:
    - Mill filling
    - Mill discharge flow-rate
    - Mill discharge density
    - Discharge density time-derivative

Summary

- Plant-wide control strategy
  - Economic objective defined in terms of grindcurves
  - Future challenge is to incorporate more complex models of down-stream processes
- Model Predictive Static Programming
  - Predictive controller with low computational complexity
  - Future challenge is to include state constraints
- State and Parameter estimation
  - Model is developed such that grinding mill conditions can be estimated
  - Future challenge is accurate measurement/calculation of derivative of discharge density

THANK YOU.

“The value and interest of life is not so much to do conspicuous things... as to do ordinary things with the perception of their enormous value.”

-Pierre Teilhard de Chardin